Volume 1, Issue 2, (2026)

1st September, 2026

DOI.org/10.71079/ASIDE.CV.1.2

ASIDE HEALTHCARE CARDIOVASCULAR

PUBLISHED BY

PUBPORTA

ISSN (Print) 3069-9851

ISSN (Online) 3069-9843

ISSN 3069-9851

9 773069 985007

Contents

ASIDE

ASIDE Cardiovascular

ASIDE CARDIOVASCULAR

Original Article

Cardiogenic Shock and Sepsis-Related Mortality in the United States, 1999-2025: National Trends, Disparities, and Forecasts to 2040

Karim Othman Abdelnaim[1], Alaa Eldeeb[2], Alyaa Ahmed Ibrahim[2], Raveen Mujeeb[3], Mohammad Rayyan Faisal[3], Amro Ali[4,*], Salem Qupp[5], Bassam Hegazy[2], Amr Ibrahim[6], Ibtissam ElGhazzani[7], Mohamed Zabady[2], Sihame ElGhazzani[7], Walid Bechibchi[8], Ilhame ElGhazzani[9], Mahdi Ahmed[10], Abdelrhman H. Mohamed[11], Mohamed Fawzi Hemida[2]

1-Faculty of Medicine, Ain Shams University, Cairo, Egypt
2-Faculty of Medicine, Alexandria University, Alexandria, Egypt
3-Department of Medicine, Dow University of Health Sciences, Karachi, Pakistan
4-Department of Medicine, Community Regional Medical Center, Fresno, CA, USA
5-Faculty of Medicine, Al-Quds University, Jerusalem, Palestine
6-Faculty of Medicine, Monoufia University, Monoufia, Egypt
7-Faculty of Medicine of Tunis, University of Tunis, Tunis, Tunisia
8-Faculty of Medicine, University of Constantine 3, Constantine, Algeria
9-Faculty of Medicine, University of Sfax, Sfax, Tunisia
10-Faculty of Medicine, Kafr El Sheikh University, Kafr El Sheikh, Egypt
11-Faculty of Medicine, Luxor University, Luxor, Egypt

ARTICLE INFO

Article history:
Received 17 Oct. 2025
Received in revised form 15 Apr. 2026
Accepted 25 Apr. 2026
Published 28 Apr. 2026

Keywords:
Cardiogenic shock
Sepsis
Mortality trends
Age-adjusted mortality rate
Health disparities
Forecasting analysis

ABSTRACT

Background: Cardiogenic shock (CS) complicated by sepsis is a life-threatening condition marked by circulatory collapse and systemic inflammation, with persistently high mortality despite critical care advances. National trends and disparities remain unclear. This study aimed to evaluate temporal mortality trends from 1999 to 2025 and project rates through 2040.
Methods: We conducted a population-based study using U.S. mortality data (1999–2025) from the CDC WONDER database. Deaths among adults aged ≥25 years with CS and sepsis were identified using ICD-10 codes. Age-adjusted mortality rates (AAMRs) per 100,000 were calculated. Joinpoint regression estimated annual percent change (APC) and average annual percent change (AAPC). Forecasting models projected mortality trends through 2040.
Results: From 1999 to 2025, 71,726 deaths occurred; 97.09% in medical facilities. Overall, AAMR rose from 0.65 to 2.16 (AAPC 5.01%, $p < 0.001$) and is projected to reach 3.62 by 2040. Men had higher mortality than women (2025: 2.78 vs 1.65; AAPC 5.06% vs 4.91%). In 2025, AAMR was 3.75 among NH Black individuals, 1.98 among NH White individuals, and 2.01 among Hispanic individuals. Adults ≥65 years had the highest CMR (7.50 in 2025; AAPC 4.63%), with the largest relative increase in ages 25–44 (AAPC 7.19%).
Conclusion: CS with sepsis mortality increased significantly from 1999 to 2025, particularly among men, NH Black individuals, and adults ≥65 years. Although recent trends have stabilized, projections indicate continued increases through 2040, highlighting persistent and widening demographic disparities in the mortality burden.

1. Introduction

Cardiogenic shock (CS) is a severe and life-threatening syndrome that arises from a primary cardiovascular disorder. It leads to tissue hypoperfusion with potential progression to multi-organ failure and death. CS has an early mortality rate of more than 50% [1, 2]. Sepsis, as defined by the Third International Consensus (Sepsis-3), is a life-threatening organ dysfunction that arises from a dysregulated immune response to an infection [3]. It affects nearly 1.7 million adults in the United States, making it one of the leading causes of death [4].

The relationship between CS and sepsis is bidirectional. CS can precipitate sepsis through impaired immune function and intestinal ischemia, leading to bacterial translocation [5]. Sepsis can frequently be found in patients with cardiogenic shock, with 15-20% of CS patients having it. This was found to significantly increase mortality [2]. One study from the Mayo Clinic has reported that 15% of all shock patients in the Cardiac Intensive Care Unit (CICU) from 2007 to 2018 had concurrent CS and sepsis, with this group of patients exhibiting higher severity, more advanced shock, and poorer survival [6].

* Corresponding author: Amro Ali, Department of Medicine, Community Regional Medical Center, Fresno, CA, USA. Email: amro.ali.md@gmail.com

Published and owned by PubPorta Publishing LLC. Academic oversight and scholarly guidance are provided by the American Society for Inclusion, Diversity, and Equity in Healthcare (ASIDE). ISSN (Print) 3069-9851, ISSN (Online) 3069-9843. Hosting by ASIDE Journals.

Citation: Abdelnaim KO, Eldeeb A, Ibrahim AA, et al. Cardiogenic Shock and Sepsis-Related Mortality in the United States, 1999-2025: National Trends, Disparities, and Forecasts to 2040. ASIDE Cardiovasc. 2026;1(2):1-8, doi:10.71079/ASIDE.CV.042826319

Sepsis can contribute to CS and myocardial dysfunction through various mechanisms, including acute changes in loading conditions, myocardial ischemia, and the toxic effects of proinflammatory cytokines on the myocardium, coronary microcirculation, and endothelium [5, 7]. An analysis of the National Inpatient Sample (NIS), which is a nationwide repository of hospital inpatient discharge data in the U.S., reported an estimated 5 million sepsis hospitalizations in the period between 2017 and 2019. Of those, one million had septic shock. Within these patients, cardiogenic shock was identified in 0.3% of patients with sepsis and 4.6% of those with septic shock. The presence of CS was associated with an increase in in-hospital mortality [8].

Despite the clinical significance of this interaction, national data describing trends and demographic disparities remain limited. Given the constraints of available datasets, we focused our analysis on mortality trends and disparities in CS and sepsis across demographic factors in the United States from 1999 to 2025. Specifically, we examined deaths in which both CS and sepsis were listed, as these provide a population-level proxy for the co-occurrence of these critical conditions.

2. Methods

2.1. Study Design and Population

We conducted a retrospective analysis using death certificate data retrieved from the Centers for Disease Control and Prevention Wide-Ranging Online Data for Epidemiologic Research (CDC WONDER) database. Data for adults aged 25 and older from 1999 to 2025 were analyzed to assess mortality from CS and sepsis in the U.S. This age cutoff has been used to define adults in a previous study [9]. Restricting to ≥25 improves robustness and reliability of estimates. The International Statistical Classification of Diseases and Related Health Problems-10th Revision (ICD-10) was used as follows: R57.0 for CS and A40-41 for sepsis. Deaths were included if CS and sepsis were listed anywhere on the death certificate, either as underlying causes or contributing causes of death. This comprehensive approach ensures the capture of all deaths where both conditions played documented roles, regardless of their position on the death certificate. Institutional review board approval was not required for this study because it used de-identified public-use data provided by the government and adhered to the STROBE (Strengthening the Reporting of Observational Studies in Epidemiology) guidelines for reporting [10].

2.2. Data Abstraction

Data on population size and demographics, including sex, age, and race, were extracted. The place of death was categorized into medical facilities, hospice, home, and nursing home/long-term care facilities. Racial and ethnic categories were classified as non-Hispanic (NH) Black or African American, NH White, and Hispanic or Latino. NH American Indian or Alaska Native and NH Asian or Pacific Islander were excluded from the trend analysis due to small numbers and data suppression. In accordance with CDC-WONDER database policies, death counts <10 are suppressed to protect confidentiality. Consequently, suppressed data were treated as missing and excluded from analysis. Age groups were divided into 3 groups: (25 – 44, 45 – 64, and ≥65 years).

Data suppression due to counts <10 did not affect any of the final analytical strata (sex, including racial/ethnic groups, and age groups) presented in this study; suppression exclusively applied to the NH American Indian or Alaskan Native and NH Asian or Pacific Islander categories, which were consequently excluded from the trend analysis.

2.3. Statistical Analysis

Crude mortality rates (CMRs) and age-adjusted mortality rates (AAMRs) per 100,000 population from 1999 to 2025 by year, sex, and race. Population denominators were derived from U.S. Census Bureau estimates (bridged-race population estimates for 1999 – 2020 and single-race estimates for 2021 – 2025, as dictated by the respective CDC WONDER archives). Age adjustment was performed using the direct standardization method, weighted to the year 2000 U.S. standard population [11]. Furthermore, 95% confidence intervals (CIs) for mortality rates were automatically generated by the CDC WONDER system; this system calculates CIs using a standard normal distribution for death counts of 100 or more, and the Tiwari modification of the gamma distribution for death counts fewer than 100. This standard was used in a previously published paper with the same study design [12]. CMRs were determined by dividing the number of CS and sepsis-related mortalities by the corresponding U.S. population of that year. It's worth mentioning that CMRs were used exclusively for age-specific analyses, as age adjustment would mask true differences between age groups. For all other variables, AAMRs were calculated to ensure comparability across populations with differing age structures. The Joinpoint Regression Program (Joinpoint V 5.4.0.0, National Cancer Institute) was used to determine the average annual percent change (AAPC) and the annual percent change (APC) with 95% CI in AAMR to quantify national annual trends in CS and sepsis-related mortality. Joinpoint regression, a segmented regression technique, was used to identify points of trend change (join points) by fitting log-linear models and using permutation tests to select the optimal number of join points, thereby ensuring model fit [13]. This method assumes independent observations; we acknowledge that mortality rates across consecutive years may be temporally autocorrelated, which could affect standard errors and the detection of joinpoints. This method allows identification of significant changes in AAMR over time by fitting log-linear regression models where temporal variation occurred. APCs were considered increasing or decreasing if the slope describing the change in mortality differed significantly from zero using two-tailed t-tests. A value of $p < 0.05$ was considered statistically significant.

2.4. Time Series Forecasting and Mortality Projections

Time series models were used to forecast the projected values of AAMRs for CS and mortality rates for sepsis in the United States, using data from 1999 to 2025, and projections for 2026 to 2040. The performance of the models was compared and evaluated for the autoregressive integrated moving average (ARIMA) and exponential smoothing state space (ETS) models. The performance was evaluated based on root mean squared error (RMSE), mean error (ME), and the autocorrelation of residuals at lag 1 (ACF1). In addition, residual diagnostics were performed to evaluate model performance and determine whether the residuals were randomly distributed and normally distributed around zero.

For sex-specific data, the ARIMA model performed better than the ETS model, with lower prediction error and minimal residual autocorrelation. The residuals of the ARIMA model were also randomly distributed and normally distributed around zero. On the other hand, for race- and age-specific data, the ETS models performed better on residual diagnostics, with residuals that were randomly distributed and normally distributed around zero, compared to the ARIMA models.

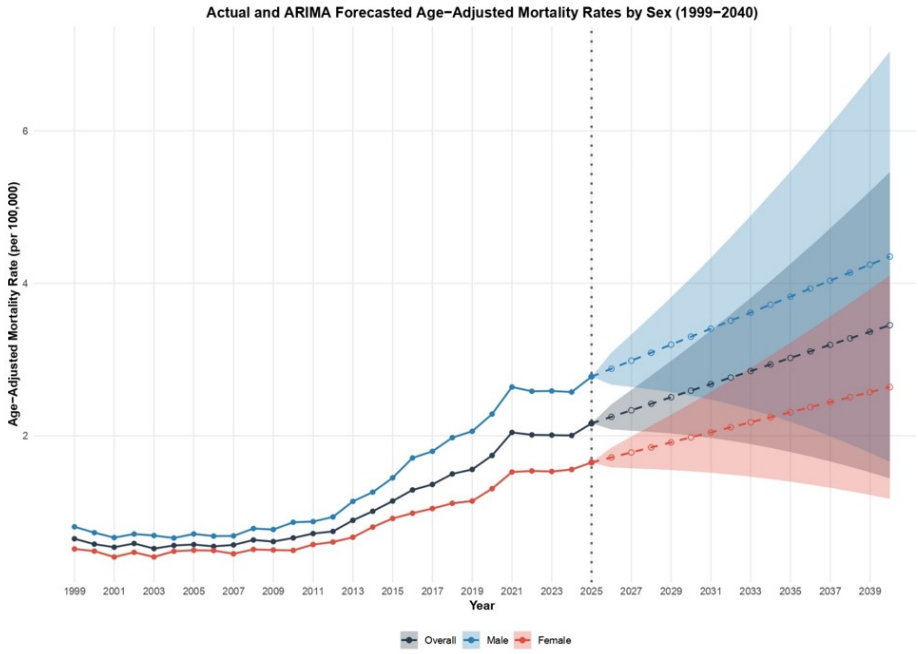

Figure 1: Cardiogenic Shock and Sepsis Comparative Longitudinal Analysis of Age-Adjusted Mortality Rates by Sex: Historical Trends and ARIMA Forecasts (1999–2040).

3. Results

From 1999 to 2025, 71,726 deaths were reported among adults aged 25 years and older in the United States with CS and sepsis. A minor limitation of our aggregate dataset is a single-death discrepancy between the total overall mortality count (71,726) and the place-of-death sub-stratification (71,725), which is likely due to incomplete categorization on the original death certificate. The majority of deaths occurred in medical facilities (97.09%), followed by nursing homes or long-term care facilities (0.95%), hospice facilities (0.83%), the decedent's home (0.61%), and other locations (0.34%). For 0.18%, the place of death was unknown **(Supplementary Table 1)**.

3.1. Overall Trends

Over the study period, the overall AAMR increased from 0.65 (95% CI: 0.61 to 0.69) in 1999 to 2.16 (95% CI: 2.11 to 2.22) in 2025, with an AAPC of 5.01 (95% CI: 4.64 to 5.43; $p < 0.001$). The mean AAMR was 1.08 (95% CI: 1.04 to 1.12). The projected mean AAMR is expected to increase to 3.02 (95% CI: 1.74 to 4.30) by 2040.

The AAMR trend demonstrated an initial period of stability from 1999 to 2008 (APC: -0.62; 95% CI: -2.58 to 1.09; p = 0.470). This was followed by a significant rise from 2008 to 2021 (APC: 10.23; 95% CI: 9.55 to 11.24; $p < 0.001$). From 2021 to 2025, the rate showed a slight non-significant increase (APC: 1.52; 95% CI: -1.74 to 3.79; p = 0.209). Forecasts suggest that the overall AAMR for cardiogenic shock with sepsis will rise to 3.62 (95% CI: 1.27 to 5.97) by 2040 **(Figure 1)** and **(Supplementary Tables 2 and 5)**.

3.2. Sex-Stratified Trends

During the study period, 41,020 deaths were reported among men and 30,706 among women. Mortality was consistently higher in men than in women. Among men, the AAMR increased from 0.81 (95% CI: 0.74 to 0.87) in 1999 to 2.78 (95% CI: 2.68 to 2.87) in 2025, with a mean AAMR of 1.39 (95% CI: 1.31 to 1.46). Among women, the AAMR rose from 0.52 (95% CI: 0.47 to 0.56) in 1999 to 1.65 (95% CI: 1.59 to 1.72) in 2025, with a mean AAMR of 0.84 (95% CI: 0.79 to 0.89) in females. The trend for both men and women increased from 1999 to 2025 [AAPC: Men: 5.06 (95% CI: 4.70 to 5.48; $p < 0.001$); AAPC: Women: 4.91 (95% CI: 4.51 to 5.37; $p < 0.001$)].

Among men, the AAMR showed a non-significant decline from 1999 to 2006 (APC: -1.66; 95% CI: -7.41 to 0.61; p = 0.102), followed by a significant increase from 2006 to 2012 (APC: 6.17; 95% CI: 1.04 to 9.72; p = 0.032). A significant steep rise was observed between 2012 and 2016 (APC: 14.93; 95% CI: 11.63 to 19.15; $p < 0.001$). Mortality continued to rise significantly from 2016 to 2021 (APC: 8.71; 95% CI: 6.24 to 10.70; p = 0.002), followed by a non-significant increase from 2021 to 2025 (APC: 1.67; 95% CI: -0.93 to 3.23; p =) 0.125). Among women, the AAMR remained relatively stable from 1999 to 2009 (APC: 0.37; 95% CI: -1.70 to 2.02; p = 0.679). A marked increase occurred between 2009 and 2021 (APC: 9.78; 95% CI: 8.93 to 11.36; $p < 0.001$). From 2021 to 2025, mortality increased modestly but not significantly (APC: 2.30; 95% CI: -1.53 to 4.92; p = 0.169). Projections suggest that the AAMR is expected to reach 2.77 (95% CI: 1.06 to 4.48) among women, and 4.56 (95% CI: 1.41 to 7.71) among men by 2040 **(Figure 1)** and **(Supplementary Tables 2 and 5)**.

3.3. Race/Ethnicity Trends

From 1999 to 2025, the AAMR increased across all racial/ethnic groups, rising from 1.24 (95% CI: 1.06 to 1.41) to 3.75 (95% CI: 3.53 to 3.98) among NH Black, 0.57 (95% CI: 0.53 to 0.61) to 1.98 (95% CI: 1.92 to 2.04) among NH White, and 0.84 (95% CI: 0.65 to 1.06) to 2.01 (95% CI: 1.86 to 2.18) among Hispanic. The highest mean AAMR was observed among NH Black (AAMR: 1.84; 95% CI: 1.67 to 2.01), followed by Hispanic (AAMR: 1.05; 95% CI: 0.91 to 1.21) and NH White (AAMR: 1.00; 95% CI: 0.95 to 1.04).

Distinct trends were observed among these groups, with NH White population experiencing the greatest increment, followed by NH Black and Hispanics [NH White: AAPC: 4.96 (95% CI: 4.42 to 5.63; $p < 0.001$); NH Black: AAPC: 4.53 (95% CI: 4.16 to 4.92; $p < 0.001$); Hispanic: AAPC: 3.77 (95% CI: 3.09 to 4.64; $p < 0.001$)].

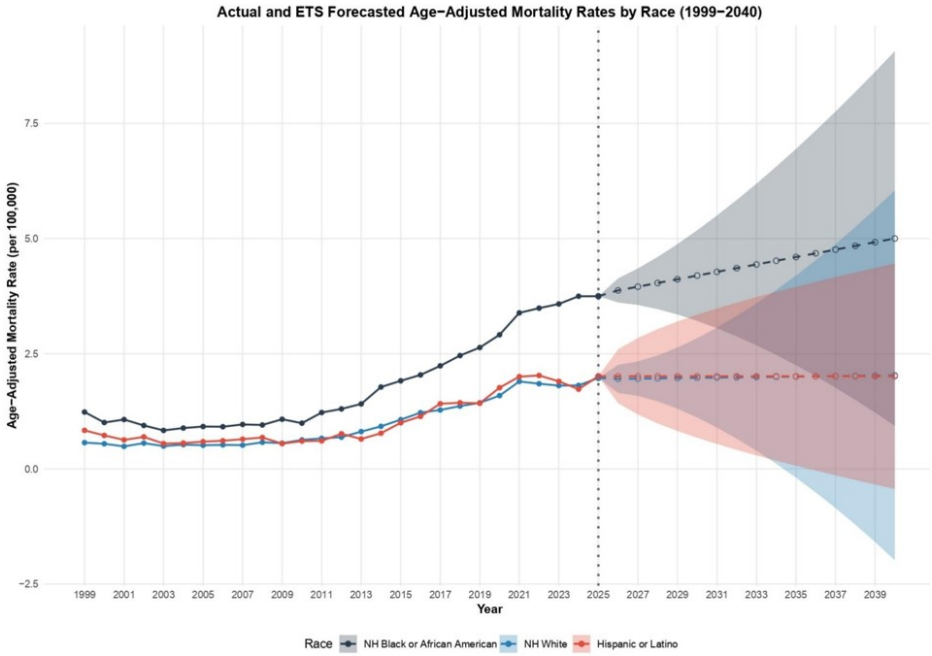

Figure 2: Cardiogenic shock and Sepsis Comparative Longitudinal Analysis of Age-Adjusted Mortality Rates by Race and Ethnicity: Historical Trends and ETS Forecasts (1999–2040).

Among NH Black individuals, the trend showed a significant decline from 1999 to 2003 (APC: -8.44; 95% CI: -13.70 to -4.84; $p < 0.001$), followed by a significant increase from 2003 to 2010 (APC: 3.63; 95% CI: 0.95 to 6.31; $p = 0.014$), a sharp rise from 2010 to 2021 (APC: 10.79; 95% CI: 10.13 to 11.85; $p < 0.001$), and a further significant increase from 2021 to 2025 (APC: 3.25; 95% CI: 0.96 to 4.99; $p = 0.012$). Among NH White individuals, the AAMR trend remained stable between 1999 and 2008 (APC: -0.46; 95% CI: -4.37 to 2.06; $p = 0.657$). A significant rise was observed from 2008 to 2021 (APC: 10.16; 95% CI: 9.31 to 12.14; $p < 0.001$). From 2021 to 2025, mortality increased slightly but not significantly (APC: 1.06; 95% CI: -3.63 to 4.07; $p = 0.410$). Among Hispanic individuals, the trend showed a slight non-significant decline from 1999 to 2010 (APC: -2.30; 95% CI: -5.59 to 0.41; $p = 0.092$). Mortality then increased sharply between 2010 and 2021 (APC: 12.17; 95% CI: 10.57 to 15.24; $p < 0.001$), and remained relatively stable from 2021 to 2025 (APC: -1.13; 95% CI: -6.11 to 2.51; pΨ0.514). The projected AAMR is expected to reach 2.01 (95% CI: -0.62 to 4.65) among Hispanics, 5.16 (95% CI: 0.33 to 10.00) among NH Black individuals, and 2.04 (95% CI: -2.84 to 6.93) among NH Whites **(Figure 2)** and **(Supplementary Tables 3 and 6)**.

3.4. Age-Specific Trends

The CMR increased across all age groups between 1999 to 2025, from 0.04 (95% CI: 0.03 to 0.05) to 0.24 (95% CI: 0.21 to 0.27) among adults aged 25-44 years, from 0.37 (95% CI: 0.32 to 0.42) to 1.63 (95% CI: 1.54 to 1.72) among those aged 45-64 years and from 2.52 (95% CI: 2.35 to 2.68) to 7.50 (95% CI: 7.28 to 7.72) among adults aged 65+ years. Adults aged 65+ years had the highest CMR (3.78; 95% CI: 3.61 to 3.95), followed by those aged 45-64 years (0.83; 95% CI: 0.77 to 0.89) and those aged 25-44 years (0.13; 95% CI: 0.11 to 0.15).

Notable trends were observed among all age groups, with adults aged 25-44 years experiencing the largest relative increase, followed by those aged 45-64 years, and 65+ years [25-44 years: AAPC: 7.19 (95% CI: 6.28 to 8.29; $p < 0.001$); 45-64 years: AAPC: 5.93 (95% CI: 5.41 to 6.65; $p < 0.001$); 65+ years: AAPC: 4.63 (95% CI: 4.21 to 5.18; $p < 0.001$)].

Among adults aged 25-44 years, the CMR increased from 1999 to 2007 with a non-significant trend (APC: 3.84; 95% CI: -9.68 to 8.63; pΨ0.327). A significant rise occurred between 2007 and 2021 (APC: 12.68; 95% CI: 11.45 to 15.99; $p < 0.001$), followed by a non-significant decline from 2021 to 2025 (APC: -4.10; 95% CI: -10.03 to 0.20; pΨ0.067). For adults aged 45-64 years, mortality remained stable from 1999 to 2007 (APC: -0.43; 95% CI: -4.81 to 2.58; pΨ 0.737). A substantial increase occurred from 2007 to 2021 (APC: 12.09; 95% CI: 11.33 to 13.35; $p < 0.001$). A slight non-significant decline occurred between 2021 and 2025 (APC: -1.61; 95% CI: -4.91 to 1.47; pΨ0.204). Among adults aged 65+ years, the trend remained stable from 1999 to 2009 (APC: -0.12; 95% CI: -2.74 to 1.69; pΨ 0.869). A marked significant increase was observed between 2009 and 2021 (APC: 9.38; 95% CI: 8.59 to 11.67; $p < 0.001$). From 2021 to 2025, rates continued to increase but not significantly (APC: 2.88; 95% CI: -1.65 to 5.49; pΨ0.090). Projections indicate that by 2040, the CMR is anticipated to reach -0.02 (95% CI: -0.77 to 0.72) among adults aged 25-44 years, 0.36 (95% CI: -4.16 to 4.89) among adults aged 45-64 years, and 12.46 (95% CI: -8.04 to 32.97) among adults aged 65+ years **(Figure 3)** and **(Supplementary Tables 4 and 7)**.

4. Discussion

This study provides a comprehensive national analysis of mortality trends associated with CS and sepsis in the United States from 1999 to 2025. Overall mortality increased substantially over the study period, with a marked acceleration after 2008 and a projected continued rise through 2040. Mortality was consistently higher among men compared to women. Racial disparities were evident, with NH Black individuals experiencing the highest mortality rates, while all racial/ethnic groups demonstrated increasing trends. Age-stratified analyses revealed the greatest relative increase among younger adults, although absolute mortality remained highest among

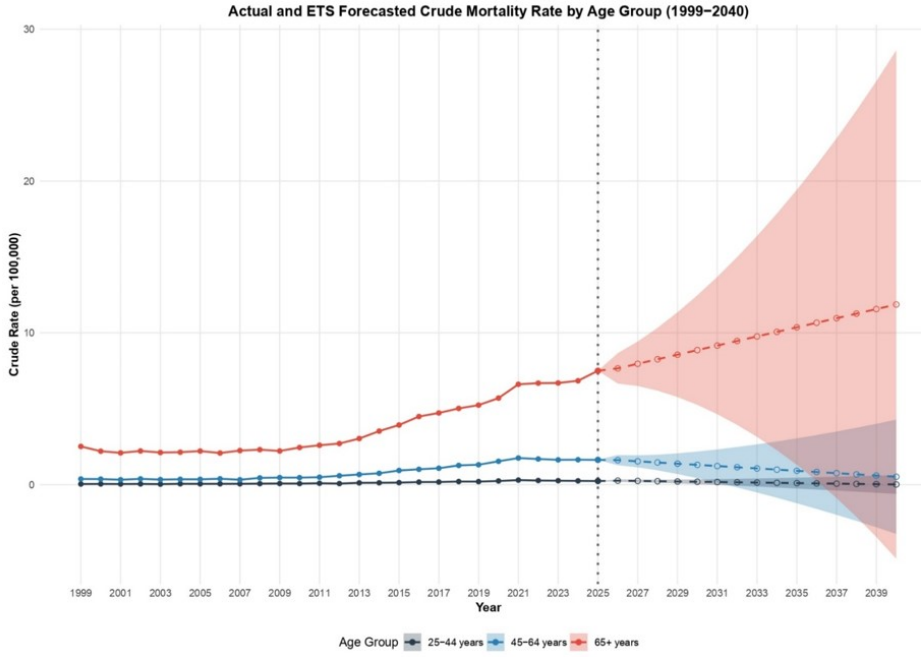

Figure 3: Cardiogenic Shock and Sepsis Comparative Longitudinal Analysis of Crude Mortality Rates by Age Group: Historical Trends and ETS Forecasts (1999–2040).

individuals aged 65 years and older. Most deaths occurred in medical facilities.

The coexistence of CS and sepsis represents a severe and increasingly recognized clinical entity associated with markedly elevated mortality. Prior studies have shown that CS complicating sepsis significantly worsens outcomes, with mortality rates exceeding 40% in contemporary cohorts [5, 6]. Mechanistically, sepsis-induced myocardial dysfunction is mediated by inflammatory cytokines, nitric oxide dysregulation, and mitochondrial impairment, leading to reversible but profound cardiac depression [14–16]. In parallel, patients with CS are highly susceptible to secondary infections due to invasive interventions and prolonged intensive care exposure, creating a bidirectional relationship that amplifies mortality risk [5, 17].

The marked increase in mortality after 2008 observed in this study is consistent with evolving epidemiological trends in both sepsis and CS. Large population-based analyses suggest that the apparent rise in sepsis incidence is partly attributable to improved recognition and coding practices, particularly following updated sepsis definitions [3, 18]. However, true increases in disease burden, driven by aging populations, multimorbidity, and improved survival following acute cardiovascular events, also play a substantial role [19, 20]. Furthermore, increasing clinical complexity, including mixed shock states and multi-organ failure, has been associated with worse outcomes despite advances in critical care [21, 22].

Sex disparities in CS and sepsis outcomes are increasingly reported. Meta-analyses indicate that women with CS may experience higher adjusted mortality and are less likely to receive mechanical circulatory support compared to men, potentially due to biological differences, later presentation, and differential treatment patterns [23, 24]. Similar disparities have been observed in acute myocardial infarction complicated by CS, where women had less revascularization and higher in-hospital mortality than men [25]. In sepsis populations, sex-based differences in clinical outcomes have been documented, with some studies showing higher in-hospital mortality among males, greater severity of organ dysfunction, and higher rates of invasive support among men [26].

Racial and ethnic disparities in critical illness outcomes are well documented. National analyses have shown that mortality associated with combined CS and sepsis is consistently higher among NH Black individuals compared with other groups [27]. Similar patterns have been observed in stand-alone CS cohorts, where NH Black and Hispanic patients with STEMI and CS had higher adjusted odds of mortality and were less likely to receive invasive procedures compared with NH White men [25].

Sepsis mortality also exhibits racial disparities. Historical sepsis data indicate higher age-adjusted mortality among Black and American Indian populations compared with NH White and Asian groups. However, some trend analyses suggest that racial mortality trajectories may vary by state and over time [28, 29].

Age is a strong determinant of mortality in both CS and sepsis. Older adults (≥65 years) have the highest absolute mortality rates, reflecting cumulative comorbidity burden, immunosenescence, and increased vulnerability to both myocardial and infectious insults. Epidemiologic studies have consistently shown that age is among the strongest predictors of mortality in shock states and sepsis, with worse outcomes among elderly, multimorbid patients [30].

The COVID-19 pandemic profoundly affected U.S. mortality patterns, with marked increases in sepsis and cardiovascular mortality during 2020 – 2021. Pandemic-related disruptions likely delayed care for acute cardiac conditions, increased infection risks, and strained critical care resources, all of which may have contributed to elevated cardiogenic shock and sepsis-related mortality rates. National sepsis mortality data show significant increases in AAMR during this period, supporting the pandemic's impact on broader mortality trends [30].

5. Clinical and Policy Implications

Building on our findings, the observed mortality trends underscore the need to evaluate targeted strategies for the early recognition and management of CS complicated by sepsis. For instance, future clinical studies should investigate whether targeted echocardiographic assessment might improve outcomes in high-risk demographic groups, such as adults ≥65 years, men, and NH Black patients presenting with sepsis and hypotension. Furthermore, the rising mortality burden highlights the potential value of evaluating bundled care approaches that integrate early fluid resuscitation, vasopressor titration, and timely mechanical support initiation. Additionally, future research could explore whether machine learning models that use vital signs, lab trends, and comorbidity profiles are useful for predicting high-risk patients and guiding escalation of care. Prospective studies are required to determine if evaluating and implementing these measures can effectively improve outcomes and mitigate the observed demographic disparities.

6. Strengths

This study leverages a comprehensive, nationally representative dataset spanning multiple decades, enabling robust analysis of long-term mortality trends across demographic groups. The use of AAMRs enhances comparability over time and between subgroups. Stratification by sex, race/ethnicity, and age provides valuable insights into disparities that are essential for targeted public health interventions. Furthermore, forecasting extends the utility of findings by projecting future mortality trajectories, which is critical for policy planning and resource allocation.

7. Limitations

Our analysis is limited by reliance on death certificate data, which may be subject to misclassification or inaccuracies in cause-of-death coding. Changes in sepsis definitions and coding practices over the study period can introduce bias in trend estimations. The lack of individual clinical data prevents adjustment for severity, comorbidities, and in-hospital management strategies (e.g., revascularization, vasopressors, mechanical support). We could not differentiate primary CS complicated by sepsis from primary sepsis with secondary cardiogenic dysfunction. Similarly, unmeasured confounders such as socioeconomic status, insurance, and healthcare delivery factors may contribute to the observed disparities but are not captured in this dataset. Our study includes multiple subgroup analyses by sex, age group, and race/ethnicity. We did not apply formal adjustments for multiple comparisons, as the analyses were primarily descriptive and hypothesis-generating. Consequently, the potential for inflated Type I error should be considered when interpreting differences across subgroups. Observed increases in mortality from CS and sepsis may reflect improved recognition and documentation rather than true increases in incidence. Changes in coding practices, the introduction of Sepsis-3 definitions (2016), Medicare SEP-1 quality measures (2015), broader adoption of electronic health records, and heightened attention during the COVID-19 era may have increased the likelihood that both conditions were recorded on death certificates. Our study cannot distinguish true changes in incidence from documentation effects.

Moreover, a methodological limitation of our forecasting analysis is the presence of negative lower confidence bounds in certain long-term projections, notably for the 25 – 44 age group by 2040. The standard ARIMA and ETS models used in this study do not inherently constrain predictions to be strictly positive. Because mortality rates cannot mathematically fall below zero, these specific lower bounds represent a statistical artifact caused by the expanding variance over a 15-year forecast horizon, rather than a biologically plausible scenario. Despite this limitation regarding the uncertainty intervals, the point estimates and the overall projected upward trajectories remain robust and provide a valuable assessment of future demographic trends.

Furthermore, our analysis relied on the inclusion of CS and sepsis as either an underlying or contributing cause of death (any mention) to capture the broadest population-level burden. We did not perform a sensitivity analysis restricting the data strictly to the underlying cause of death (UCD), nor did we mandate the presence of specific ICD-10 codes for severe sepsis (e.g., R65.2). We acknowledge that lacking a UCD restriction or a severe sepsis code requirement limits the clinical specificity of our cohort. Consequently, our mortality estimates reflect the overall epidemiological burden of these co-occurring critical conditions, which may include patients for whom they were present but not the primary driver of mortality.

Additionally, a minor limitation of our aggregate dataset is a single-death discrepancy between the total overall mortality count (71,726) and the place-of-death sub-stratification (71,725), which is likely due to incomplete categorization on the original death certificate.

8. Conclusion

This national analysis demonstrates a marked and sustained increase in mortality related to CS complicated by sepsis among U.S. adults between 1999 and 2025. Age-adjusted mortality rates more than tripled during the study period, with the steepest rise occurring between 2008 and 2021. Mortality remained consistently higher among men compared with women and was disproportionately elevated among NH Black individuals. Although older adults (≥65 years) bore the highest absolute mortality burden, younger adults experienced the greatest relative increases over time. Forecasting models project continued growth in mortality rates through 2040, particularly among men and the NH Black populations. These findings highlight a worsening national mortality trajectory with persistent demographic disparities, underscoring the need for targeted surveillance and intervention strategies.

Conflicts of Interest

The authors declare no competing interests that could have influenced the objectivity or outcome of this research.

Funding Source

No financial support was received for the study.

Acknowledgments

None.

Institutional Review Board (IRB)

No ethical approval was required for the study.

Large Language Model

No artificial intelligence (AI) tools or large language models were used in the design, analysis, interpretation, or writing of this manuscript.

Author Contributions

KOA and MFH contributed to the conceptualization of the study, while AE, AAI, and RM were responsible for data collection. MRF and AA performed the statistical analysis, and SQ, BH, and AI contributed to the interpretation of results. IE, MZ, SE, WB, IE, MA, and AM assisted in drafting the manuscript, while MFH supervised the study. All authors reviewed and approved the final manuscript.

Data Availability

Mortality data were obtained from the CDC WONDER Multiple Cause of Death database https://wonder.cdc.gov/. To ensure reproducibility, we queried deaths among adults aged ≥25 years from 1999–2025 listing R57.0 (cardiogenic shock) and A40–A41 (sepsis) as any mention (underlying or multiple cause of death). Analyses were stratified by sex, age group (25–44, 45–64, ≥65 years), and race/ethnicity (Non-Hispanic White, Non-Hispanic Black, Hispanic). All query parameters are described here to allow exact replication of the data extraction.

References

1. Delmas C, Roubille F, Lamblin N, Bonello L, Leurent G, Levy B, et al. Baseline characteristics, management, and predictors of early mortality in cardiogenic shock: insights from the FRENSHOCK registry. ESC Heart Fail. 2022;9(1):408-19. [PMID: 34973047, PMCID: PMC8788015, https://doi.org/10.1002/ehf2.13734].
2. Jung RG, Stotts C, Gupta A, Prosperi-Porta G, Dhaliwal S, Motazedian P, et al. Prognostic Factors Associated with Mortality in Cardiogenic Shock - A Systematic Review and Meta-Analysis. NEJM Evid. 2024;3(11):EVIDoa2300323. [PMID: 39437131, https://doi.org/10.1056/EVIDoa2300323].
3. Singer M, Deutschman CS, Seymour CW, Shankar-Hari M, Annane D, Bauer M, et al. The Third International Consensus Definitions for Sepsis and Septic Shock (Sepsis-3). JAMA. 2016;315(8):801-10. [PMID: 26903338, PMCID: PMC4968574, https://doi.org/10.1001/jama.2016.0287].
4. Rhee C, Dantes R, Epstein L, Murphy DJ, Seymour CW, Iwashyna TJ, et al. Incidence and Trends of Sepsis in US Hospitals Using Clinical vs Claims Data, 2009-2014. JAMA. 2017;318(13):1241-9. [PMID: 28903154, PMCID: PMC5710396, https://doi.org/10.1001/jama.2017.13836].
5. Cherbi M, Merdji H, Labbe V, Bonnefoy E, Lamblin N, Roubille F, et al. Cardiogenic shock and infection: A lethal combination. Arch Cardiovasc Dis. 2024;117(8-9):470-9. [PMID: 39048471, https://doi.org/10.1016/j.acvd.2024.04.005].
6. Jentzer JC, Ahmed AM, Vallabhajosyula S, Burstein B, Tabi M, Barsness GW, et al. Shock in the cardiac intensive care unit: Changes in epidemiology and prognosis over time. Am Heart J. 2021;232:94-104. [PMID: 33257304, https://doi.org/10.1016/j.ahj.2020.10.054].
7. Sato R, Hasegawa D, Guo S, Nuqali AE, Moreno JEP. Sepsis-induced cardiogenic shock: controversies and evidence gaps in diagnosis and management. J Intensive Care. 2025;13(1):1. [PMID: 39748440, PMCID: PMC11694368, https://doi.org/10.1186/s40560-024-00770-y].
8. Sato R, Hasegawa D, Nishida K, Dugar S. Cardiogenic shock complicating sepsis and septic shock: A national inpatient sample analysis. Med Intensiva (Engl Ed). 2023;47(9):547-51. [PMID: 37270337, https://doi.org/10.1016/j.medine.2023.05.005].
9. Hemida MF, Ibrahim AA, Zeeshan N, Faisal MR, Patel K, Hussein M, et al. Trends and disparities in aortic dissection mortality in the united states: a retrospective analysis. BMC Cardiovasc Disord. 2026;26(1):66. [PMID: 41572202, PMCID: PMC12825201, https://doi.org/10.1186/s12872-025-05446-5].
10. von Elm E, Altman DG, Egger M, Pocock SJ, Gotzsche PC, Vandenbroucke JP, et al. The Strengthening the Reporting of Observational Studies in Epidemiology (STROBE) statement: guidelines for reporting observational studies. J Clin Epidemiol. 2008;61(4):344-9. [PMID: 18313558, https://doi.org/10.1016/j.jclinepi.2007.11.008].
11. Anderson RN, Rosenberg HM. Age standardization of death rates: implementation of the year 2000 standard. Natl Vital Stat Rep. 1998;47(3):1-16, 20. [PMID: 9796247].
12. Hemida MF, Ibrahim AA, Shahriar Z, Khalid M, Zeeshan N, Qaisi W, et al. Mortality trends in multiple sclerosis and cardiovascular disease in adults in the United States: A 25-year mortality perspective. Mult Scler Relat Disord. 2026;105:106861. [PMID: 41308235, https://doi.org/10.1016/j.msard.2025.106861].
13. National Cancer Institute. Joinpoint trend analysis software [Internet]; 2025. Joinpoint Regression Program, Surveillance Research Program: National Cancer Institute, Bethesda, MD. Available from: https://surveillance.cancer.gov/joinpoint/.
14. Liu C, Liu H, Li Y, Zeng Y, Wang X, Mou Y, et al. Combatting sepsis-induced myocardial dysfunction: emerging mechanisms and immunomodulatory breakthroughs. Front Immunol. 2025;16:1643048. [PMID: 41256846, PMCID: PMC12620270, https://doi.org/10.3389/fimmu.2025.1643048].
15. Padureanu V, Caragea DC, Pirscoveanu DFV, Dop D, Munteanu AC, Radulescu D, et al. Association Between Myocardial Dysfunction and Septic Shock. Int J Mol Sci. 2026;27(6). [PMID: 41898416, PMCID: PMC13026803, https://doi.org/10.3390/ijms27062552].
16. Tartavoulle T, Fowler L. Cardiogenic Shock in the Septic Patient: Early Identification and Evidence-Based Management. Crit Care Nurs Clin North Am. 2018;30(3):379-87. [PMID: 30098741, https://doi.org/10.1016/j.cnc.2018.05.006].
17. Kosaraju A, Pendela VS, Hai O. Cardiogenic Shock. StatPearls Publishing, Treasure Island (FL); 2026. Available from: https://www.ncbi.nlm.nih.gov/books/NBK482255/.
18. Seymour CW, Liu VX, Iwashyna TJ, Brunkhorst FM, Rea TD, Scherag A, et al. Assessment of Clinical Criteria for Sepsis: For the Third International Consensus Definitions for Sepsis and Septic Shock (Sepsis-3). JAMA. 2016;315(8):762-74. [PMID: 26903335, PMCID: PMC5433435, https://doi.org/10.1001/jama.2016.0288].
19. Benjamin EJ, Virani SS, Callaway CW, Chamberlain AM, Chang AR, Cheng S, et al. Heart Disease and Stroke Statistics-2018 Update: A Report From the American Heart Association. Circulation. 2018;137(12):e67-e492. [PMID: 29386200, https://doi.org/10.1161/CIR.0000000000000558].
20. Dunlay SM, Chamberlain AM. Multimorbidity in Older Patients with Cardiovascular Disease. Curr Cardiovasc Risk Rep. 2016;10. [PMID: 27274775, PMCID: PMC4889124, https://doi.org/10.1007/s12170-016-0491-8].
21. Asim M, Amin F, El-Menyar A. Multiple organ dysfunction syndrome: Contemporary insights on the clinicopathological spectrum. Qatar Med J. 2020;2020(1):22. [PMID: 33628712, PMCID: PMC7884906, https://doi.org/10.5339/qmj.2020.22].
22. Basodan N, Al Mehmadi AE, Al Mehmadi AE, Aldawood SM, Hawsawi A, Fatini F, et al. Septic Shock: Management and Outcomes. Cureus. 2022;14(12):e32158. [PMID: 36601152, PMCID: PMC9807186, https://doi.org/10.7759/cureus.32158].
23. Fisher T, Hill N, Kalakoutas A, Lahlou A, Rathod K, Proudfoot A, et al. Sex differences in treatments and outcomes of patients with cardiogenic shock: a systematic review and epidemiological meta-analysis. Crit Care. 2024;28(1):192. [PMID: 38845019, PMCID: PMC11157877, https://doi.org/10.1186/s13054-024-04973-5].
24. Takla A, Mostafa MR, Eid MM, Abuelazm M, Hassan AR, Katamesh B, et al. Sex difference in outcomes and management of cardiogenic shock: A systematic review and meta-analysis. Curr Probl Cardiol. 2024;49(11):102777. [PMID: 39103132, https://doi.org/10.1016/j.cpcardiol.2024.102777].
25. Ya'qoub L, Lemor A, Dabbagh M, O'Neill W, Khandelwal A, Martinez SC, et al. Racial, Ethnic, and Sex Disparities in Patients With STEMI and Cardiogenic Shock. JACC Cardiovasc Interv. 2021;14(6):653-60. [PMID: 33736772, https://doi.org/10.1016/j.jcin.2021.01.003].
26. Zhao H, Yang B, Dai H, Li C, Ruan H, Li Y. Sex Differences in Sepsis-Related Acute Respiratory Distress Syndrome and Other Short-Term Outcomes among Critically Ill Patients with Sepsis: A Retrospective Study in China. Shock. 2025;63(5):733-42. [PMID: 39965585, PMCID:

PMC12039918, https://doi.org/10.1097/SHK.0000000000002555].
27. Hemida MF, Saghir M, Ibrahim AA, Ishtiaq S, Mohamed A, Faisal MR, et al. TCT-291 Cardiogenic Shock and Septicemia: National Trends in Co-Occurrence, Mortality, and Critical Care Outcomes in the U.S. (1999–2023). Jacc. 2025;86(17). [https://doi.org/10.1016/j.jacc.2025.09.390].
28. Melamed A, Sorvillo FJ. The burden of sepsis-associated mortality in the United States from 1999 to 2005: an analysis of multiple-cause-of-death data. Crit Care. 2009;13(1):R28. [PMID: 19250547, PMCID: PMC2688146, https://doi.org/10.1186/cc7733].
29. Oud L, Garza J. Trajectories of State-Level Sepsis-Related Mortality by Race and Ethnicity Group in the United States. J Clin Med. 2024;13(10). [PMID: 38792390, PMCID: PMC11122657, https://doi.org/10.3390/jcm13102848].
30. Morrissey R, Lee J, Baral N, Tauseef A, Sood A, Mirza M, et al. Demographic and regional trends of sepsis mortality in the United States, 1999-2022. BMC Infect Dis. 2025;25(1):504. [PMID: 40211200, PMCID: PMC11987265, https://doi.org/10.1186/s12879-025-10921-7].

ASIDE

ASIDE Cardiovascular

ASIDE CARDIOVASCULAR

Original Article

Ac-SDKP Maintains Coronary Microvascular Barrier Function and Prevents Radiation-induced Cardiac Injury

Sarmila Nepali[1], Badri Karthikeyan[1], Swati D Sonkawade[2], Supriya D Mahajan[2], Joseph Spernyak[3], Umesh C Sharma[3], Saraswati Pokharel[1,*]

1-Department of Pathology and Laboratory Medicine, Roswell Park Comprehensive Cancer Center, Buffalo, NY, USA
2-Department of Medicine, Jacob's School of Medicine and Biomedical Sciences, University at Buffalo, Buffalo, NY, USA
3-Translational Imaging Shared Resources, Roswell Park Comprehensive Cancer Center, Buffalo, NY, USA

ARTICLE INFO

Article history:
Received 26 Mar. 2026
Received in revised form 17 Apr. 2026
Accepted 21 Apr. 2026
Published 13 May 2026

Keywords:
Radiation
Cardiomyopathy
Ac-SDKP
Claudin-1
Endothelial dysfunction
Vascular permeability

ABSTRACT

Background: Radiation-induced cardiomyopathy is a significant late complication in cancer survivors treated with thoracic radiation, with few preventive options. Early injury is characterized by coronary microvascular endothelial dysfunction and increased vascular permeability. Claudin 1 (Cldn1), a tight junction protein in endothelial cells, plays a key role in maintaining vascular barrier integrity. This study investigated whether the endogenous tetrapeptide N acetyl Ser Asp Lys Pro (Ac SDKP) preserves cardiac microvascular barrier function and mitigates early radiation-associated cardiac injury in preclinical models.

Methods: Human coronary microvascular endothelial cells (HMVECs) were exposed to ionizing radiation (IR) with preventive Ac SDKP treatment. Endothelial barrier function was assessed using FITC dextran permeability and transendothelial electrical resistance (TEER). In vivo, mice received fractionated left thoracic irradiation (3 Gy/day, 5 days/week; total 45 Gy). Ac SDKP (3.2 mg/kg/day) was administered via a subcutaneous osmotic minipump, starting 1 day prior to irradiation and continuing throughout the study. Cardiac vascular leakage was measured by Evans blue extravasation at early and chronic time points, and left ventricular (LV) function was evaluated by cardiac MRI.

Results: IR decreased Cldn1 expression, increased endothelial permeability, and reduced TEER in HMVECs. Preventive Ac SDKP preserved Cldn1 expression and significantly reduced IR-induced permeability, although TEER recovery was partial. In mice, irradiation reduced cardiac Cldn1 levels, increased vascular leakage, and impaired LV function. Ac SDKP reduced early leakage and improved selected functional measures, with no significant effect on chronic permeability.

Conclusion: Preventive Ac SDKP attenuates radiation-related cardiac microvascular dysfunction and partially preserves cardiac function, likely through maintenance of endothelial barrier integrity and Cldn1 expression, suggesting potential vascular protective pathways.

1. Introduction

Thoracic radiation therapy (RT) is one of the major treatment modalities for various cancers, including breast, lung, and mediastinal malignancies [1]. However, incidental exposure of the heart to ionizing radiation (IR) is a well-established contributor to radiation-induced heart disease (RIHD), often presenting as delayed cardiovascular toxicity [2]. Clinical and experimental evidence suggests that microvascular injury is among the earliest events in the pathogenesis of RIHD. In particular, disruption of the coronary microvascular endothelial barrier often precedes myocardial inflammation, fibrosis, and contractile dysfunction [3].

The endothelial barrier is tightly regulated by intercellular junctional complexes, of which tight junctions (TJs) are essential components[4]. TJs are formed by transmembrane proteins, including occludins, junctional adhesion molecules, and claudins, which work collectively to restrict paracellular flux and maintain vascular homeostasis [5]. Among these, claudin-1 (Cldn1) is an important TJ protein implicated in barrier integrity by forming selective channels that regulate solute and ion permeability [6, 7]. While Cldn1 has been extensively characterized in epithelial tissues, its role in cardiac vasculature is less well understood. We recently demonstrated that claudin 1 (Cldn1) is enriched in coronary microvascular endothelial cells and that chest irradiation reduces its mRNA and protein expression [8]. However, those studies primarily focused on structural remodeling and myocardial blood flow. They did not address whether Cldn1 is a candidate pathway involved in radiation-induced vascular leakage, or whether restoring Cldn1 is associated with improved radiation-induced disruption of the cardiac vascular barrier. Increased vascular permeability can promote myocardial edema and tissue remodeling, ultimately contributing to ventricular dysfunction [9]. Identifying agents that preserve endothelial barrier integrity may therefore offer new strategies to prevent or mitigate radiation induced cardiac injury.

* Corresponding author: Saraswati Pokharel, Department of Pathology and Laboratory Medicine, Roswell Park Comprehensive Cancer Center, Buffalo, NY, USA. Email: saraswati.pokharel@roswellpark.org

Published and owned by PubPorta Publishing LLC. Academic oversight and scholarly guidance are provided by the American Society for Inclusion, Diversity, and Equity in Healthcare (ASIDE). ISSN (Print) 3069-9851, ISSN (Online) 3069-9843.

Citation: Nepali S, Karthikeyan B, D Sonkawade S, et al. Ac-SDKP maintains coronary microvascular barrier function and prevents radiation-induced cardiac injury. ASIDE Cardiovasc. 2026;1(2):9-18, doi:10.71079/ASIDE.CV.051326685

Consistent with this gap, our prior studies examining AcSDKP in radiation-induced cardiac injury focused predominantly on late myocardial remodeling outcomes, including fibrosis and coronary blood flow, without directly assessing early vascular barrier dysfunction or endothelial cell tight-junction integrity. Whether radiation disrupts cardiac vascular endothelial barrier functions early, and whether these early changes contribute to later cardiac injury, remains incompletely defined.

N-acetyl-Ser-Asp-Lys-Pro (Ac-SDKP) is an endogenous tetrapeptide generated through the enzymatic hydrolysis of its precursor, thymosin $\beta 4$ [10]. Although primarily synthesized in the bone marrow and mononuclear cells, Ac-SDKP has also been detected in various organs, including the heart, kidneys, and vasculature [11–13]. We have previously demonstrated that Ac-SDKP exerts potent anti-inflammatory and antifibrotic effects in preclinical models of cardiac fibrosis [14, 15]. In our most recent work, we identified additional protective actions of Ac-SDKP in reducing myocardial fibrosis and enhancing coronary blood flow following chest irradiation [16]. While Ac-SDKP has been shown to preserve endothelial function in multiple organ systems, its effects on endothelial barrier integrity, especially in the context of radiation-induced vascular injury, remain poorly understood.

In this study, we investigated whether radiation-induced down-regulation of Cldn1 is associated with impairment of the cardiac vascular endothelial barrier and whether Ac-SDKP can attenuate these changes. Using in vitro and in vivo models, we evaluated endothelial permeability, cardiac vascular leak, and cardiac function to determine whether preservation of barrier integrity is associated with Ac SDKP – mediated protection following thoracic irradiation.

Our findings indicate that Ac-SDKP could mitigate radiation-induced cardiac vascular injury while concurrently preserving Cldn1 expression.

2. Methods

2.1. Cell culture and irradiation

Human Cardiac Microvascular Endothelial Cells (HMVECs) (Lonza, CC-7030) were cultured in EGM-2MV medium (Lonza, CC-3156) supplemented with the EGM-2V BulletKit (Lonza, CC-3202) at 37°C in a humidified incubator with 5% CO_2. For irradiation experiments, HMVECs were seeded at 2×10^5 cells per well in 12-well insert plates (Corning, 3460) and incubated for 24 hours. The medium was then replaced, and a subgroup of cells was treated with Ac-SDKP (100 nM) for 4 hours prior to irradiation. Cells were subsequently exposed to 9 Gy of ionizing radiation using a specialized orthovoltage radiation chamber, as previously described [17]. Following irradiation, cells were returned to standard culture conditions for an additional 48-72 hours before additional assays.

2.2. In vitro permeability assay

Seventy-two hours after irradiation, HMVECs were subjected to a permeability assay using fluorescein isothiocyanate (FITC)-dextran (25 μg/mL; Sigma-Aldrich, NC0689651). FITC-dextran was added to each insert, and the plate was incubated in the dark at room temperature for 20 minutes. Following incubation, the inserts were removed, and 100 μL of media from each receiver well was transferred to a 96-well black opaque plate (Greiner Bio-One, 655076). Permeability was quantified by measuring fluorescence intensity at 485 nm excitation and 535 nm emission using a plate reader (Synergy H1, BioTek). Permeability assays were performed in at least three independent experiments, with a total of 10 - 19 sample wells analyzed per condition across all experiments. Replicate wells were averaged, and experiment-level means were used for statistical analysis.

2.3. Animal studies

The animal care and experimental protocols were carried out in accordance with the US National Institutes of Health guidelines and were approved by the Institutional Animal Care and Use Committees of the Roswell Park Comprehensive Cancer Center (Institutional Animal Care and Use Committee #1336M). Both male and female mice (6-7 weeks old) were used for in vivo studies. Mice were euthanized using CO_2 overexposure followed by cervical dislocation.

2.4. Mouse radiation therapy

Experimental mice were subjected to fractionated left chest irradiation at a dose of 3 Gy/day, five days per week, for a total of 45 Gy over three weeks. The X-ray beam was targeted to the left thorax using an orthovoltage irradiator equipped with a Thoreau's filter, as previously described [17]. A subset of mice was sacrificed at the end of the three-week radiation protocol for permeability assays. In contrast, a second subset was sacrificed 18-20 weeks after the start of radiation for long-term analysis. Additional age-matched radiation-unexposed mice were used as biological controls. Unilateral left thoracic irradiation was selected to approximate clinically relevant cardiac exposure during thoracic radiotherapy while limiting off-target organ injury and enabling long term survival.

2.5. Ac-SDKP therapy

Ac-SDKP therapy: Mice were treated with continuous subcutaneous infusion of Ac-SDKP (3.2 mg/kg/day) for 3 weeks (acute study) or 18-20 weeks (chronic study) using ALZET® Mini-Osmotic Pumps (infusion was started 24 h before radiation exposure). After the completion of the treatment protocol, animals were sacrificed (with CO_2 overexposure), and organs were harvested for additional histopathological and molecular analysis.

2.6. Study design

We used three experimental groups of sex- and age-matched mice (6-7 weeks) for both acute and chronic studies: (I) sham-irradiated control mice, (II) mice receiving thoracic irradiation alone, and (III) mice receiving thoracic irradiation with Ac-SDKP treatment. For the acute study, mice from each group were sacrificed at the early (3 weeks) post-irradiation time point (n = 7-9 per group). For the chronic study, separate cohorts were followed long term (18-20 weeks) and sacrificed at the chronic endpoint (n = 7-9 per group). All animal procedures were performed under anesthesia to minimize discomfort and were conducted in accordance with protocols approved by the Institutional Animal Care and Use Committee (IACUC). Euthanasia was performed in compliance with the guidelines of the Panel on Euthanasia of the American Veterinary Medical Association. All image-based analyses of cardiac imaging, histological, and immunohistochemical quantification were performed by investigators blinded to group allocation. No animals or samples were excluded from analysis unless pre-specified technical criteria were not met, and no post hoc exclusions were applied.

2.7. Cardiac magnetic resonance imaging (MRI) for the assessment of myocardial morphology and function

Between 18 and 20 weeks after IR, a subset of mice was anesthetized and maintained under 2 – 2.5% isoflurane throughout the imaging procedure. Body temperature and vital signs were continuously monitored and controlled using an MR-compatible gating and monitoring system (Model 1025, SA Instruments, Stony Brook, NY). Cardiac-gated steady-state free precession scans were obtained

in apical 2- and 4-chamber views using the following parameters: TE/TR = 2.0/4.0 ms, flip angle = 25°, field of view (FOV) = 4.0 × 2.8 cm, matrix size = 128 × 96, slice thickness = 1 mm, six averages, and 16 frames per cardiac cycle. Left ventricular (LV) volumes and function were analyzed using Segment software (version 3.0 R7732; http://segment.heiberg.se). LV endocardial and epicardial borders were delineated from the short-axis cine images acquired at the mid-papillary muscle level. LV diameters and volumes were estimated geometrically from these images, and volume-versus-time curves were generated across 16 frames to characterize systolic and diastolic phases.

To evaluate time-dependent changes in myocardial contractility, radial velocities were measured across six myocardial segments (anterior, anteroseptal, inferoseptal, inferior, inferolateral, and anterolateral), using the mid-septum as the reference for rotation. The velocity mapping algorithm was validated by comparison with prior Doppler echocardiography data assessing average systolic radial velocities in adult male rodents. Quantitative analysis of radial velocity (cm/s) was performed at peak systole (vS), the maximal point on individual segmental velocity curves, which reflects peak contractile force generation. Acceleration was calculated by taking the time derivative of the radial velocity. This imaging and analysis protocol has been previously validated and published [18].

2.8. In vivo cardiac vascular leakage (Miles' assay)

Miles' assay is based on the intravenous injection of Evans Blue, a dye with high affinity for albumin, in mouse models. Under physiological conditions, albumin does not cross the endothelial barrier, and Evans Blue-bound albumin is restricted within blood vessels. In pathologic conditions with increased vascular permeability, the endothelium becomes permeable to small proteins such as albumin, and albumin-bound Evans Blue will appear in the organs with increased permeability. The extent of vascular permeability can be quantified by measuring the dye incorporated into the tissue. Evans blue dye (0.5%; Sigma-Aldrich, E2129) was prepared in PBS, and each mouse was injected with 200 μL of the solution (1.04 mM) via the tail vein. Thirty minutes post-injection, mice were euthanized, and heart tissue was harvested. Each sample was incubated in 500 μL of formamide at 55 °C for 24 hours to extract the dye. Vascular permeability was quantified by measuring the optical density of the extracted dye at 610 nm, as previously described [19].

2.9. Quantitative real-time polymerase chain reaction (qPCR)

Total RNA was extracted using the Quick-RNA MiniPrep Plus Kit (Zymo Research, CA, USA) and quantified with a NanoDrop 1000 spectrophotometer (Thermo Fisher, MA, USA). One microgram of RNA was reverse transcribed into cDNA using the Verso cDNA Synthesis Kit (Thermo Fisher, MA, USA), following the manufacturer's protocol. qPCR was then performed using the SsoAdvanced™ Universal SYBR® Green Supermix (Bio-Rad, USA) on a CFX96 Real-Time PCR Detection System (Bio-Rad, CA, USA). The primer sequence used were Cldn1 Forward (5'-TGA GTT GAA TAC CCC AGG CA-3') and Reverse (5'-GAC ATC CAC AGT CCC TCG TA-3'), GAPDH, forward (5'-TCC TGT TCG ACA GTC AGC CGC A-3') and reverse (5'-GCG CCC AAT ACG ACC AAA TCC GT-3'); CD163, forward (5'- TGC CTC TGC TGT CAC TAA CG -3') and reverse (5'- TTC ATT CAT GCT CCA GCC GT -3'); CD68, forward (5'- TTC TCC AGC TGT TCA CCT TGA CCT -3') and reverse (5'- GTT GCA AGA GAA ACA TGG CCC GAA -3'); F4/80 forward (5'- CCT GGA CGA ATC CTG TGA AG -3') and reverse (5'- GGT GGG ACC ACA GAG AGT TG -3'); eNOS, forward (5'- GTG ATG GCG AAG CGA GTG AAG G -3') and reverse (5'- ACC ACC AGC ACC AGC GTC TC -3'). The thermal cycling conditions consisted of an initial denaturation at 95 °C, followed by 39 amplification cycles, and melt-curve analysis from 65 °C to 95 °C to confirm amplification specificity. Threshold cycle (Ct) values were obtained for each gene, and mRNA expression was quantified using the Ct method, normalized to GAPDH as the endogenous control. Relative expression levels were calculated and expressed relative to control samples.

2.10. Western blot

HMVECs were washed with PBS, and heart tissue was finely ground prior to lysis in RIPA buffer (Thermo Fisher, 89900) supplemented with protease (Thermo Fisher, PI87786) and phosphatase inhibitors (Thermo Fisher, PI78420). Lysates were centrifuged at 1,000 g for 10 minutes at 4 °C, and supernatants were collected for protein quantification using a BCA Protein Assay Kit (Thermo Fisher, 23227). Equal amounts of protein were resolved on 4 – 20% gradient SDS PAGE gels (Bio Rad, 4561094) and transferred to PVDF membranes (Thermo Fisher, 88520). Membranes were blocked with 5% BSA (Fisher Scientific, BP1600 100) for 1 hour at room temperature and incubated overnight at 4 °C with primary antibodies against Cldn1 (EPR9306, Abcam, ab180158). After washing, the membranes were incubated with HRP-conjugated secondary antibodies for 1 hour at room temperature. After detection of Cldn1, membranes were reprobed with GAPDH as a loading control (mouse monoclonal anti-GAPDH antibody; clone 6C5; Santa Cruz Biotechnology, sc 32233; 1:5000 dilution). Protein bands were visualized using enhanced chemiluminescence (Thermo Scientific, 32106) on a ChemiDoc™ Imaging System (Bio Rad). Band intensities were quantified using ImageJ software. Cldn1 protein levels were normalized to the corresponding GAPDH loading control within the same lane, and data are presented as relative expression compared with control samples.

2.11. Tissue morphometry

For hematoxylin and eosin (H&E) staining, 4 μm-thick sections from formalin-fixed, paraffin-embedded heart tissue were deparaffinized, rehydrated, stained with hematoxylin and eosin, dehydrated, and mounted. Images were acquired using a Leica Biosystem ScanScope® (Aperio Technologies, Vista, CA, USA) at 40x magnification and saved in TIFF format. Cardiomyocyte size and nuclear density were quantified using the ruler tool in ImageScope, specifically evaluating circular myocytes with centrally located nuclei. Masson's trichrome staining was performed using the Epredia™ Richard-Allan Scientific Masson Trichrome Kit (Epredia, 87109) according to the manufacturer's instructions. Slides were deparaffinized, rehydrated, and treated with Bouin's solution, and stained sequentially with Weigert's Iron Hematoxylin, Biebrich Scarlet-Acid Fuchsin, and Aniline Blue, then dehydrated and mounted. Collagen appeared blue, nuclei black, and myocardium red. Interstitial fibrosis was quantified using the Positive Pixel Count v9 algorithm in ImageScope, excluding perivascular regions using the negative pen tool. Trichrome staining was used to assess vascular and perivascular fibrosis in medium and small sized coronary vessels within the myocardium. Fibrosis quantification was performed using whole heart sections from each animal. Total vascular area and the area of positive fibrotic staining were measured using NIH ImageJ/Fiji software (National Institutes of Health, Bethesda, MD, USA). Coronary luminal size was determined using Fiji's measurement tools. Luminal area was initially measured in pixels² and converted to μm² using an adjusted conversion factor of 8.26 pixels²/μm². Because larger vessels exhibited proportionally greater fibrosis than smaller vessels, the fibrotic area was normalized to the corresponding luminal area.

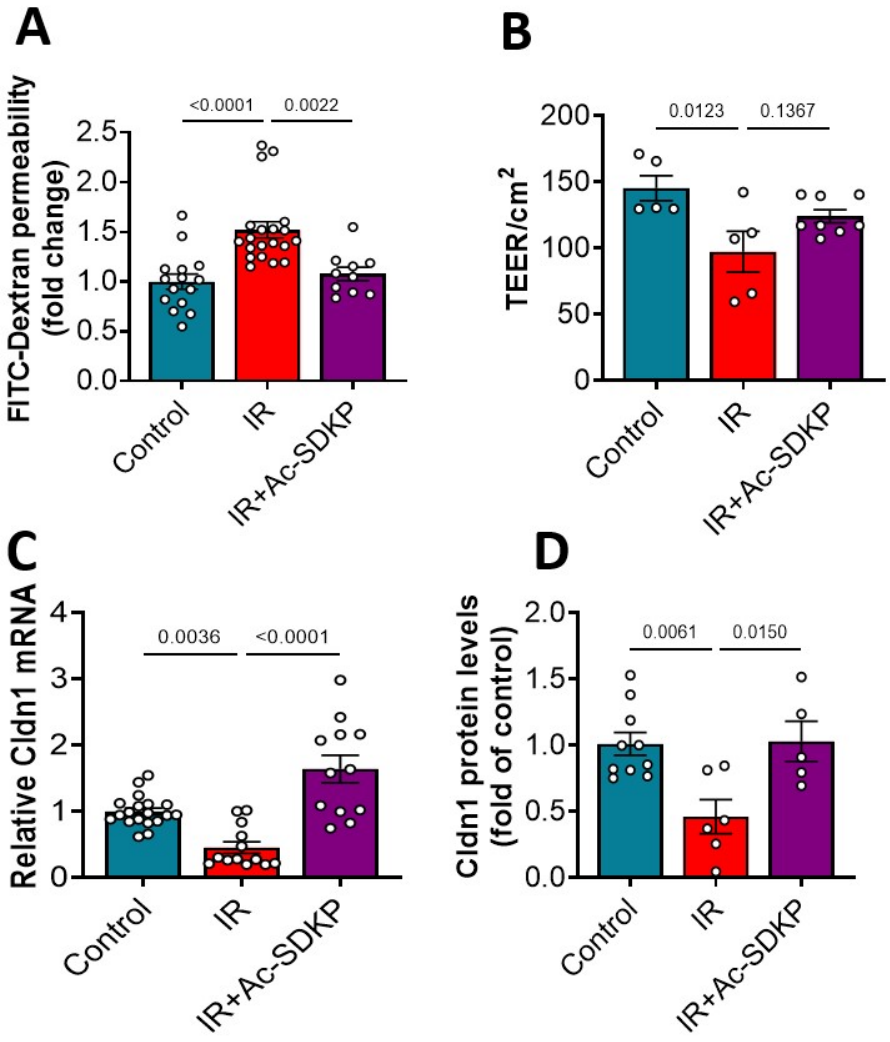

Figure 1: Effects of radiation and Ac-SDKP on coronary vascular endothelial cell (HMVEC) Cldn1 expression, vascular permeability, and endothelial barrier integrity. Radiation exposure (9 Gy) increased endothelial permeability, as measured by the FITC-dextran assay (A), and impaired endothelial barrier function, as indicated by a decrease in TEER (B). Similarly, radiation downregulated both mRNA (C) and protein levels (D) of Cldn1 in HMVECs. Ac-SDKP mitigated radiation-induced FITC-dextran permeability, but the effects on TEER were not statistically significant. All data are expressed as mean ± SEM, $n = 5–20$.

2.12. Transmission Electron Microscopy (TEM)

Ultrastructural analysis was performed using a Hitachi HT7800 High-Resolution 120 kV Transmission Electron Microscope. Heart tissues were fixed overnight at room temperature in 2% formaldehyde and 2% EM-grade glutaraldehyde (Electron Microscopy Sciences, Hatfield, PA, USA) in 0.1 M cacodylate buffer (pH 7.2). After fixation, samples were washed in cacodylate buffer (without aldehydes) and post-fixed in 1% osmium tetroxide in 0.1 M cacodylate buffer for 1 hour. Tissues were then washed and dehydrated through a graded ethanol series (30%, 50%, 70%, and 95% for 10 minutes each), followed by two changes in 100% ethanol. Ultrathin sections were obtained, and images were acquired by an observer blinded to the experimental group from blood vessels of comparable size across conditions to allow comparison of ultrastructural features.

2.13. Statistical analysis

Results are expressed as means ± SEM, and analysis was done using GraphPad Prism software (version 9.0, GraphPad Software, San Diego, California, USA). The study was not powered to detect sex specific differences, and preliminary analyses did not reveal qualitative differences between sexes. Therefore, data were pooled across sex to focus on the primary experimental effects. For radial velocity analysis, peak systolic velocity, acceleration, and deceleration values from the six myocardial segments were averaged per animal to generate a single representative value prior to group-level statistical comparison. Quantitative endpoints were summarized by group using the mean and standard error of mean (SEM). When appropriate, endpoints were analyzed using an unpaired t-test or one-way ANOVA, with treatment group (control, radiation alone, and radiation + Ac-SDKP) as a factor. When significant effects were detected, pairwise between-group comparisons were conducted using Tukey's multiple comparisons test, based on a single pooled variance from the ANOVA model. P-values <0.05 were considered significant.

3. Results

3.1. Ac-SDKP inhibits radiation-induced vascular permeability in HMVECs

Radiation significantly increased endothelial permeability in HMVECs, as measured by FITC-dextran assay. Irradiated cells exhibited a 52%

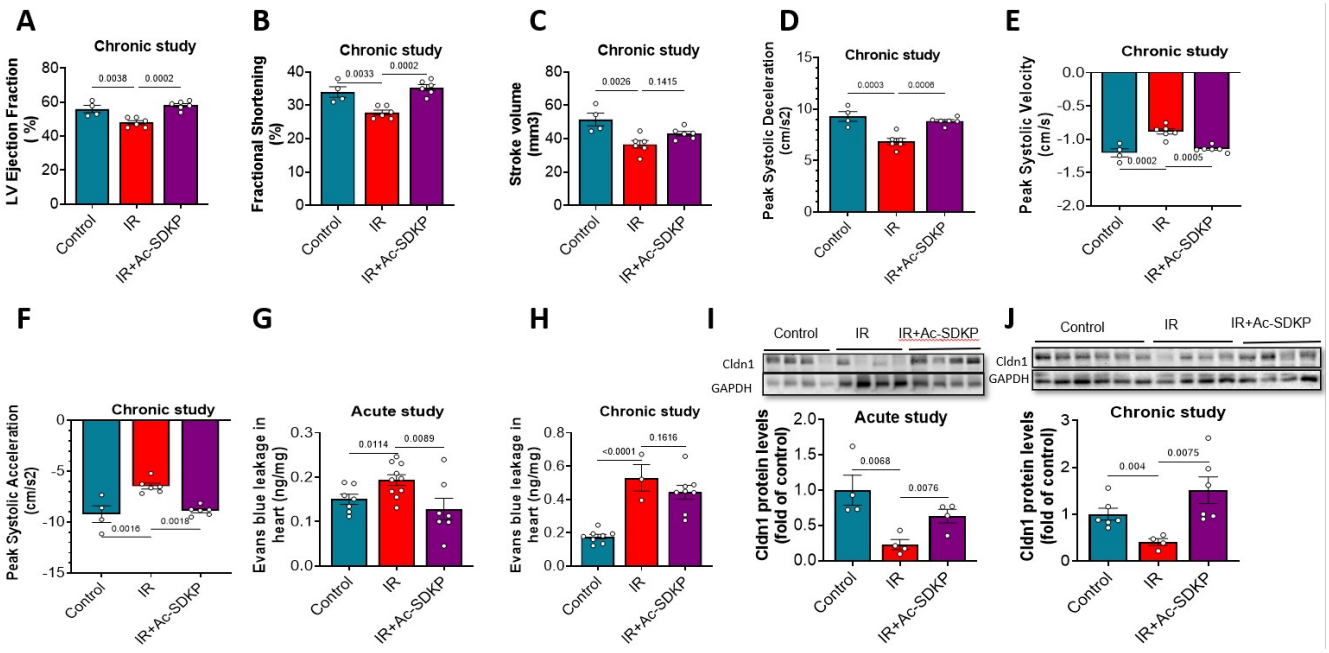

Figure 2: Effects of radiation and Ac-SDKP on cardiac function, cardiac vascular permeability, and Cldn1 levels. Radiation exposure (45 Gy, 15 fractions) impaired left ventricular ejection fraction (A), fractional shortening (B), stroke volume (C), peak systolic deceleration (D), peak systolic velocity (E), and peak systolic acceleration (F) in the chronic study model. Similarly, IR exposure increased Evans blue dye leakage (G, H) and decreased Cldn1 protein expression (I, J) in both acute and chronic models. These effects were mitigated by Ac-SDKP (3.2 mg/kg/day) in the acute setting, whereas the effect on cardiac vascular permeability was not statistically significant in the chronic setting. All data are expressed as mean ± SEM, $n = 3–9$.

rise in permeability compared to controls (fluorescence intensity-relative expression: control, 1.00 ± 0.029; IR, 1.52±0.37; p<0.0001, n=15-20). Ac-SDKP treatment normalized permeability levels (0.71 ± 0.14; p = 0.0022 vs. IR, n = 9), indicating its role in preserving endothelial barrier function and membrane integrity **(Fig. 1A)**.

3.2. Effects on endothelial cell barrier integrity

Transendothelial electric resistance (TEER) measurements were performed, with 5 - 8 wells analyzed per condition across all experiments. Radiation significantly impaired endothelial barrier function, as evidenced by decreased TEER. Forty-eight hours after 9 Gy irradiation, TEER was reduced by approximately 33% in HMVECs (control: 145.3 ±21.12 vs. IR: 97.2 ±34.47; p = 0.0123, n=5). Pre-treatment with Ac SDKP was associated with a tendency to increase TEER in irradiated cells; however, this change did not reach statistical significance (IR + Ac SDKP: 123.86 ± 13.85 vs. IR: 97.2 ± 34.47; p = 0.1367, n = 5-8). Data are shown in **(Fig. 1B)**.

3.3. Ac-SDKP inhibits radiation-induced downregulation of Cldn-1 in HMVECs

Radiation exposure (9 Gy) significantly downregulated both mRNA and protein levels of Cldn1 in HMVECs. Compared to the control, irradiated cells showed a reduction of 55% in Cldn1 mRNA expression (relative expression: control, 1.00 ± 0.23; IR, 0.45 ± 0.31; p = 0.0036, n= 13-19) and a decrease of 54% in Cldn1 protein levels (relative expression: control, 1.00 ± 0.27; IR, 0.46 ± 0.31; p = 0.0061 n= 6-10) **(Figure 1)**. Treatment with Ac-SDKP restored Cldn1 expression (mRNA: 3.61± 0.68; p < 0.0001 vs. IR, n=12; protein: 2.24± 0.74; p = 0.015 vs. IR, n=5), suggesting a protective effect on the tight junction protein, which could contribute to membrane integrity following radiation **(Figs. 1C and 1D)**.

3.4. Effects of Ac-SDKP on radiation-induced cardiac damage

Cardiac MRI performed 19 weeks post-radiation revealed significant functional impairment in irradiated mice. Ejection fraction was reduced in irradiated mice but improved with Ac-SDKP therapy (control: 56.12±4.25%; IR: 48.05±2.67%; IR + Ac-SDKP: 58.23±2.63%; p = 0.0038, n= 4-6) **(Fig. 2A)**. Similarly, fractional shortening was reduced in irradiated mice but improved with Ac-SDKP therapy (control: 34.00±2.74%; IR: 27.83±1.67%; IR + Ac-SDKP: 35.33±1.97%; p = 0.0033 control vs IR and p= 0.0002 IR vs IR + Ac-SDKP, n=4-6) **(Fig. 2B)**. Stroke volume was reduced in the IR group compared to controls (control: 51.56±7.67 mm3; IR: 36.62±5.54 mm3; p = 0.0026, n= 4-6). Ac-SDKP treatment did not significantly improve stroke volume after IR (IR + Ac-SDKP: 43.04±3.36 mm3; p = 0.14, n=6) **(Fig. 2C)**. Radial velocity analysis demonstrated significant reductions in peak systolic velocity, peak systolic acceleration, and peak systolic deceleration following IR, all of which were improved by Ac-SDKP (deceleration: control: 9.30± 0.93 cm/s2; IR: 6.88 ± 0.73; IR + Ac-SDKP: 8.84± 0.37; p = 0.0003 control vs. IR, and 0.0006 IR vs. IR+ Ac-SDKP; velocity: control: -1.20 ± 0.12 cm/s; IR: -0.88 ± 0.10; IR + Ac-SDKP: -1.15± 0.05; p = 0.0002 control vs. IR, and 0.0005 IR vs. IR+ Ac-SDKP; acceleration: control: -9.20±1.63 cm/s2; IR: -6.45± 0.70; IR + Ac-SDKP: -8.87± 0.47; p = 0.0016 control vs. IR, and 0.0018 IR vs. IR+ Ac-SDKP, n=4-6) **(Fig. 2D-F)**.

3.5. Effects of Ac-SDKP on radiation-induced cardiac vascular leakage and Cldn1 levels

Radiation exposure (acute study) led to increased cardiac vascular permeability, demonstrated by a 29% increase in Evans blue dye extravasation compared to controls (ng/mg tissue: control: 0.15± 0.03; IR: 0.19 ± 0.04; p = 0.0114, n=7-10), indicating endothelial barrier disruption after 3 weeks. Treatment with Ac-SDKP significantly reduced cardiac vascular leakage in irradiated mice, restoring

permeability levels closer to baseline (IR + Ac-SDKP: 0.13±0.06; p =0.0089 vs IR, n=7) **(Fig. 2G)**. At 19 weeks, cardiac vascular permeability remained significantly elevated in irradiated animals compared to controls (ng/mg tissue: control: 0.18 ± 0.04; IR: 0.53 ± 0.14; p < 0.0001, n=3-8). Ac SDKP – treated irradiated mice showed a minor decrease in permeability compared to irradiated mice alone; however, this difference was not statistically significant (IR + Ac SDKP: 0.44 ± 0.12; IR vs. IR + Ac SDKP, p = 0.1616, n=8) **(Fig. 2H)**.

Radiation exposure significantly reduced cardiac Cldn1 expression in mice compared with non-irradiated controls at 3 weeks post-irradiation. Treatment with Ac-SDKP restored Cldn1 protein levels in irradiated animals (relative expression in densitometric units: control: 1.00 ± 0.42; IR: 0.23± 0.14; IR + Ac-SDKP: 0.63±0.19; p = 0.0068 control vs IR, p=0.0076 IR vs IR+ Ac-SDKP, n=4 each group) **(Fig. 2I)**. These effects of radiation and Ac-SDKP on Cldn1 protein levels persisted for 19 weeks after IR (relative expression in densitometric units: control: 1.00 ± 0.31; IR: 0.41± 0.14; IR + Ac-SDKP: 1.51±0.69; p = 0.004 control vs IR, p=0.0075 IR vs IR+ Ac-SDKP, n= 4-6) **(Fig. 2J)**.

3.6. Effects of IR and Ac-SDKP on fibroinflammatory response

To assess the impact of radiation and Ac-SDKP on macrophage-associated gene expression, we analyzed mRNA levels of CD68, F4/80, and CD163 in cardiac tissue at 3- and 19-weeks post-radiation.

At 3 weeks (acute phase), IR significantly increased CD163 expression compared to control (CD163: control, 1.00 ± 0.36; IR, 2.25 ± 1.27; p = 0.0035, n=4 per group), while CD68 (control, 1.00 ± 0.25; IR, 0.88 ± 0.07; p=NS, n=4 per group) and F4/80 (control, 1.00 ± 0.19; IR, 1.28 ± 0.37; p=NS, n=4 per group) levels remained unchanged. Treatment with Ac-SDKP significantly attenuated IR-induced CD163 expression (IR + Ac-SDKP, 0.26± 0.08; p = 0.0002 vs. IR, n=4 per group), with no significant effect on CD68 or F4/80 **(Fig. 3A)**. At 19 weeks (chronic phase), CD163 expression was significantly reduced in irradiated hearts compared to controls (CD163: control, 1.00 ± 0.19; IR, 0.07 ± 0.04; p = 0.0003, n=4-6), while F4/80 expression was increased (control, 1.00 ± 0.27; IR, 2.27 ± 0.82; p<0.0001, n=4-6). CD68 expression remained unchanged (control, 1.00 ± 0.21; IR, 1.22 ± 0.82; p = NS, n=4-6). Ac-SDKP did not alter CD163 levels (IR + Ac-SDKP, 1.31 ± 0.27; p = NS vs. IR, n=5) and CD68 mRNA levels (IR + Ac-SDKP, 0.97± 0.13; p = NS vs. IR, n=4), but significantly reduced F4/80 expression induced by radiation (IR + Ac-SDKP, 0.63 ± 0.20; p = 0.0016 vs. IR, n=5) **(Fig. 3B)**.

Additionally, after 3 weeks, IR decreased eNOS mRNA expression (control, 1.00 ± 0.23; IR, 0.74 ± 13; p = 0.0477), n=4 per group, while Ac-SDKP modestly increased eNOS levels, though not significantly (IR + Ac-SDKP, 1.29 ± 0.33; p = 0.08 vs. IR, n=4) **(Fig. 3C)**. As with the acute study, IR significantly suppressed eNOS expression (control, 1.00 ± 0.16; IR, 0.70 ± 0.08; p = 0.00380 n=4-6), and Ac-SDKP restored eNOS levels to near control values (IR + Ac-SDKP, 1.35 ± 0.28; p = 0.027, n=5) in chronic studies (19 weeks) **(Fig. 3D)**.

Radiation-induced fibrotic remodeling, however, was not evident either at 3 or 19 weeks as assessed by interstitial collagen deposition (interstitial collagen volume fraction at 3 weeks, fold of control: control: 1.00 ± 0.18; IR: 1.05± 0.07; IR + Ac-SDKP: 1.03± 0.31; p = NS, n=5-9; collagen volume fraction at 19-weeks post IR, fold of control: control: 1.00 ± 0.22; IR: 1.11± 0.20; IR + Ac-SDKP: 1.09± 0.27; p =NS, n=5-8) **(Fig. 3E-F)**, Similarly, Ac-SDKP treatment did not alter interstitial and perivascular fibrotic changes (relative % area stained at 19-weeks post IR: control: 1.00 ± 0.20; IR: 1.19±0.16; IR + Ac-SDKP: 1.35± 0.35; p =NS, n=5-9) **(Fig. 3G-H)**. Similarly, there was no significant difference in cardiomyocyte size or nuclear density across groups. Results are shown in **(Fig. 3I-K)**.

3.7. Electron microscopic findings

Electron microscopy revealed distinct ultrastructural changes in the coronary microvascular endothelium following radiation exposure and peptide treatment. In control hearts, endothelial cells displayed an intact and continuous basement membrane with well-apposed nuclei, indicating normal vascular ultrastructure. In contrast, hearts from irradiated mice showed marked endothelial damage, including nuclear dropout, and reduced basement membrane density, indicative of radiation-induced vascular injury. Notably, treatment with Ac-SDKP following irradiation preserved endothelial integrity. Endothelial nuclei remained visible, and the basement membrane exhibited increased density compared to irradiated hearts without treatment, suggesting a protective effect of the peptide against radiation-induced microvascular damage **(Figure 4)**. These observations, however, are descriptive in nature and reflect qualitative comparisons rather than quantitative morphometric assessment.

4. Discussion

Coronary vasculopathy is a well-known and serious complication of radiotherapy involving the thoracic region. While most prior research has examined post-radiation coronary artery atherosclerosis, the current study focuses on the coronary microvascular endothelial barrier dysfunction, with particular attention to the tight junction (TJ) protein Cldn1. This study identifies vascular barrier disruption as an early feature of radiation injury, and examines the association between Ac SDKP treatment, endothelial barrier-associated protein Cldn1, and functional outcomes. Using a combination of in vitro and in vivo experiments, we show that radiation exposure significantly disrupts endothelial tight junctions, impairs barrier function, and has partial, time-dependent downstream effects on cardiac function. Several of these radiation-associated changes were attenuated in the presence of Ac SDKP, although not uniformly across all endpoints.

Radiation-induced endothelial dysfunction is a well-recognized contributor to delayed cardiovascular complications after thoracic irradiation. Radiation injury leads to impaired endothelial functions such as reduced vasodilation, diminished capillary formation, and increased permeability [20, 21]. Previous studies have shown that ionizing radiation negatively affects endothelial cell integrity, which is expected given that endothelial cells are among the most radiosensitive cell types [22]. Endothelial cell paracellular permeability depends on tight junction (TJ) proteins, primarily the claudin and occludin families, as well as intracellular partners like JAM-2 and ZO-1, to maintain vessel wall integrity. Among these, Cldn1 plays a key role in maintaining the tight seal between endothelial cells, thereby preventing paracellular permeability [23]. Disruption or altered expression of Cldn1 in response to radiation can compromise endothelial barrier function and contribute to vascular dysfunction.

Our findings align with prior reports demonstrating that radiation disrupts epithelial cell tight junction proteins such as claudins, occludins, and ZO-1, leading to increased cell permeability and tissue injury[24]. We have previously noted that Cldn1 is expressed in coronary vascular endothelial cells and plays an important role in maintaining coronary vascular barrier integrity [8]. In the present study, Cldn1 expression was markedly reduced at both the mRNA and protein levels following radiation in human microvascular endothelial cells (HMVECs). Functionally, this was associated with increased paracellular permeability and reduced transendothelial electrical resistance (TEER), a marker of compromised endothelial

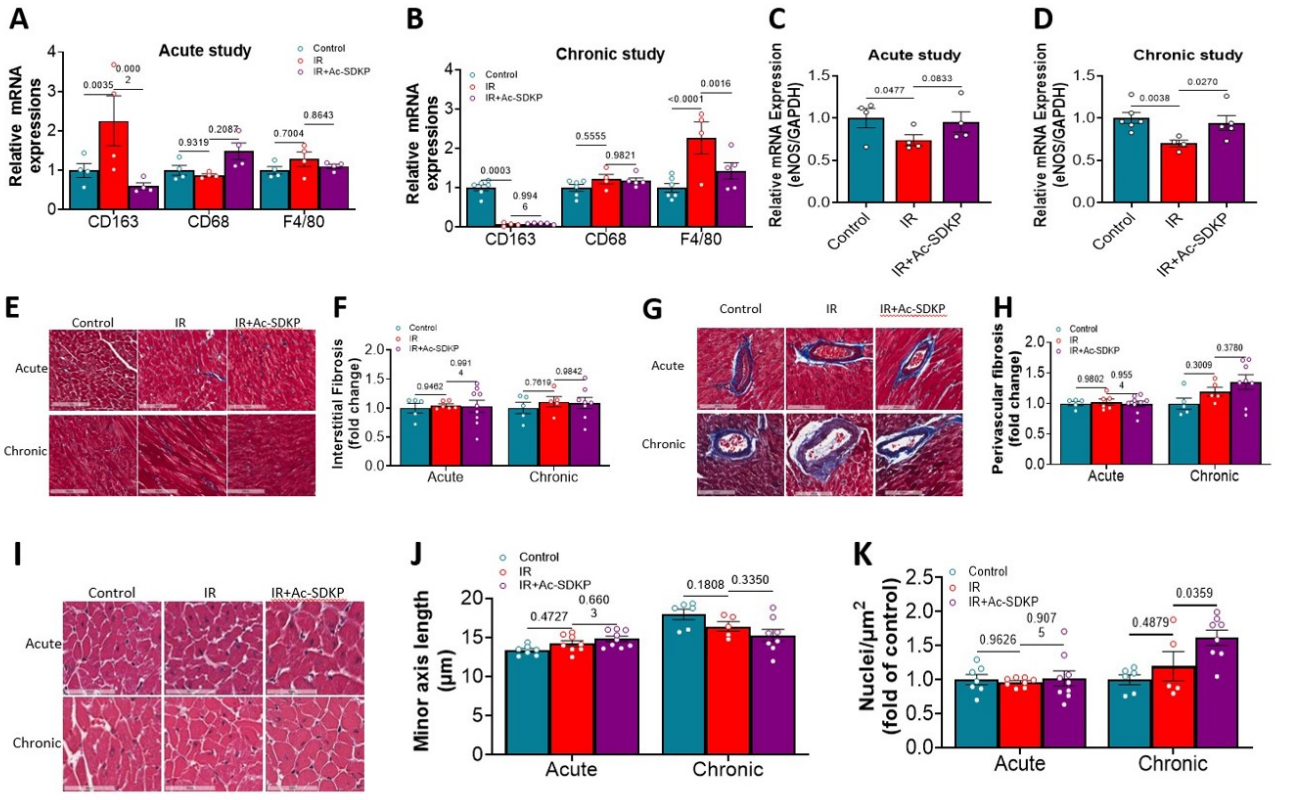

Figure 3: Effects of radiation and Ac-SDKP on fibroinflammatory response. Effects of radiation and Ac-SDKP on macrophage-associated inflammatory markers (CD163, CD68, and F4/80) in acute (A) and chronic (B) study models. mRNA expression of eNOS is shown for acute (C) and chronic (D) models. Representative trichrome-stained myocardial sections and quantification of interstitial (E–F) and perivascular (G–H) collagen are presented for both studies. Representative hematoxylin and eosin (H&E)–stained myocardial sections (I) illustrate cardiomyocyte morphology, with no significant differences observed in cardiomyocyte size (J) or nuclear density (K) among groups. All data are expressed as mean ± SEM, $n = 4–9$.

barrier integrity. Notably, treatment with Ac-SDKP restored Cldn1 levels and normalized endothelial permeability, suggesting that Ac-SDKP may protect tight junctions and membrane integrity after radiation injury. It should, however, be emphasized that Ac SDKP treatment was associated with higher Cldn1 expression and decreased endothelial cell permeability (in HMVECs); the recovery of TEER did not reach statistical significance, underscoring the partial nature of this effect. Since we did not use a genetic loss-of-function or gain-of-function model, Cldn1 preservation in this context should be interpreted as a parallel observation that reflects barrier status, rather than as direct evidence of a mechanistic pathway.

In vivo, irradiated mice exhibited increased coronary vascular permeability, sustained reductions in Cldn1 protein levels, and impaired cardiac function, as measured by ejection fraction, fractional shortening, and radial strain. Ac SDKP treatment was associated with improved early permeability measures and selected MRI parameters; however, chronic permeability reduction did not reach statistical significance. These findings are consistent with our prior studies implicating endothelial damage and microvascular rarefaction in the pathogenesis of radiation-induced cardiomyopathy [16] while also highlighting that the degree of protection observed here is incomplete and time-dependent.

Previous studies using electron microscopy have demonstrated that radiation induces profound ultrastructural changes in cardiac microvascular endothelium. In rabbit models exposed to 10 – 13 Gy, investigators reported increased pinocytic vesicle transport across endothelial cells along intercellular junctional gaps and disruption of endothelial sheets, as evidenced by leakage of carbon particles [25, 26]. Additionally, elevated endothelial phagocytic activity, including erythrophagocytosis, was observed in a dose-dependent manner [27]. These findings provided early evidence that radiation impairs both intracellular trafficking and intercellular connectivity, contributing to increased vascular permeability. Consistent with these reports, our electron microscopy analysis revealed hallmark features of radiation-induced endothelial injury in the heart, including nuclear dropout, thinning and rarefaction of basement membranes, and focal loss of basement membrane continuity. In AcSDKP – treated irradiated hearts, ultrastructural features appeared qualitatively less severe, with preserved endothelial nuclei and a continuous basement membrane. However, these observations are descriptive in nature, based on blinded image acquisition from vessels of comparable size, and were not supported by morphometric quantification. Therefore, TEM findings are presented as supportive evidence rather than definitive mechanistic proof.

The protective role of Ac-SDKP in radiation-induced cardiovascular injury is supported by prior studies demonstrating its antifibrotic, anti-inflammatory, and endothelial-protective properties in various models of cardiac injury [14, 15, 28, 29]. Mechanistically, Ac-SDKP is known to enhance endothelial nitric oxide synthase (eNOS) activity, inhibit TGF-β signaling, and reduce reactive oxygen species, all of which may contribute to its effects observed here [13, 17, 30].

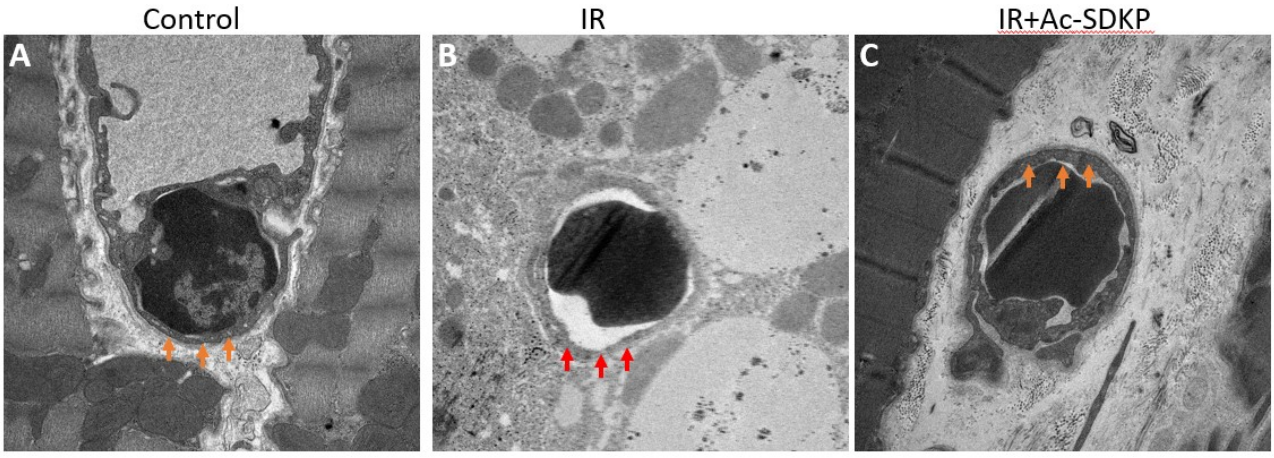

Figure 4: Effects of radiation and Ac-SDKP on the myocardial coronary vasculature examined by transmission electron microscopy (acute study). Representative images from control, IR, and IR + Ac-SDKP–treated mouse hearts show coronary vasculature with radiation-induced endothelial injury characterized by nuclear dropout and reduced basement membrane density. Treatment with Ac-SDKP mitigated these changes. Denser basement membranes are indicated by orange arrows, and paler basement membranes by red arrows.

In the present study, molecular markers such as eNOS and selected inflammatory transcripts, including CD163 and F4/80, increased with radiation exposure and decreased with AcSDKP treatment, suggesting an anti-inflammatory response; however, these data do not establish immune cell infiltration or phenotype at the tissue level.

Interestingly, despite the evidence of vascular injury, we did not observe significant interstitial or perivascular fibrosis at either 3 or 19 weeks, nor changes in cardiomyocyte size or nuclear density. This suggests that the injury phenotype captured here represents a vascular dominant and pre fibrotic stage of radiation-induced cardiac injury. Unlike the rat model, in which interstitial fibrosis is prominent at 18 weeks after IR [17], the mouse model appears more resistant to fibrosis. This temporal pattern is consistent with prior reports indicating that overt radiation-induced fibrosis in mice typically emerges at later time points, often beyond 24 weeks post-irradiation [31]. The absence of fibrosis in this study, therefore, likely reflects the examined time frame rather than inconsistency with established models. Furthermore, cardiomyocyte hypertrophy and nuclear density were unchanged across groups, suggesting that early cardiac dysfunction in this context is driven primarily by vascular mechanisms rather than myocyte remodeling. These findings align with earlier reports indicating minimal effects on cardiomyocyte size or BNP expression after radiation injury in some animal models [32].

Several limitations should be acknowledged. This study was preventive in design and did not evaluate Ac SDKP as a therapeutic intervention after established injury, nor did it include a dose-response analysis or an Ac SDKP-only control arm. Although associations between Cldn1 expression, vascular permeability, and functional outcomes were observed, no targeted mechanistic interventions were performed to establish causality. Because radiation was delivered unilaterally while outcomes were assessed at the whole heart level, regional effects may be diluted in global analyses. Accordingly, the findings reflect integrated whole heart consequences of localized radiation exposure rather than spatially resolved regional pathology. Whole-heart lysates and permeability assays were used to limit endothelial specificity, and permeability was assessed using Evans blue uptake as a surrogate for coronary leakage. LV volumes and ejection fraction were derived from a single mid-ventricular short-axis cine acquisition rather than a contiguous short-axis stack with disk summation. This approach is appropriate given the absence of regional wall-motion abnormalities in this model, but it is a limitation; future studies should incorporate whole-LV volumetry. Ultrastructural analyses were qualitative, and inflammatory assessments relied on bulk gene expression rather than cell level validation. Collectively, these constraints limit mechanistic inference and translational extrapolation.

5. Conclusions

In summary, this study identifies disruption of the cardiac vascular barrier as an early feature of radiation-associated cardiac injury and demonstrates that preventive Ac-SDKP administration reduces cardiac vascular leakage and partially preserves cardiac function in experimental models. Changes in Cldn1 expression closely paralleled alterations in vascular permeability, supporting its utility as a marker of endothelial barrier status. However, because direct genetic or pharmacologic manipulation of Cldn1 was not performed, these observations should be interpreted as correlative rather than causal. Accordingly, Cldn1 is best considered a candidate pathway associated with barrier regulation in this context. Future studies incorporating targeted mechanistic interventions and endothelial specific analyses will be required to define causal relationships and assess translational relevance.

Conflicts of Interest

The authors declare no competing interests that could have influenced the objectivity or outcome of this research.

Funding Source

Roswell Park and the National Cancer Institute supported this research under award number P30CA016056. S.P. is supported by a grant from NIH/NHLBI (Grant No. R01HL150266). U.C.S is supported by a grant from NIH/NHLBI (Grant R01HL152090).

Acknowledgments

None.

Institutional Review Board (IRB)

All animal experiments were approved by the Institutional Animal Care and Use Committee (IACUC) of Roswell Park Comprehensive Cancer Center and conducted in accordance with institutional guidelines.

Large Language Model

During the preparation of this work, the author(s) used ChatGPT to edit the language. After using this tool/service, the author(s) reviewed and edited the content as needed and take full responsibility for the content of the publication.

Author Contributions

SN contributed to methodology, validation, formal analyses, investigation, and writing the original draft, SDS participated in methodology and investigation, BK contributed to analyses of imaging data, JS provided image acquisition and resources, SDM was responsible for in vitro experimental resources, review, and editing, UCS contributed to conceptualization, review, and editing, SP led conceptualization, funding acquisition, supervision, and review and editing.

Data Availability

Raw data generated and included in this article are available upon reasonable request.

References

1. Miller KD, Siegel RL, Lin CC, Mariotto AB, Kramer JL, Rowland JH, et al. Cancer treatment and survivorship statistics, 2016. CA Cancer J Clin. 2016;66(4):271-89. [PMID: 27253694, https://doi.org/10.3322/caac.21349].
2. Aronow H, Kim M, Rubenfire M. Silent ischemic cardiomyopathy and left coronary ostial stenosis secondary to radiation therapy. Clin Cardiol. 1996;19(3):260-2. [PMID: 8674269, https://doi.org/10.1002/clc.4960190325].
3. Abe JI, Allen BG, Beyer AM, Lewandowski D, Mapuskar KA, Subramanian V, et al. Radiation-Induced Macrovessel/Microvessel Disease. Arterioscler Thromb Vasc Biol. 2024;44(12):2407-15. [PMID: 39445428, PMCID: PMC11842029, https://doi.org/10.1161/ATVBAHA.124.319866].
4. Komarova YA, Kruse K, Mehta D, Malik AB. Protein Interactions at Endothelial Junctions and Signaling Mechanisms Regulating Endothelial Permeability. Circ Res. 2017;120(1):179-206. [PMID: 28057793, PMCID: PMC5225667, https://doi.org/10.1161/CIRCRESAHA.116.306534].
5. Lee WL, Slutsky AS. Sepsis and endothelial permeability. N Engl J Med. 2010;363(7):689-91. [PMID: 20818861, https://doi.org/10.1056/NEJMcibr1007320].
6. Furuse M, Hata M, Furuse K, Yoshida Y, Haratake A, Sugitani Y, et al. Claudin-based tight junctions are crucial for the mammalian epidermal barrier: a lesson from claudin-1-deficient mice. J Cell Biol. 2002;156(6):1099-111. [PMID: 11889141, PMCID: PMC2173463, https://doi.org/10.1083/jcb.200110122].
7. Xia Y, Cao H, Zheng J, Chen L. Claudin-1 Mediated Tight Junction Dysfunction as a Contributor to Atopic March. Front Immunol. 2022;13:927465. [PMID: 35844593, PMCID: PMC9277052, https://doi.org/10.3389/fimmu.2022.927465].
8. Nepali S, Chen M, Karthikeyan B, Sonkawade SD, Mahajan SD, Spernyak J, et al. Claudin 1 dysregulation disrupts coronary microvascular integrity and impairs cardiac function. Atherosclerosis. 2025;403:119149. [PMID: 40068507, PMCID: PMC12070307, https://doi.org/10.1016/j.atherosclerosis.2025.119149].
9. Vasques-Novoa F, Angelico-Goncalves A, Alvarenga JMG, Nobrega J, Cerqueira RJ, Mancio J, et al. Myocardial oedema: pathophysiological basis and implications for the failing heart. ESC Heart Fail. 2022;9(2):958-76. [PMID: 35150087, PMCID: PMC8934951, https://doi.org/10.1002/ehf2.13775].
10. Cavasin MA, Rhaleb NE, Yang XP, Carretero OA. Prolyl oligopeptidase is involved in release of the antifibrotic peptide Ac-SDKP. Hypertension. 2004;43(5):1140-5. [PMID: 15037553, PMCID: PMC4677773, https://doi.org/10.1161/01.HYP.0000126172.01673.84].
11. Azizi M, Ezan E, Nicolet L, Grognet JM, Menard J. High plasma level of N-acetyl-seryl-aspartyl-lysyl-proline: a new marker of chronic angiotensin-converting enzyme inhibition. Hypertension. 1997;30(5):1015-9. [PMID: 9369248, https://doi.org/10.1161/01.hyp.30.5.1015].
12. Lenfant M, Wdzieczak-Bakala J, Guittet E, Prome JC, Sotty D, Frindel E. Inhibitor of hematopoietic pluripotent stem cell proliferation: purification and determination of its structure. Proc Natl Acad Sci U S A. 1989;86(3):779-82. [PMID: 2915977, PMCID: PMC286560, https://doi.org/10.1073/pnas.86.3.779].
13. Sonkawade SD, Xu S, Kim M, Nepali S, Karambizi VG, Sexton S, et al. Phospholipid Encapsulation of an Anti-Fibrotic Endopeptide to Enhance Cellular Uptake and Myocardial Retention. Cells. 2023;12(12). [PMID: 37371059, PMCID: PMC10296995, https://doi.org/10.3390/cells12121589].
14. Peng H, Carretero OA, Vuljaj N, Liao TD, Motivala A, Peterson EL, et al. Angiotensin-converting enzyme inhibitors: a new mechanism of action. Circulation. 2005;112(16):2436-45. [PMID: 16216963, PMCID: PMC6824430, https://doi.org/10.1161/CIRCULATIONAHA.104.528695].
15. Pokharel S, van Geel PP, Sharma UC, Cleutjens JP, Bohnemeier H, Tian XL, et al. Increased myocardial collagen content in transgenic rats overexpressing cardiac angiotensin-converting enzyme is related to enhanced breakdown of N-acetyl-Ser-Asp-Lys-Pro and increased phosphorylation of Smad2/3. Circulation. 2004;110(19):3129-35. [PMID: 15520311, https://doi.org/10.1161/01.CIR.0000147180.87553.79].
16. Sharma UC, Sonkawade SD, Baird A, Chen M, Xu S, Sexton S, et al. Effects of a novel peptide Ac-SDKP in radiation-induced coronary endothelial damage and resting myocardial blood flow. Cardiooncology. 2018;4. [PMID: 31057947, PMCID: PMC6497419, https://doi.org/10.1186/s40959-018-0034-1].
17. Sharma UC, Sonkawade SD, Spernyak JA, Sexton S, Nguyen J, Dahal S, et al. A Small Peptide Ac-SDKP Inhibits Radiation-Induced Cardiomyopathy. Circ Heart Fail. 2018;11(8):e004867. [PMID: 30354563, PMCID: PMC6205206, https://doi.org/10.1161/CIRCHEARTFAILURE.117.004867].
18. Karthikeyan B, Sonkawade SD, Pokharel S, Preda M, Schweser F, Zivadinov R, et al. Tagged cine magnetic resonance imaging to quantify regional mechanical changes after acute myocardial infarction. Magn Reson Imaging. 2020;66:208-18. [PMID: 31668928, PMCID: PMC7031039, https://doi.org/10.1016/j.mri.2019.09.010].
19. Radu M, Chernoff J. An in vivo assay to test blood vessel permeability. J Vis Exp. 2013;(73):e50062. [PMID: 23524912, PMCID: PMC3639515, https://doi.org/10.3791/50062].
20. Beckman JA, Thakore A, Kalinowski BH, Harris JR, Creager MA. Radiation therapy impairs endothelium-dependent vasodilation in humans. J Am Coll Cardiol. 2001;37(3):761-5. [PMID: 11693749, https://doi.org/10.1016/s0735-1097(00)01190-6].
21. Suvorava T, Luksha LS, Lobanok LM. The effects of acute and chronic radiation on endothelium- and no-dependent vascular reactivity. Cell Mol Biol (Noisy-le-grand). 2005;51(3):321-7. [PMID: 16191400].
22. Reinhold HS, Buisman GH. Radiosensitivity of capillary endothelium. Br J Radiol. 1973;46(541):54-7. [PMID: 4683331, https://doi.org/10.1259/0007-1285-46-541-54].
23. Gunzel D, Fromm M. Claudins and other tight junction proteins. Compr Physiol. 2012;2(3):1819-52. [PMID: 23723025,

https://doi.org/10.1002/cphy.c110045].

24. Shukla PK, Gangwar R, Manda B, Meena AS, Yadav N, Szabo E, et al. Rapid disruption of intestinal epithelial tight junction and barrier dysfunction by ionizing radiation in mouse colon in vivo: protection by N-acetyl-l-cysteine. Am J Physiol Gastrointest Liver Physiol. 2016;310(9):G705-15. [PMID: 26822914, PMCID: PMC4867328, https://doi.org/10.1152/ajpgi.00314.2015].
25. Khan MY, Ohanian M. Radiation-Induced Cardiomyopathy: II. An Electron Microscopic Study of Myocardial Microvasculature. Am J Pathol. 1974;74(1):125-36. [PMID: 19971051, PMCID: PMC1910718].
26. Bouten RM, Young EF, Selwyn R, Iacono D, Rittase WB, Day RM. Effects of radiation on endothelial barrier and vascular integrity. Tissue Barriers in Disease, Injury and Regeneration. 2021:43–94.
27. Bari WA, Sorenson GD. Ultrastructural Alterations in X-Irradiated Spleen. Pathol Microbiol (Basel). 1964;27:257-75. [PMID: 14132879, https://doi.org/10.1159/000161473].
28. Peng H, Xu J, Yang XP, Kassem KM, Rhaleb IA, Peterson E, et al. N-acetyl-seryl-aspartyl-lysyl-proline treatment protects heart against excessive myocardial injury and heart failure in mice. Can J Physiol Pharmacol. 2019;97(8):753-65. [PMID: 30998852, PMCID: PMC6824427, https://doi.org/10.1139/cjpp-2019-0047].
29. Sharma U, Rhaleb NE, Pokharel S, Harding P, Rasoul S, Peng H, et al. Novel anti-inflammatory mechanisms of N-Acetyl-Ser-Asp-Lys-Pro in hypertension-induced target organ damage. Am J Physiol Heart Circ Physiol. 2008;294(3):H1226-32. [PMID: 18178715, PMCID: PMC6824420, https://doi.org/10.1152/ajpheart.00305.2007].
30. Pokharel S, Rasoul S, Roks AJ, van Leeuwen RE, van Luyn MJ, Deelman LE, et al. N-acetyl-Ser-Asp-Lys-Pro inhibits phosphorylation of Smad2 in cardiac fibroblasts. Hypertension. 2002;40(2):155-61. [PMID: 12154106, https://doi.org/10.1161/01.hyp.0000025880.56816.fa].
31. Dreyfuss AD, Goia D, Shoniyozov K, Shewale SV, Velalopoulou A, Mazzoni S, et al. A Novel Mouse Model of Radiation-Induced Cardiac Injury Reveals Biological and Radiological Biomarkers of Cardiac Dysfunction with Potential Clinical Relevance. Clin Cancer Res. 2021;27(8):2266-76. [PMID: 33542079, PMCID: PMC9215266, https://doi.org/10.1158/1078-0432.CCR-20-3882].
32. Tokatli F, Uzal C, Doganay L, Kocak Z, Kaya M, Ture M, et al. The potential cardioprotective effects of amifostine in irradiated rats. Int J Radiat Oncol Biol Phys. 2004;58(4):1228-34. [PMID: 15001267, https://doi.org/10.1016/j.ijrobp.2003.09.071].

ASIDE

ASIDE Cardiovascular

ASIDE CARDIOVASCULAR

Case Report

Acute Decompensated Heart Failure with Severe Left Ventricular Systolic Dysfunction of Undetermined Etiology in a 26-Year-Old Male: A Case Report

Abdul Eizad Asif[1], Ahmad Mustafa Butt[2], Syed Tahir Hussain[3], Aqsa Ibrahim[2], Muhammad Hassaan Javaid[4,*]

1-Shalamar Medical and Dental College, Lahore, Pakistan
2-Central Park Medical College, Lahore, Pakistan
3-Central Park Teaching Hospital, Lahore, Pakistan
4-Shifa College of Medicine, Islamabad, Pakistan

ARTICLE INFO

Article history:

Received 23 Apr. 2026

Received in revised form 8 Jun. 2026

Accepted 30 Jun. 2026

Published 18 Aug. 2026

Keywords:
Heart failure with reduced ejection fraction

Undetermined etiology cardiomyopathy

Ischemic cardiomyopathy

Acute pulmonary edema

Hypertension

ABSTRACT

Heart failure with reduced ejection fraction (HFrEF) is rare in young adults but may develop when multiple uncontrolled cardiovascular risk factors are present. The diagnosis of an underlying cause of heart failure among younger patients is difficult due to multiple possible etiologies of LV systolic dysfunction, which might have similar clinical manifestations and imaging features. A 26-year-old man with a past medical history of uncontrolled hypertension and smoking, who came to hospital with complaints of sudden onset of dyspnea and chest pain on the left side, was investigated further to have sinus tachycardia with abnormal R-wave progression on electrocardiogram, cardiomegaly with pulmonary congestion on chest X-ray, and significantly impaired global systolic function of the left ventricle with ejection fraction of 25% on transthoracic echocardiogram. Troponins showed no dynamic change in their rise-and-fall pattern, ruling out acute coronary syndrome. He was stabilized on CPAP breathing and IV nitroglycerine and loop diuretics, with marked relief in symptoms. Following hemodynamic stabilization, guideline-directed medical therapy for HFrEF was initiated. In this case, there is acute decompensated heart failure with reduced ejection fraction (HFrEF) characterized by severe systolic dysfunction occurring in a relatively young individual suffering from numerous risk factors for cardiovascular disorders. The etiology of the condition could not be precisely determined due to the unavailability of coronary angiography and other advanced diagnostic methods. Ischemic cardiomyopathy is just one of the potential causes that also include hypertensive cardiomyopathy, idiopathic dilated cardiomyopathy, toxic cardiomyopathy, and inflammatory cardiomyopathy. The present report highlights the need for careful etiologic assessment of patients presenting with recently developed ventricular dysfunction, appropriate diagnosis in the absence of evidence of coronary disease, and prompt initiation of appropriate therapy.

1. Introduction

The number of people affected by heart failure globally continues to increase significantly, leading to morbidity, disability, and deaths [1]. This has been attributed to an increasing prevalence of risk factors for cardiovascular disease that can be modified [2]. Among the types of heart failure, heart failure with reduced ejection fraction (HFrEF) is very prevalent. HFrEF occurs when there is a decrease in ventricular systolic function. Ischemic cardiomyopathy results from long-term myocardial ischemia and infarction due to coronary artery disease [3]. Ischemic cardiomyopathy is one of the most prevalent causes of HFrEF among older populations [4, 5]. Myocardial injury caused by ischemia eventually leads to ventricular remodeling, resulting in systolic dysfunction. While ischemic cardiomyopathy mostly affects the middle-aged and elderly population, early-onset coronary artery disease is becoming more frequent among younger people, owing to the high prevalence of risk factors such as smoking, high blood pressure, and diabetes [6, 7].

The INTERHEART study revealed that a limited number of reversible risk factors, such as smoking, high blood pressure, abnormal lipids, and psychosocial stress, are responsible for the majority of myocardial infarction risk among populations from 52 different countries and various demographics [8]. The accumulation of these risk factors early on can contribute to heart damage and the development of heart failure among younger patients. According to the literature, acute decompensated heart failure occurs when there is sudden onset or progression of symptoms like dyspnea, orthopnea, paroxysmal nocturnal dyspnea, and pulmonary congestion [9]. Radiographic findings of cardiogenic pulmonary edema include cardiomegaly, Kerley B lines, and the appearance of a "bat-wing" perihilar pattern of alveolar edema [10]. Transthoracic echocardiography remains the mainstay for assessing cardiac morphology and ventricular function [11].

Determination of the cause of the left ventricular systolic dysfunction in younger patients poses a considerable diagnostic difficulty as various conditions such as hypertensive, ischemic, idiopathic dilated, inflammatory, and toxic cardiomyopathy may present with identical symptoms. The important consideration here is that the absence of imaging test results, infarction, and abnormal motion of the affected

* Corresponding author: Muhammad Hassaan Javaid, Shifa College of Medicine, Islamabad, Pakistan. Email: hassaanjavaid3@gmail.com

Published and owned by PubPorta Publishing LLC. Academic oversight and scholarly guidance are provided by the American Society for Inclusion, Diversity, and Equity in Healthcare (ASIDE). ISSN (Print) 3069-9851, ISSN (Online) 3069-9843. Hosting by ASIDE Journals.

Citation: Asif AE, Butt AM, Hussain ST, Ibrahim A, Javaid MH. Acute Decompensated Heart Failure with Severe Left Ventricular Systolic Dysfunction of Undetermined Etiology in a 26-Year-Old Male: A Case Report. ASIDE Cardiovasc. 2026;1(2):19-25, doi:10.71079/ASIDE.CV.081826789

area makes it impossible to confirm ischemic cardiomyopathy; it can only be termed suspected or possible. Here we consider the case of a 26-year-old man with acute decompensation of HFrEF as a consequence of significant left ventricular systolic dysfunction of unknown origin, and illustrate the clinical, diagnostic, and therapeutic approach in a resource-limited setting.

2. Case Presentation

A 26-year-old male was brought to the emergency department on December 20, 2025, due to acute onset of shortness of breath associated with orthopnea and paroxysmal nocturnal dyspnoea, with concomitant left-sided chest pain of eight hours' duration. No symptoms like nausea, vomiting, palpitations, syncope, or diaphoresis were seen.

History of hypertension of two years' duration, managed by an amlodipine/valsartan combination 5 mg/80 mg taken intermittently. He reported having chest pain twice in the past that he termed a "heart attack" due to self-management of medication when there is relief from symptoms. Documentation for any such episode, including ECG tracing, troponin levels at different time points, angiographic findings, any interventions, and discharge prescriptions, in support of an acute coronary syndrome (ACS) diagnosis, was not present; hence, these are considered self-reported suspected ACS cases. There was a history of admission for acute pulmonary edema twice and meningoencephalitis once during the year 2025 in his report. Family history was positive for hypertension in both parents and one sibling. He had been smoking cigarettes and snuff for four years.

Findings from physical examination showed that the patient was suffering from acute breathlessness and distress. The following findings were noted regarding his vital signs: blood pressure 150/100 mmHg, pulse 110 beats/min, respiratory rate 24 breaths/min, and afebrile. Bilateral crackles were noted in the mid lung zone. No jugular venous distension was noted, nor was any evidence of lower limb edema. No extra heart sounds or murmurs were present at the first assessment. The abdomen was soft and non-tender.

The chest X-ray (**Figure 1**) showed cardiomegaly with bilateral hilar haziness, Kerley B lines, and batwing appearance of alveolar infiltrates suggestive of cardiogenic pulmonary edema. Electrocardiography (**Figure 2**) showed sinus tachycardia with non-progressing R waves in anterior precordial leads (V1 to V4). Acute ST-segment elevation, pathologic Q waves, or hemodynamically significant arrhythmia was not noted.

2.1. Investigations

Serial troponin-I was performed to rule out acute myocardial injury. The initial result was 0.02 ng/mL (reference lab value: 0.16 ng/mL). Another test was performed 6 hours after admission and yielded 0.03 ng/mL, still below the cutoff level. Another test, twelve hours after admission, showed a level of 0.02 ng/mL. In all these results, there was no evidence of rise and fall of levels characteristic of STEMI or NSTEMI. Therefore, there was no diagnosis of acute type 1 myocardial infarction based on the kinetics of troponin. It may be considered that there was a completed myocardial infarction with normalized troponin, especially with consideration of the medical history given by the patient; however, no objective documentation of prior ischemic events was available.

The basic metabolic panel showed no electrolyte abnormalities and intact renal function (normal serum creatinine), allowing initiation of medically indicated therapy. No anemia or leukocytosis was found in the complete blood count. Liver function tests were normal. Importantly, however, several critical laboratory studies were not performed due to financial limitations, namely: fasting lipids, hemoglobin A1c levels, thyroid hormones, markers for viral infections (coxsackievirus, parvovirus B19, and adenovirus), autoimmune antibodies, and a urine toxicology screen. Testing for brain natriuretic peptide (BNP)/NT-proBNP was not done. The lack of these tests is a major disadvantage in diagnosing the cause of cardiomyopathy.

2.2. Echocardiographic Findings

Transthoracic echocardiography revealed a slight enlargement of the left ventricle along with mild concentric hypertrophy of the left ventricle. There was severe impairment of the systolic function of the left ventricle, with a biventricular Simpson estimation of the left ventricle's ejection fraction of 25%. Importantly, there were no regional abnormalities in left ventricular wall motion within the coronary artery territories; instead, there was diffuse, global hypokinesis. This presentation is less indicative of ischemic cardiomyopathy, which causes regional wall abnormalities. It rather points towards a possible diagnosis of hypertensive, idiopathic dilated, inflammatory, or toxic cardiomyopathy, although this does not rule out an ischemic process. Mild dilation of the left atrium was seen. Normal dimensions and functions were observed for both the right atrium and ventricle. Mitral valve insufficiency and mild tricuspid regurgitation were present. There was no pericardial effusion.

2.3. Differential Diagnosis

In view of the clinical and echocardiographic findings, it was impossible to make an etiological diagnosis. Below are some differential diagnoses to be considered:

Hypertrophic Cardiomyopathy: A strong possibility due to a two-year history of poorly controlled hypertension, with mild concentric LV hypertrophy and LV global dysfunction. This is the most plausible diagnosis in light of the information available. Dilated Cardiomyopathy: A possibility due to LV global hypokinesia without regional involvement. Idiopathic and genetic causes are still possible. Ischemic Cardiomyopathy: Although premature coronary artery disease may be seen in patients with risk factors, there were no imaging studies performed for the coronary arteries.

The lack of regional wall motion abnormalities and the indeterminate nature of troponin kinetics make this a probable, rather than a confirmed, diagnosis. Acute severe left ventricular dysfunction associated with myocarditis is well documented in young adults. No viral antibody tests were performed; a cardiac MRI, needed to evaluate for myocardial inflammation or late gadolinium enhancement, was unavailable. Toxic cardiomyopathy: There was no systematic history-taking regarding alcohol consumption.

2.4. Management

As soon as the patient arrived in the emergency room, CPAP ventilation therapy and urinary catheter insertion were initiated to ensure proper fluid balance. Nitroglycerine intravenously, along with furosemide 80 mg IV, was given to the patient. These measures helped in achieving immediate and impressive improvement in symptoms. Dyspnea resolved, and there was no sign of lung congestion. The patient was transferred to the coronary care unit.

After hemodynamic stability was achieved and there was evidence of adequate renal function, guideline-directed medical therapy for HFrEF was initiated: sacubitril/valsartan 50 mg BD, metoprolol succinate 25 mg OD, spironolactone 25 mg OD, dapagliflozin 10 mg OD, and rosuvastatin 20 mg OD. Co-administration of

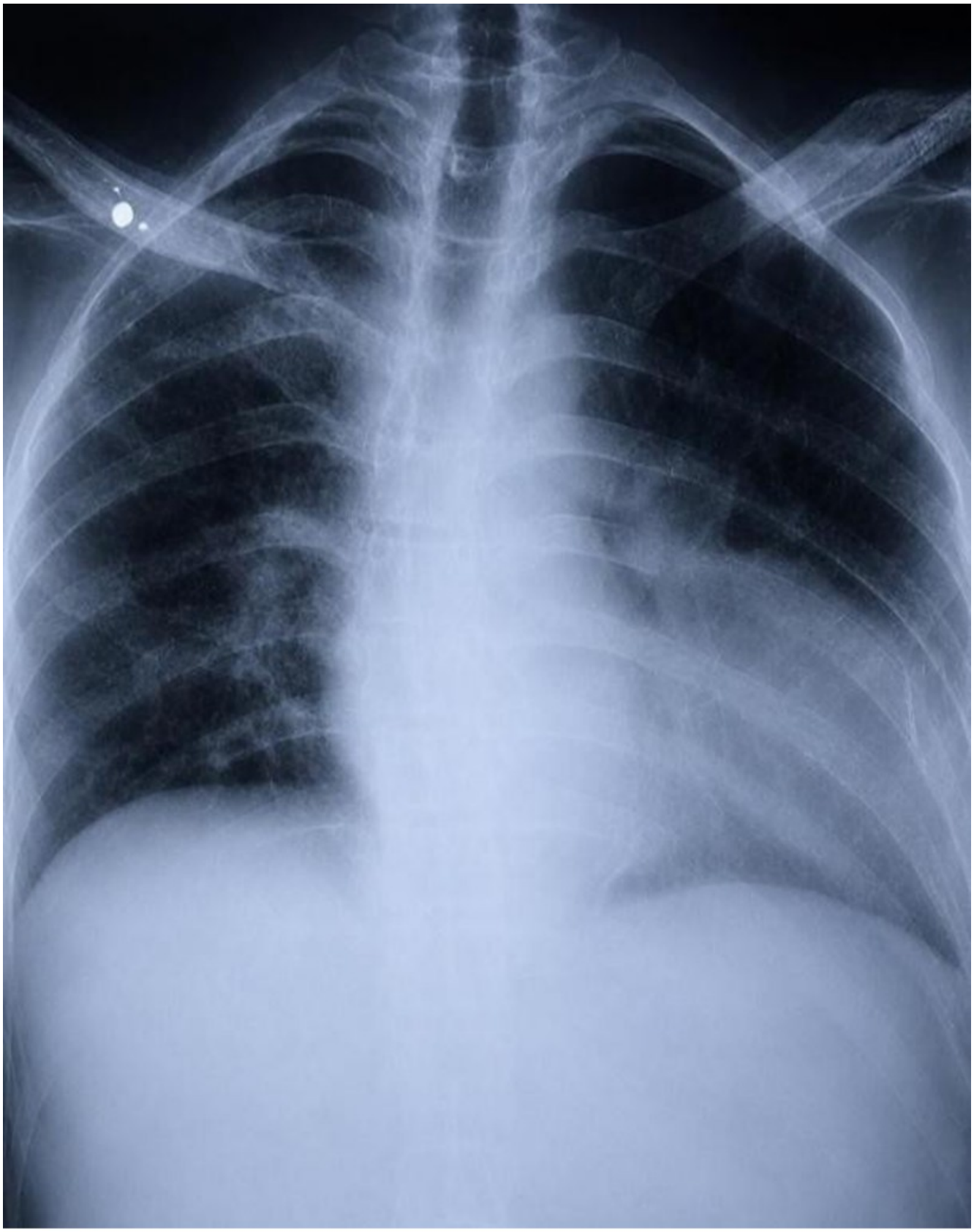

Figure 1: Posteroanterior chest radiograph obtained at admission. The image demonstrates cardiomegaly (cardiothoracic ratio >0.5), bilateral perihilar alveolar infiltrates in a "bat-wing" pattern, and horizontal linear opacities at the lung bases consistent with Kerley B lines, in keeping with cardiogenic pulmonary edema. All patient and institutional identifiers have been removed from the final image before submission.

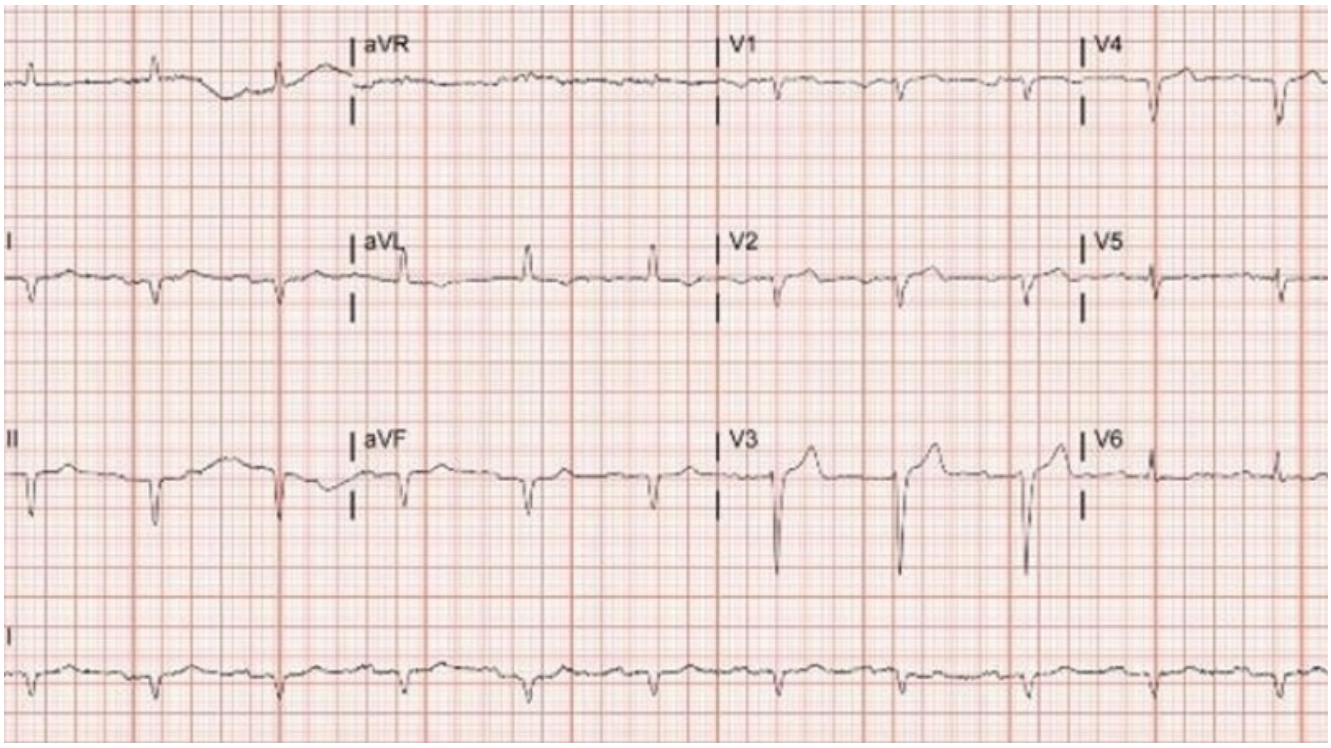

Figure 2: Twelve-lead electrocardiogram obtained at admission. The tracing demonstrates sinus tachycardia (rate approximately 110 bpm) with poor R-wave progression in the anterior precordial leads (V1–V4), suggesting anterior inactivation or prior anterior injury. No acute ST-segment elevation, pathological Q waves, or significant arrhythmia are identified. The ECG pattern is consistent with left ventricular dysfunction but is nonspecific and does not establish a diagnosis of acute myocardial infarction or confirm prior ischemic events. All patient and institutional identifiers have been removed from the final image before submission.

pantoprazole 40 mg OD was considered necessary to minimize gastrointestinal adverse effects. Regarding antiplatelet therapy: aspirin 75 mg daily and clopidogrel 75 mg daily were administered based on the presumed history of past acute coronary syndromes and considering the high cardiovascular risk profile of the patient. It is important to consider that, since the presence of confirmed ACS or obstructive coronary disease is unconfirmed at this admission, the treating team should review the use of dual antiplatelet therapy (DAPT), with documentation of the indication for such therapy, its intended duration, and a risk-benefit analysis. Where ACS cannot be confirmed, a review of the indication for dual antiplatelet therapy will be necessary during outpatient follow-up based on coronary assessment. The duration of dual antiplatelet therapy was not predefined at discharge and was planned to be reassessed following outpatient coronary evaluation.

It is important to differentiate between acute stabilization and treatment of disease processes. Acute recovery from the symptoms that led to the admission to the hospital can be traced to decongestion using positive pressure ventilation, nitrates, and intravenous diuretics. Sacubitril/valsartan, beta-blockers, mineralocorticoid receptor antagonists, and SGLT-2 inhibitors have been associated with improved outcomes in HFrEF but do not confer symptomatic benefit.

2.5. Discharge Status

Improvement was observed in the patient's clinical course during his three-day hospital stay. On discharge, the patient was able to walk around without any dyspnea. His blood pressure was 130/85 mmHg, and his resting heart rate was 82 beats per minute while on medication. The results of his tests for kidney function and potassium levels before starting sacubitril/valsartan and spironolactone were normal (the numerical readings could not be quantified, which is a limitation of this report).

The patient had been successfully weaned off oxygen supplementation and had been tolerating ambient air saturation levels adequately before his discharge from the hospital. His urine output had been satisfactory while he was receiving his diuretics, but no precise figures on his fluid balance were recorded. Unfortunately, this information was not fully reflected in the original case notes, and its absence constitutes a known limitation of this case study.

Table 1 presents a timeline of the case, based on the patient's self-reports during the index admission. There were no records other than those from the patient himself to verify the sequence of events. The prior history of chest pain described by the patient as "heart attacks" will be considered cases of self-reported suspected acute coronary syndrome.

3. Discussion

In this particular scenario, an example of acute heart failure has been provided in the form of a case where a 26-year-old male had presented with acute decompensation of HFrEF resulting from significant systolic dysfunction in the left ventricle. However, it could not be determined whether there was a specific cause of such heart failure. In other words, the condition can be considered as heart failure of unknown cause, as opposed to the term ischemic cardiomyopathy that may have also applied to this patient.

Table 1: Self-Reported Timeline of Clinical Events

Date / Period	Clinical Event	Symptoms / Findings	Evaluation / Documentation	Treatment / Outcome
Approximately 2023	Diagnosis of hypertension	Recurrent headaches and elevated blood pressure	Diagnosed locally; exact records unavailable	Started on amlodipine/valsartan (5 mg/80 mg); poor medication adherence reported
July 2023	First self-reported suspected ACS episode	Severe chest pain with shortness of breath	No ECG, troponin, or angiographic documentation available; event classification based on patient self-report only.	Symptomatic treatment at local clinic; discharged without documented cardiac workup; no revascularization or ACS-consistent discharge prescriptions on record
2024	Hospital admission for meningoencephalitis	Fever and neurological symptoms	Details unavailable; no cardiac evaluation documented	Treated conservatively; full recovery reported
During 2025 (before current admission)	Two admissions for acute pulmonary edema	Acute dyspnea and respiratory distress	No echocardiographic or angiographic records available; events based on patient self-report	Managed with supportive and decongestive therapy; outcomes and discharge medications unknown.
May 2025	Second self-reported suspected ACS episode	Chest pain requiring hospital visit	No catheterization or coronary imaging records available; no ECG or troponin documentation; event classification based on patient self-report only	Medical management reported; discharge medications and revascularization status unknown.
December 20, 2025	Current presentation with acute decompensated heart failure	Sudden severe breathlessness, orthopnea, paroxysmal nocturnal dyspnea, and left-sided chest pain	Chest X-ray: cardiomegaly, perihilar haziness, Kerley B lines. ECG: sinus tachycardia, poor R-wave progression, no acute ST elevation. Serial troponin-I: 0.02, 0.03, 0.02 ng/mL (non-diagnostic). Echo: global LV hypokinesia, EF 25%, no regional wall-motion abnormality	CPAP ventilation, IV nitroglycerine, IV furosemide 80 mg; rapid symptomatic improvement achieved
Hospital stay (3 days)	Stabilization and initiation of GDMT	Progressive improvement in dyspnea and pulmonary congestion; ambulatory at discharge	Severe global LV systolic dysfunction confirmed (EF 25%); renal function and electrolytes within acceptable limits at discharge.	Sacubitril/valsartan 50 mg BD, metoprolol succinate 25 mg OD, spironolactone 25 mg OD, dapagliflozin 10 mg OD, rosuvastatin 20 mg OD, aspirin 75 mg OD, clopidogrel 75 mg OD, pantoprazole 40 mg OD
Post-discharge	Follow-up unavailable	—	No outpatient records available	Long-term outcome unknown

Abbreviations: ACS, acute coronary syndrome; BD, twice daily; CPAP, continuous positive airway pressure; ECG, electrocardiogram; EF, ejection fraction; GDMT, guideline-directed medical therapy; IV, intravenous; LV, left ventricular; OD, once daily.

Notably, the echocardiogram results, which demonstrate generalized hypokinesia without regional wall motion abnormalities, are more suggestive of non-ischemic cardiomyopathy. Traditionally, in ischemic cardiomyopathy, wall motion abnormalities can be mapped to the territories supplied by the coronary arteries. Global dysfunction is suggestive of hypertensive, dilated, inflammatory, or toxic cardiomyopathy. In this case, the troponin results were negative for any diagnosis, and an acute coronary syndrome could not be confirmed. Previous ischemic episodes cannot be ruled out, but there is no evidence to document their occurrence.

Self-reported history of any previous episodes of chest pain needs proper interpretation. Although these were attributed to "heart attacks" by the patient, lack of supporting evidence from ECG during the episode(s), serial troponins, coronary angiogram findings, evidence of revascularization, and discharge medications in line with ACS would preclude classification as documented coronary artery disease. Any misclassification would have significant implications for diagnosis, dual antiplatelet therapy, and subsequent management in this particular case.

Limited resources constitute another important contextual consideration within the current scenario. Advanced heart scanning techniques such as coronary angiography, coronary CT angiography, and cardiac magnetic resonance imaging may not be available or affordable in low- and middle-income nations. Consequently, a provisional diagnosis of heart disease must be based on clinical examination, bedside echocardiography, and risk factor assessment, and must guide the initiation of appropriate treatment.

Where cardiac MRI is available, it remains the gold standard for differentiating ischemic from non-ischemic cardiomyopathy based on late gadolinium enhancement patterns in the myocardium. In ischemic cardiomyopathy, there is subendocardial or transmural late enhancement in a coronary territory pattern, whereas in inflammatory cardiomyopathy, the enhancement occurs at the level of midwall or epicardium. The investigation to rule out/confirm coronary artery disease would include either a coronary angiogram or a coronary CTA. These are an essential part of this patient's follow-up.

Several etiologies require individual discussion. The possibility of hypertensive cardiomyopathy is substantiated by the presence of two years of uncontrolled hypertension, mild concentric LVH, and recurrent episodes of acute pulmonary edema, one of the well-known phenotypes of pressure-overload cardiomyopathy that develops into dilated-phase hypertensive heart disease. As far as idiopathic dilated cardiomyopathy that presents with similar symptoms and global hypokinesia, its differential diagnosis is needed with exclusion of any other etiology and, possibly, genetic testing due to the positive family history of cardiovascular disorders. The diagnosis of myocarditis needs to be considered in young patients with recent onset of LV dysfunction because viral cardiomyopathy could result from previous viral infections, even though the previously experienced meningoencephalitis does not mean that it was caused by it. The role of toxic cardiomyopathy due to the abuse of stimulants and illicit drugs, as well as that of alcohol cardiomyopathy, was also not ruled out in this particular patient.

This particular case further emphasizes the importance of the association of lack of adherence with early cardiovascular disease. Young patients suffering from diseases such as hypertension show very low levels of adherence to their medications, as they stop taking their medications once the symptoms abate, something that has been observed in this particular patient, and might contribute to myocardial damage. Registry data have confirmed increasing rates of cardiovascular disease in younger adults globally [6].

HFrEF treatment strategies today rely on four evidence-based medication classes: angiotensin receptor–neprilysin inhibitors, beta-blockers, mineralocorticoid receptor antagonists, and sodium glucose cotransporter 2 inhibitors [3, 12]. Sacubitril/valsartan was shown to be superior to enalapril with respect to cardiovascular mortality and HF admissions, as shown by the PARADIGM-HF trial [13]. Similarly, empagliflozin was found to be effective in reducing cardiovascular mortality and HF hospitalizations among HFrEF patients in the EMPEROR-Reduced trial [14]. All four medications have been prescribed to the patient after hemodynamic stabilization, consistent with current guidelines.

Follow-up studies among young patients with severe left ventricular systolic dysfunction are critical in determining the effectiveness of their medications and whether they are following their medical advice, performing their evaluation, and assessing them for eligibility for device therapy. It is currently recommended that an assessment of the LV ejection fraction be performed three to six months after optimizing their medical management regimen if there is still severe systolic dysfunction (LVEF $\leq$35%) despite optimal therapy, which may warrant consideration of an implantable cardioverter-defibrillator for primary prevention of sudden cardiac death.

4. Conclusion

This is an example of acute decompensation of HFrEF associated with severe impairment of the function of the left ventricle in the context of multiple cardiovascular risk factors in a young male patient, namely poorly controlled hypertension and active smoking. The underlying etiology is unknown in this case, primarily due to the lack of coronary imaging and other sophisticated diagnostic tests. Ischemic cardiomyopathy is a possibility, but without coronary angiography, we cannot confirm that diagnosis; hypertensive cardiomyopathy and idiopathic dilated cardiomyopathy are at least equally likely. Reported episodes of chest pain in the past are not documented objectively and thus cannot serve as evidence for coronary artery disease. This case illustrates several key principles of management in patients like this, such as: (1) correct diagnosis, recognizing unconfirmed ischemic cardiomyopathy as suspicious or possible but not confirmed; (2) systematic etiological investigation; (3) prompt initiation of medical treatment according to recommendations regardless of the underlying pathology; and (4) appropriate follow-up with coronary and cardiac MRI examination as soon as possible.

Conflicts of Interest

The authors have no conflicts of interest to declare.

Funding Source

No funding sources to declare.

Acknowledgments

Not applicable.

Institutional Review Board (IRB)

Ethical approval is not required for case reports at our institution.

Informed Consent

Written informed consent was obtained from the patient for publication of this case report.

Large Language Model

No generative artificial intelligence (AI) tools or large language models were used in the preparation, writing, editing, analysis, or revision of this manuscript. The authors take full responsibility for the content of the published work.

Author Contributions

AEA, STH, and MHJ contributed to the conceptualization of the study, while AEA, AMB, STH, and AI were responsible for investigation and data collection. AEA, AMB, STH, AI, and MHJ contributed to the methodology, and AI performed the literature review. AEA, AMB, and AI assisted in drafting the manuscript, while STH and MHJ supervised the study and MHJ was responsible for project administration. All authors reviewed and approved the final manuscript.

Data Availability

Data are available from the corresponding author on request.

References

1. Savarese G, Lund LH. Global public health burden of heart failure. Card Fail Rev. 2017;3(1):7-11. [doi:10.15420/cfr.2016:25:2].

2. Tsao CW, Aday AW, Almarzooq ZI, et al. Heart disease and stroke statistics—2023 update: a report from the American Heart Association. Circulation. 2023;147(8):e93-e621. [doi:10.1161/CIR.0000000000001123].
3. McDonagh TA, Metra M, Adamo M, et al. 2021 ESC Guidelines for the diagnosis and treatment of acute and chronic heart failure. Eur Heart J. 2021;42(36):3599-726. [doi:10.1093/eurheartj/ehab368].
4. Felker GM, Shaw LK, O'Connor CM. A standardized definition of ischemic cardiomyopathy for use in clinical research. J Am Coll Cardiol. 2002;39(2):210-8. [doi:10.1016/s0735-1097(01)01738-7].
5. Gheorghiade M, Bonow RO. Chronic heart failure in the United States: a manifestation of coronary artery disease. Circulation. 1998;97(3):282-9. [doi:10.1161/01.cir.97.3.282].
6. Sharma SK, Makkar JS, Bana A, et al. Premature coronary artery disease, risk factors, clinical presentation, angiography and interventions: hospital-based registry. Indian Heart J. 2022;74(5):391-7. [doi:10.1016/j.ihj.2022.08.003].
7. Smith CL, Seigerman M, Adusumalli S, et al. Evolution and outcomes of premature coronary artery disease. Curr Cardiol Rep. 2021;23(4):36. [doi:10.1007/s11886-021-01457-8].
8. Yusuf S, Hawken S, Ounpuu S, INTERHEART Study Investigators, et al. Effect of potentially modifiable risk factors associated with myocardial infarction in 52 countries: case-control study. Lancet. 2004;364(9438):937-52. [doi:10.1016/S0140-6736(04)17018-9].
9. Gheorghiade M, Pang PS. Acute heart failure syndromes. J Am Coll Cardiol. 2009;53(7):557-73. [doi:10.1016/j.jacc.2008.10.041].
10. Milne EN, Pistolesi M, Miniati M, Giuntini C. The radiologic distinction of cardiogenic and noncardiogenic edema. AJR Am J Roentgenol. 1985;144(5):879-94. [doi:10.2214/ajr.144.5.879].
11. Lang RM, Bierig M, Devereux RB, American Society of Echocardiography, et al. Recommendations for chamber quantification. Eur J Echocardiogr. 2006;7(2):79-108. [doi:10.1016/j.euje.2005.12.014].
12. Yancy CW, Jessup M, Bozkurt B, et al. 2017 ACC/AHA/HFSA focused update of the 2013 ACCF/AHA guideline for the management of heart failure. Circulation. 2017;136(6):e137-61. [doi:10.1161/CIR.0000000000000509].
13. McMurray JJ, Packer M, Desai AS, PARADIGM-HF Investigators, et al. Angiotensin-neprilysin inhibition versus enalapril in heart failure. N Engl J Med. 2014;371(11):993-1004. [doi:10.1056/NEJMoa1409077].
14. Packer M, Anker SD, Butler J, EMPEROR-Reduced Trial Investigators, et al. Cardiovascular and renal outcomes with empagliflozin in heart failure. N Engl J Med. 2020;383(15):1413-24. [doi:10.1056/NEJMoa2022190].

ASIDE

ASIDE Cardiovascular

ASIDE CARDIOVASCULAR

Case Report

Dysphagia Megalatriensis Secondary to Rheumatic Severe Mitral Regurgitation with Giant Left Atrium: A Case Report

Jaweria Farman[1], Alina Batool[1], Okasha Tahir[2], Muhammad Hassaan Javaid[3,*], Abbas Khan[4], Hakim Ullah Wazir[5]

1-Khyber Girls Medical College, Peshawar, Pakistan
2-Khyber Medical University, Peshawar, Pakistan
3-Shifa College of Medicine, Islamabad, Pakistan
4-Hayatabad Medical Complex, Peshawar, Pakistan
5-Lady Reading Hospital, Peshawar, Pakistan

ARTICLE INFO

Article history:

Received 12 May 2026

Received in revised form 1 Aug. 2026

Accepted 25 Aug. 2026

Published 15 Sep. 2026

Keywords:
Dysphagia Megalatriensis

Giant Left Atrium

Rheumatic Heart Disease

Mitral Regurgitation

Esophageal Compression

Left Atrial Enlargement

ABSTRACT

Dysphagia megalatriensis is a rare condition caused by extensive left atrial dilatation, usually due to chronic rheumatic mitral valvular heart disease. It causes esophageal compression, which can be mistaken for primary esophageal conditions. A 45-year-old female patient with a 10-year history of rheumatic heart disease presented with gradually progressive dysphagia for solids and liquids, worsening breathlessness, orthopnea, poor appetite, and weight loss. Physical examination revealed signs of severe mitral regurgitation and chronic heart failure. Echocardiography revealed severe rheumatic mitral regurgitation with substantial leaflet thickening, commissural fusion, subvalvular involvement, giant left atrium (87 mm; left atrial volume index 148 mL/m^2), atrial fibrillation, and pulmonary hypertension. No significant mitral stenosis was found. Quantitative assessment of mitral valve area and mean transmitral gradient was unavailable because comprehensive Doppler assessment was not completed before referral. Contrast-enhanced computed tomography revealed signs of a markedly enlarged left atrium with external compression of the thoracic esophagus. In contrast, barium swallow confirmed smooth extrinsic compression of the esophagus without any obstructive luminal mass. The patient underwent medical optimization with diuretics, rate control, anticoagulation, nutritional support, and initiation of secondary prophylaxis for rheumatic fever before being referred to a cardiothoracic center for planned mitral valve replacement with left atrial reduction plasty. Dysphagia megalatriensis should be considered in patients with dysphagia and chronic rheumatic mitral valve disease after exclusion of primary esophageal pathology. Multimodality imaging is essential for diagnosis. Medical stabilization followed by referral for definitive surgical management is appropriate; however, the planned operation had not yet been performed, and postoperative outcomes were unavailable at the time of manuscript preparation.

1. Introduction

Acute rheumatic fever (ARF) is an immune-mediated inflammatory disease that develops following pharyngeal infection with Group A *Streptococcus* (*Streptococcus pyogenes*), typically two to three weeks after the initial infection.[1] The disease may affect the joints, skin, heart, and central nervous system, with diagnosis based on the Jones criteria.[1] Cardiac involvement most commonly manifests as valvulitis affecting the mitral and aortic valves, leading to valvular insufficiency and, over time, stenosis.[2] Recurrent episodes of ARF may result in progressive fibrosis, commissural fusion, and distortion of the mitral valve, ultimately leading to chronic rheumatic heart disease (RHD).

Giant left atrium (GLA) is a recognized but rare consequence of RHD of the mitral valve, resulting from sustained volume and pressure loads that cause progressive left atrial dilatation. Giant left atrium is classically defined as a parasternal long axis diameter of the left atrium >65 mm or a left atrial volume index of greater than 100 mL/m^2, with left atrial dimensions greater than 80 mm seen in more advanced and prolonged cases.[3, 4] The massive increase in size of the left atrium causes mass effects on nearby structures. Compression of the respiratory airways leads to carina splaying and atelectasis; compression of the recurrent left laryngeal nerve causes hoarseness (Ortner's syndrome); posterior displacement of the thoracic esophagus causes dysphagia or dysphagia megalatriensis.[3, 5] Transesophageal echocardiography is associated with high procedure-related risks in cases of esophageal compression; hence, it should be performed if its benefits clinically justify the risk and other imaging techniques are not applicable.[5]

Though the occurrence of RHD has declined worldwide due to the availability of more antibiotics, the disease continues to be a serious problem in developing nations, where late diagnosis and inadequate prevention systems result in the development of complications like GLA.[6] Dysphagia megalatriensis is observed very infrequently today, with fewer than a couple of dozen cases being mentioned in the literature.[3, 4] In most cases, the patients are adults who have

* Corresponding author: Muhammad Hassaan Javaid, Shifa College of Medicine, Islamabad, Pakistan. Email: hassaanjavaid3@gmail.com

Published and owned by PubPorta Publishing LLC. Academic oversight and scholarly guidance are provided by the American Society for Inclusion, Diversity, and Equity in Healthcare (ASIDE). ISSN (Print) 3069-9851, ISSN (Online) 3069-9843. Hosting by ASIDE Journals.

Citation: Farman J, Batool A, Tahir O, Javaid MH, Khan A, Wazir HU. Dysphagia Megalatriensis Secondary to Rheumatic Severe Mitral Regurgitation with Giant Left Atrium: A Case Report. ASIDE Cardiovasc. 2026;1(2):26-31, doi:10.71079/ASIDE.CV.091126846

rheumatic mitral disease that has been left untreated for long periods of time.

There are several educational aspects related to this particular case: it describes the problem of differential diagnosis between cardiac esophageal compression and intrinsic esophageal disease; it draws attention to the risks associated with the delayed diagnosis of RHD as well as the lack of secondary prophylaxis in a country where RHD is endemic; and it demonstrates that a complex diagnostic procedure including echocardiography, HRCT, and barium swallow should be used to make an accurate diagnosis. This report has been written in accordance with the CARE criteria.[7]

2. Case Presentation

2.1. Patient History and Timeline

A 45-year-old woman came to our cardiology ward with complaints of progressive breathlessness on exercise as well as at rest, poor appetite, orthopnea, and non-productive cough. Of importance was the progressive dysphagia, starting from solids to fluids, which had occurred within two to three weeks, along with weight loss.

She had been diagnosed with rheumatic heart disease about 10 years ago when she first presented with symptoms of exertional dyspnea. She recalled an episode of fever associated with migratory polyarthritis during childhood, although no medical documentation was available. In the course of the next 10 years, her symptoms had gradually increased even though she had been intermittently receiving medications like diuretics at the peripheral health center. She had never been put on secondary prophylaxis using benzathine penicillin G throughout this period. She had no complaints of throat infection, joint pain, skin rashes, or neurological symptoms during the present admission. A summary chronological timeline is presented in **Table 1**.

Table 1: Chronological clinical timeline of the case

Timepoint	Event
Childhood (recalled)	Episode of fever and migratory polyarthritis; no formal diagnosis or documentation available.
2014	Formal diagnosis of rheumatic heart disease at a peripheral facility; initiated on diuretics. No echocardiography documented at that time. Secondary prophylaxis not commenced.
2014–2024	Progressive worsening of exertional dyspnea; intermittent diuretic use without specialist follow-up. No secondary prophylaxis throughout this period.
~3 weeks before admission	Onset of rapidly progressive dysphagia, initially to solids then to liquids; associated with anorexia and weight loss.
~4 weeks prior to admission	Worsening dyspnea at rest; onset of orthopnea, non-productive cough.
Day 1 (Admission)	Admitted to cardiology unit; physical examination, ECG, chest X-ray, and laboratory investigations performed.
Day 2–3	Transthoracic echocardiography, HRCT chest, and barium swallow performed. Diagnosis of dysphagia megalatriensis established.
Day 3–5	Medical optimization initiated: diuresis, rate control, afterload reduction, anticoagulation. Dietitian and speech-language pathology consulted. Nasogastric feeding commenced.
Day 5–7	Cardiothoracic surgical consultation. Patient and family counseled regarding mitral valve replacement and left atrial reduction plasty.
Day 7 (Discharge planning)	Patient clinically stabilized; referred to tertiary cardiothoracic surgery center for elective surgical intervention.

ECG, electrocardiogram; HRCT, high-resolution computed tomography.

2.2. Physical Examination

The patient appeared chronically ill and cachectic, with bilateral temporal wasting. Physical examination results were as follows: blood pressure 110/70 mm Hg; pulse rate 88 beats per minute, with the pulse being irregularly irregular; respiratory rate 18 breaths per minute; oxygen saturation 96% on room air; body temperature 37.1°C. The BMI was not measured; however, mid-upper arm circumference was reduced.

The findings from the cardiovascular assessment included the apex impulse located laterally to the sixth intercostal space in the anterior axillary line, along with an apical palpable thrill. Auscultation revealed a grade 4/6 systolic murmur at the apex that radiated to the left axilla during all respiratory activities, indicative of severe mitral valve regurgitation. Bilateral crackles up to the mid-zones and mild expiratory wheezes bilaterally were heard on auscultation. There was no elevated jugular venous pressure, but there was mild bilateral pedal edema.

2.3. Imaging Investigations

Chest X-ray (**Figure 1**) showed gross cardiomegaly with splitting of the tracheal carina, which is typical of giant left atrial dilatation. Cardiothoracic ratio exceeded 0.65. Bilateral perihilar haziness was noted, indicative of increased pulmonary venous pressure.

A 12-lead ECG confirmed atrial fibrillation with a ventricular rate of approximately 90 beats per minute. There were no features of pre-excitation or acute ischemia. P waves suggestive of left atrial enlargement had been noted on an earlier recording in 2014, but were no longer visible because of atrial fibrillation. Left ventricular hypertrophy by voltage criteria was not confirmed. The exact duration of atrial fibrillation before admission could not be determined, although the patient reported palpitations for at least two years.

Transthoracic echocardiography (**Figure 2** and **Figure 3**) demonstrated a giant left atrium measuring 87 mm in the parasternal long-axis view with a left atrial volume index of 148 mL/m^2. The mitral valve showed diffuse leaflet thickening, commissural fusion, and subvalvular thickening consistent with chronic rheumatic involvement. Severe mitral regurgitation was present with an effective regurgitant orifice area of 0.52 cm^2, regurgitant volume of 75 mL/beat, vena contracta width of 8 mm, and a wide eccentric posterolateral regurgitant jet on color Doppler. Left ventricular end-diastolic diameter measured 62 mm with preserved systolic function (LVEF 53%). Moderate pulmonary hypertension was present with an estimated right ventricular systolic pressure of 62 mm Hg. No clinically significant mitral stenosis was demonstrated. Quantitative assessment of mitral valve area and mean transmitral gradient was unavailable because comprehensive Doppler assessment was not completed before referral.

The chest CT scan with contrast (**Figure 4**) revealed an extremely enlarged left atrium, resulting in mass effect in the posterior mediastinum, causing anterior displacement and external compression of

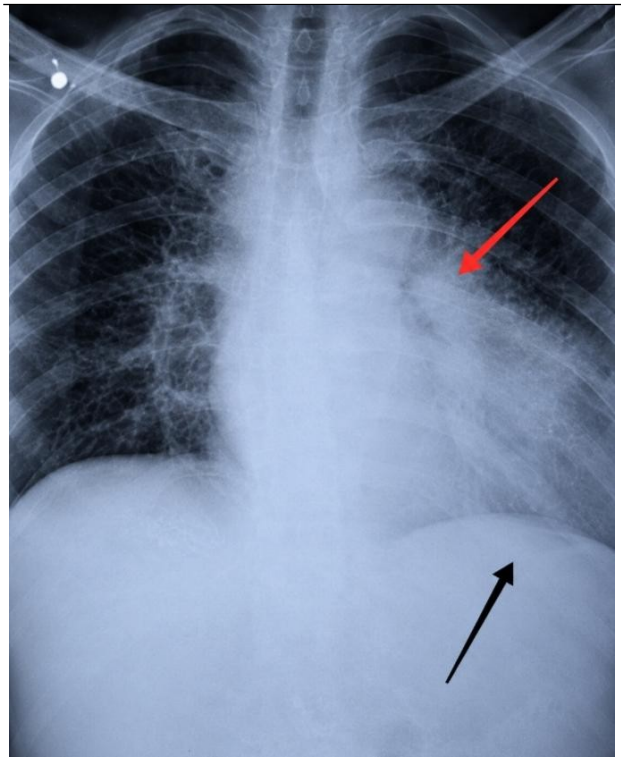

Figure 1: Chest radiograph demonstrating marked cardiomegaly with widening of the carinal angle (2 arrows), consistent with giant left atrial enlargement.

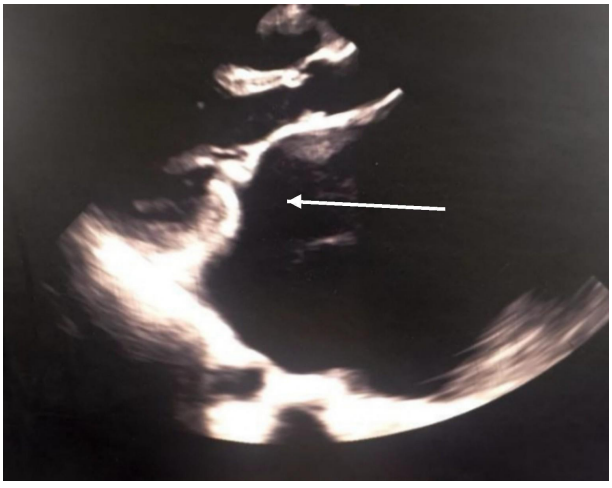

Figure 2: Transthoracic echocardiography showing rheumatic thickening of the mitral valve leaflets.

the mid-to-lower esophagus. The condition correlated exactly with the clinical presentation of dysphagia.

The barium swallow demonstrated smooth extrinsic compression of the mid-esophagus without an obstructing intraluminal lesion. These findings supported cardiac compression as the cause of dysphagia; however, intrinsic mucosal disease could not be completely excluded because upper gastrointestinal endoscopy was deferred owing to the patient's clinical condition and the anticipated procedural risk.

2.4. Laboratory Investigations

Selected laboratory values are summarized in **Table 2**.

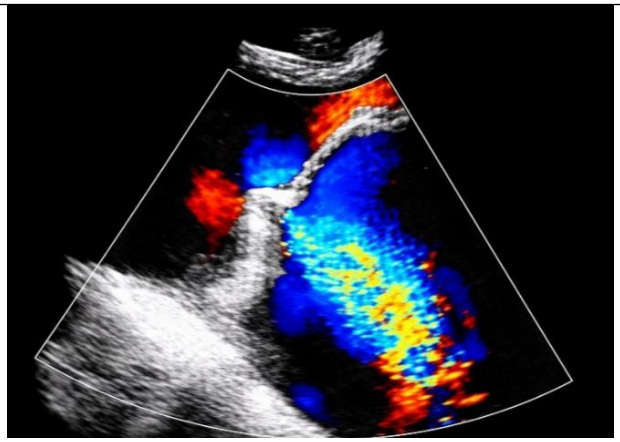

Figure 3: Color Doppler echocardiography demonstrating a severe eccentric posterolateral mitral regurgitant jet.

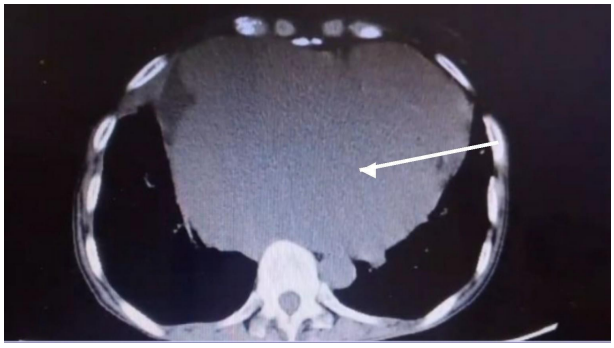

Figure 4: Contrast-enhanced CT of the chest showing giant left atrial enlargement causing posterior mediastinal mass effect with anterior displacement and compression of the thoracic esophagus (white arrow).

Transesophageal echocardiography (TEE) was considered for further evaluation of mitral valve anatomy and left atrial appendage thrombus. However, it was deferred because of the increased procedural risk associated with significant esophageal compression by the enlarged left atrium. Following multidisciplinary discussion, alternative imaging modalities, including repeat transthoracic echocardiography and cardiac magnetic resonance imaging, were planned at the receiving tertiary center if clinically indicated before surgery.

2.5. Management

After admission, management of decompensated heart failure was undertaken using the below-mentioned strategy. Intravenous administration of furosemide 40 mg once daily, followed by oral therapy, to obtain a net negative fluid balance, in addition to careful monitoring of kidney function tests and electrolyte levels. Administration of spironolactone 25 mg once daily, which is an aldosterone antagonist that works on neurohormonal blocking in heart failure. Once-daily administration of losartan 25 mg was used to reduce afterload by inhibiting angiotensin II receptor activity. However, losartan was preferred because of its better tolerability compared with ACE inhibitors, given the risk of cough. Nebivolol 2.5 mg was administered once daily to control the rate of atrial fibrillation. However, since there was a borderline state of decompensation, it was administered cautiously while monitoring hemodynamics and development of bronchospasm. Warfarin was started at a target INR of 2.0–3.0 to prevent blood clot formation due to AF in a patient

Table 2: *Summary of selected laboratory investigations.*

Parameter	Result	Reference Range
Hemoglobin	12.9 g/dL	12.0–16.0 g/dL
Mean corpuscular volume	88 fL (normocytic)	80–100 fL
Serum creatinine	0.9 mg/dL	0.5–1.1 mg/dL
eGFR (CKD-EPI)	78 mL/min/1.73 m^2	≥60
Serum potassium	3.8 mmol/L	3.5–5.0 mmol/L
Serum sodium	136 mmol/L	136–145 mmol/L
HbA1c	6.1% (prediabetes range)	<5.7% (normal)
Anti-streptolysin O (ASO) titre	400 IU/mL (elevated)	<200 IU/mL
INR (on warfarin, Day 5)	2.4	Target 2.0–3.0
Serum albumin	28 g/L (low)	35–50 g/L
HBsAg	Non-reactive	—
HIV antibody	Non-reactive	—
Blood group	AB positive	—

eGFR, estimated glomerular filtration rate; CKD-EPI, Chronic Kidney Disease Epidemiology Collaboration; HbA1c, glycated hemoglobin; ASO, anti-streptolysin O; INR, international normalized ratio; HBsAg, hepatitis B surface antigen; HIV, human immunodeficiency virus.

with rheumatic mitral valve disease. INR monitoring was performed every 48 hours during the inpatient period.

Digoxin 0.125 mg once daily was added due to the poor effect of nebivolol alone on ventricular rate control. The reduced dose was chosen in view of the patient's low body weight, normal-to-mildly reduced renal function, and hypoalbuminemia**.** Because the admission serum potassium was 3.8 mmol/L, electrolyte replacement was prescribed with a target serum potassium level above 4.0 mmol/L during treatment to reduce the risk of digoxin toxicity.

The patient had never received secondary prophylaxis against recurrent *Streptococcus* infections before now, even though the patient had been suffering from this condition for 10 years. During this admission, benzathine penicillin G 1.2 million units intramuscularly was administered every 4 weeks, and plans for further secondary prophylaxis were coordinated with the tertiary surgical facility and the patient's local clinic. Penicillin allergy was excluded by history.

With the rapid progression of both solids and liquids dysphagia, presence of cachexia with serum albumin level of 28 g/L, and high aspiration risk due to almost total esophageal blockage, it was decided to consult the dietitian and speech pathology as soon as possible. All oral intake was stopped until safe swallowing could be assessed. Feeding via nasogastric tube was initiated on Day 3 of admission with a high-protein, high-calorie formula to deliver 1,800–2,000 kcal/day and 1.5 g protein/kg/day to overcome severe malnutrition before surgery. Aspiration precautions, including head-of-bed elevation (30–45°), confirmation of nasogastric tube placement, and avoidance of oral intake, were implemented. Nutritional reassessment was planned at the receiving surgical center as part of preoperative optimization.

After hemodynamic stabilization and multidisciplinary review involving cardiology, cardiothoracic surgery, anesthesia, and nutrition teams, the patient was referred to a tertiary cardiothoracic center for planned mitral valve replacement with left atrial reduction plasty. The procedure had not yet been performed at the time of manuscript preparation; therefore, postoperative outcomes were unavailable.

3. Discussion

Giant left atrium is a well-recognized but rare condition seen later in cases of chronic mitral valve disease associated with rheumatic heart disease. The continuous volume overload from mitral regurgitation, combined with rheumatic inflammatory remodeling of the atrial wall, leads to dilation. Excessive enlargement of the left atrium (diameter ≥65–80 mm) leads to mechanical pressure effects on adjacent mediastinal structures, resulting in left main bronchus compression with resultant carina deviation and atelectasis, recurrent left laryngeal nerve compression with subsequent hoarseness of voice (Ortner's syndrome), and posterior displacement of the thoracic esophagus resulting in mechanical dysphagia known as dysphagia megalatriensis.[4, 8, 9] At the same time, left atrial fibrosis-related atrial fibrillation, pulmonary hypertension, and the risks of thromboembolism add to the disease severity.[10, 11]

The difficulty with diagnosing dysphagia megalatriensis lies in the symptomatology being very similar to primary esophageal disorders. In the past, it was mistaken for achalasia, esophageal cancer, and even mediastinal tumors. Furthermore, the enlargement of the left atrium can give the impression of an aortic aneurysm or pleural effusion on a plain chest X-ray examination.[4, 12] It is therefore important to adopt a systematic multimodality approach to diagnosing this condition. Two-dimensional echocardiography will confirm the presence of the valve disorder and left atrial enlargement.[4, 9] Barium swallow is useful for demonstrating smooth extrinsic esophageal compression. However, it does not exclude intrinsic mucosal disease, and upper gastrointestinal endoscopy should be considered when clinically appropriate. In our patient, endoscopy was deferred because of clinical instability and concern regarding procedural risk associated with severe esophageal compression.[3] As has been pointed out above, transesophageal echocardiography carries a high procedural risk when there is significant esophageal compression, and its use should be limited to patients who stand to benefit from the information provided by the test, such as mitral valve shape and the ability to repair.[3, 5]

The rheumatic cause of valvular pathology in this patient is evidenced by the concordance of echocardiographic valve anatomy (thickening of leaflets, commissural fusion, subvalvular involvement), a 10-year illness duration, a childhood history of fever with arthritis, and an elevated ASO titer. An elevated ASO titer indicates previous exposure to Group A *Streptococcus* but is not diagnostic of chronic rheumatic heart disease. In this patient, the diagnosis was supported primarily by the characteristic echocardiographic findings together with the clinical history of previous acute rheumatic fever and chronic valvular disease.

Management of GLA requires two phases: first, medical stabilization of hemodynamic abnormalities, followed by surgical correction of the structural defect. Medical management, which includes loop diuretics, afterload reduction, rate control in AF, and anticoagulant therapy, helps mitigate the effects of heart failure and reduce the risk of thromboembolic complications. However, it does not help correct the mechanical compression of the esophagus caused by the dilated atrium.[13] There has not been any substantial evidence of successful non-surgical treatment for GLA, nor of significant improvement in symptoms of dysphagia megalatriensis without correcting the structural defects. Surgical management, typically consisting of mitral valve repair or replacement with concomitant

left atrial reduction plasty, has been reported to relieve esophageal compression and improve symptoms in appropriately selected patients.[8, 12] Series performed in dedicated centers show a perioperative mortality of 2–3%, a significant reduction from the previous value of around 20%, due to improvements in surgical techniques, cardioplegic strategies, and perioperative management.[8] Despite this considerable reduction, the risk associated with surgery in a cachectic and malnourished patient with pulmonary hypertension and chronic AF is still not insignificant and should be decided on an individual basis after optimizing the patient preoperatively.

There are several points in this case worth elaborating upon. Firstly, the lack of secondary prevention for a decade likely played a significant role in the recurrence of subclinical rheumatism and the subsequent deterioration of valvular structures. Benzathine penicillin G was administered during this hospitalization in accordance with standard treatment protocols for RHD and will be continued after surgery. Secondly, the condition of malnutrition, hypoproteinemia, and severe dysphagia is a factor not only relevant but potentially overlooked in terms of preoperative risks in GLA. Nutritional optimization with enteral feeding before surgery is appropriate and was achieved in this case. Thirdly, the digoxin dose was deliberately reduced from 0.25 mg to 0.125 mg based on the patient's low body weight and normal-to-mildly reduced renal function; this demonstrates the appropriateness of individualization when prescribing drugs to high-risk individuals and underscores the importance of clearly stating the dose used in case reports.

This current case contributes to the small but increasing body of literature regarding dysphagia megalatriensis. It serves as an additional case of the late presentation of advanced rheumatic heart disease in South Asia. This illustrates the importance of considering cardiac compression as a cause of dysphagia for practitioners in endemic regions of RHD, especially when routine investigation of the esophagus proves inconclusive.

4. Conclusion

Dysphagia megalatriensis is a rare but important manifestation of giant left atrial enlargement and should be considered in patients presenting with dysphagia after primary esophageal disease has been excluded. In patients with chronic rheumatic mitral valve disease, multimodality imaging with transthoracic echocardiography, contrast-enhanced computed tomography, and barium swallow can establish the diagnosis and define the extrinsic nature of esophageal compression. Medical stabilization, nutritional optimization, anticoagulation, and secondary prophylaxis for rheumatic fever are essential before referral for definitive surgery. In this case, the patient was stabilized and referred for planned mitral valve replacement with left atrial reduction plasty. Still, the operation had not yet been performed, and postoperative outcomes were unavailable.

Conflicts of Interest

The authors declare no conflicts of interest.

Funding Source

This research received no specific grant from any funding agency in the public, commercial, or not-for-profit sectors.

Institutional Review Board (IRB)

The case was managed in accordance with the Declaration of Helsinki. Formal ethical approval was not required for a single-patient, de-identified case report at the participating institutions.

Informed Consent

Written informed consent was obtained from the patient for publication of this case report and any associated clinical images. All images presented in this report have been reviewed to ensure that patient-identifying information has been removed.

Large Language Model

None

Authors Contribution

JF, AB, MHJ, and AK were responsible for case selection, while JF and AB were responsible for data collection. MHJ and AK wrote the first draft of the manuscript, and OT compiled the references. HUW was responsible for patient follow-up and obtaining informed consent, while OT and HUW contributed to reviewing, editing, and final formatting. All authors reviewed and approved the final manuscript.

Data Availability

Data sharing does not apply to this article as no datasets were generated or analyzed during the current study.

References

1. Gewitz MH, Baltimore RS, Tani LY, et al. Revision of the Jones criteria for the diagnosis of acute rheumatic fever in the era of Doppler echocardiography: a scientific statement from the American Heart Association. Circulation. 2015;131(20):1806-18. [PMID: 25908771, doi:10.1161/CIR.0000000000000205].
2. Cannon J, Roberts K, Milne C, Carapetis JR. Rheumatic heart disease severity, progression and outcomes: a multi-state model. J Am Heart Assoc. 2017;6(3):e003498. [PMID: 28255075, doi:10.1161/JAHA.116.003498].
3. Deschepper C, Devos D, DePauw M. Cardiac dysphagia — a ghost of the past? A case report. Eur Heart J Case Rep. 2021;5(9):ytab338. [PMID: 34527858, doi:10.1093/ehjcr/ytab338].
4. Pandit BN, Aggarwal P, Subramaniyan S, Gujral JS, Nath RK. Largest giant left atrium in rheumatic heart disease. J Cardiol Cases. 2021;24(1):10-3. [PMID: 34257753, doi:10.1016/j.jccase.2020.11.022].
5. Bugra AK, Kadirogullari E, Onan B. Reduction plasty for giant left atrium causing dysphagia: a case report. Gen Thorac Cardiovasc Surg. 2021;69(3):546-9. [PMID: 32965607, doi:10.1007/s11748-020-01490-4].
6. Steer AC, Carapetis JR. Acute rheumatic fever and rheumatic heart disease in indigenous populations. Pediatr Clin North Am. 2009;56(6):1401-19. [PMID: 19962028, doi:10.1016/j.pcl.2009.09.011].
7. Gagnier JJ, Kienle G, Altman DG, et al. The CARE guidelines: consensus-based clinical case reporting guideline development. J Med Case Rep. 2013;7:223. [PMID: 24228906, doi:10.1186/1752-1947-7-223].
8. Apostolakis E, Shuhaiber JH. The surgical management of giant left atrium. Eur J Cardiothorac Surg. 2008;33(2):182-90. [PMID: 18096399, doi:10.1016/j.ejcts.2007.11.003].
9. Gajanana D, Morris DL, Janzer SF, George JC, Figueredo VM. Giant left atrium causing dysphagia. Tex Heart Inst J. 2016;43(5):469-71. [PMID: 27777540, doi:10.14503/THIJ-15-5682].

10. Patel DA, Lavie CJ, Milani RV, Shah S, Gilliland Y. Clinical implications of left atrial enlargement: a review. Ochsner J. 2009;9(4):191-6. [PMID: 21603443].
11. Zilberszac R, Gleiss A, Massetti M, et al. Left atrial size predicts outcome in severe but asymptomatic mitral regurgitation. Sci Rep. 2023;13(1):3892. [PMID: 36890195, doi:10.1038/s41598-023-31163-0].
12. Santra G, Paul R, Pradhan S, Choudhury PS, Das S. A case of giant left atrium mimicking pleural effusion. Oman Med J. 2014;29(4):e077. [PMID: 30996820, doi:10.5001/omj.2014.82].
13. Greenberg B. Medical management of patients with heart failure and reduced ejection fraction. Korean Circ J. 2022;52(3):173-97. [PMID: 35257531, doi:10.4070/kcj.2021.0401].

ASIDE

ASIDE Cardiovascular

ASIDE CARDIOVASCULAR

Original Article

Trends in Mortality Involving Ischemic Heart Disease and Procedure-related Conditions in U.S. Adults, 1999–2023

Mohamed Alatfawy[1], Youssef Ramadan[2,*], Abdelrhman H. Mohamed[3], Maryam Saghir[4], Alyaa Ahmed Ibrahim[5], Anika Goel[6], Waheed Qaisi[7], Krish Patel[8], Mostafa Mohamed Abdelmoneam Elsawy[2], Omar Khaled Elsalhy[2], Ibtissam ElGhazzani[9], Sihame ElGhazzani[9], Alaa Eldeeb[5], Walid Bechibchi[10], Mohamed Fawzi Hemida[5]

1-Faculty of Medicine, Kafrelsheikh University, Kafr Elsheikh, Egypt
2-Faculty of Medicine, October 6 University, Giza, Egypt
3-Faculty of Medicine, Luxor University, Luxor, Egypt
4-Jinnah Sindh Medical University, Karachi, Pakistan
5-Faculty of Medicine, Alexandria University, Alexandria, Egypt
6-Kakatiya Medical College, Warangal, Telangana, India
7-An-Najah National University, Nablus, Palestine
8-C. U. Shah Medical College, Surendranagar, Gujarat, India
9-Faculty of Medicine of Tunis, University of Tunis El Manar, Tunis, Tunisia
10-Faculty of Medicine, University of Constantine 3 Salah Boubnider, Constantine, Algeria

ARTICLE INFO

Article history:
Received 21 May 2026
Received in revised form 9 Sep 2026
Accepted 12 Sep 2026
Published 16 Sep 2026

Keywords:
Ischemic heart disease
Procedure-related mortality
Mortality trends
CDC WONDER
Epidemiology

ABSTRACT

Background: Ischemic heart disease (IHD) is a leading cause of death in the United States, and death certificates may contain medical or surgical care-related codes among decedents with IHD. However, these codes do not establish procedural exposure, postoperative status, timing, or causality. This study assesses 25-year trends in mortality involving IHD and Y83–Y84 codes.

Methods: Nationwide multiple-cause-of-death (MCOD) death-certificate records were obtained from the CDC WONDER database for U.S. adults aged ≥25 years from 1999–2023. Death records containing IHD (ICD-10 codes I20–I25) and medical/surgical care-related codes (Y83–Y84) were identified. We calculated age-adjusted mortality rates (AAMRs) per 100,000 people in the general U.S. population. We used joinpoint regression to estimate annual percentage changes (APCs) and average annual percentage changes (AAPCs).

Results: From 1999–2023, a total of 144,644 deaths were reported. The AAMR significantly decreased from 4.19 in 1999 to 1.13 in 2023 (AAPC: −5.51; $p = 0.000021$). The overall AAMR was 3.78 (AAPC: −5.26) among males and 1.71 (AAPC: −6.12) among females. By race, AAMRs declined substantially among all groups from 1999 to 2023, with the highest 1999 AAMR observed among NH White individuals (4.35). Regionally, the Midwest had the highest overall AAMR (2.75). Adults aged ≥65 years had the highest overall CMR (10.34). From 1999 to 2020, the population-level AAMR was 3.21 in nonmetropolitan areas and 2.45 in metropolitan areas.

Conclusions: Mortality involving IHD and medical/surgical procedure-related codes declined in recent years, particularly during 2021–2023. Higher population-level mortality rates were observed among males and in the Midwest region.

1. Introduction

Ischemic heart disease (IHD), commonly referred to as coronary artery disease (CAD) or coronary heart disease, continues to represent one of the most significant public health challenges in the United States, remaining the leading cause of mortality and morbidity among adults. Recent nationally representative survey data indicate that CAD affects approximately 4.9% of U.S. adults, with slightly higher rates in men and markedly increasing prevalence with age. This translates to millions of Americans living with clinically diagnosed CAD, and the burden is disproportionately greater among older individuals and male adults, underscoring persistent demographic disparities [1, 2]. IHD accounts for more than one in seven deaths in the United States, with coronary heart disease specifically responsible for over 371,000 deaths annually [3]. Despite advances in medical and interventional therapies, projections suggest that the prevalence of IHD will continue to rise, with estimates indicating a potential 31% increase by 2060, largely attributed to population aging and persistent risk factors including diabetes, hypertension, and dyslipidemia [4].

Patients with IHD represent a particularly vulnerable population in the context of medical and surgical procedures, facing substantially elevated risks compared to those without cardiac disease. Studies demonstrate that patients with significant cardiac disease who

* Corresponding author: Email: mmmk15424@gmail.com

Published and owned by PubPorta Publishing LLC. Academic oversight and scholarly guidance are provided by the American Society for Inclusion, Diversity, and Equity in Healthcare (ASIDE). ISSN (Print) 3069-9851, ISSN (Online) 3069-9843. Hosting by ASIDE Journals.

Citation: Alatfawy M, Ramadan Y, Mohamed AH, et al. Trends in mortality involving ischemic heart disease and procedure-related conditions in U.S. adults, 1999–2023. ASIDE Cardiovasc. 2026;1(2):32-41, doi:10.71079/ASIDE.CV.091626873

undergo vascular or major surgery may face up to a 10% risk of major morbidity and mortality. However, these findings from clinical surgical cohorts should be distinguished from death-certificate data containing medical/surgical procedure-related codes, which cannot establish whether a procedure occurred, the timing of the procedure, postoperative status, or a causal relationship between the procedure-related condition and death [5, 6]. Postoperative myocardial injuries and infarction occur in approximately 18–20% of patients undergoing noncardiac surgery, with peak incidence within the first 48 hours post-operatively [7, 8]. The pathophysiology underlying increased risk associated with medical and surgical procedures involves multiple mechanisms, including increased myocardial oxygen demand during procedural stress, hemodynamic fluctuations, and prothrombotic states [9, 10]. Advanced age, emergency surgery, and multiple comorbidities further amplify the risk of adverse postoperative outcomes in this population [11].

While substantial attention has been directed toward understanding cardiac risk associated with medical and surgical procedures in patients with IHD, comprehensive long-term population-level analyses of mortality involving IHD and medical/surgical procedure-related codes remain limited. Most existing studies have focused on short-term outcomes or specific surgical procedures, leaving a gap in understanding how mortality involving IHD and medical/surgical procedure-related codes has evolved over extended periods. In the U.S. Multiple Cause of Death (MCOD) database, procedure-related conditions identify death records in which medical or surgical care was documented; however, these records do not establish the timing of the procedure relative to IHD or death or confirm a causal relationship. The changing landscape of cardiac care suggests that mortality trends may have shifted considerably. Yet, the magnitude of these changes and potential disparities across demographic and geographic subgroups have not been systematically characterized. This study examines 25-year trends in mortality records involving IHD and medical/surgical procedure-related codes among U.S. adults aged ≥25 years.

2. Methods

2.1. Study setting and population

In this descriptive study, we analyzed national mortality trends using MCOD records from the Centers for Disease Control and Prevention Wide-Ranging Online Data for Epidemiologic Research (CDC WONDER) database for U.S. adults aged ≥25 years from 1999 to 2023, as shown in a previous CDC study [12]. We identified IHD using ICD-10 codes I20–I25, and medical/surgical procedure-related events using Y83–Y84 [13, 14]. We identified both code groups regardless of their position on the death certificate, and included records containing both I20–I25 and Y83–Y84. Thus, the analysis identified death certificates documenting both IHD and medical/surgical procedure-related codes rather than a clinically defined postoperative cohort. Deaths among individuals younger than 25 years and records without both coding criteria were excluded. Because MCOD data are based on death certificates, we could not establish the timing of the procedure relative to IHD or death, or any causal relationship. Institutional review board approval was not required because the study used publicly available, de-identified mortality data. The study was reported in accordance with the Strengthening the Reporting of Observational Studies in Epidemiology (STROBE) guidelines [15].

2.2. Outcome definition

The primary outcome was defined as mortality records documenting both IHD and medical/surgical procedure-related conditions on the death certificate. This outcome represents deaths in which IHD and procedure-related conditions were concurrently documented and should not be interpreted as confirmed postoperative deaths or as evidence that a medical or surgical procedure caused the death.

2.3. Data abstraction

We extracted data on population size, year, and demographic characteristics, including sex, age, race and ethnicity, and region. We classified racial and ethnic categories as non-Hispanic (NH) White, NH Black or African American, Hispanic or Latino, NH American Indian or Alaska Native, and NH Asian or Pacific Islander. Mortality estimates for NH American Indian or Alaska Native individuals were suppressed when counts were too small to produce reliable estimates and were therefore not interpreted. The National Center for Health Statistics (NCHS) 2013 Urban-Rural Classification Scheme classified counties as metropolitan or nonmetropolitan [16, 17]. Metropolitan counties included large central metropolitan, large fringe metropolitan, medium metropolitan, and small metropolitan counties, whereas nonmetropolitan counties included micropolitan and noncore counties. Because CDC WONDER provided urban-rural classification data through 2020, we restricted the urban-rural analysis to 1999–2020. We stratified regions into Northeast, Midwest, South, and West according to U.S. Census Bureau definitions. We categorized age groups as 25–44 years, 45–64 years, and ≥65 years.

2.4. Statistical analysis

We calculated crude mortality rates (CMRs) and age-adjusted mortality rates (AAMRs) per 100,000 population from 1999 to 2023. We stratified them by year, sex, and race/ethnicity, with urban-rural analyses restricted to 1999–2020. We standardized AAMRs to the 2000 U.S. standard population across all age groups, with corresponding 95% confidence intervals (CIs) [18]. We calculated CMRs by dividing the number of deaths involving IHD and medical/surgical procedure-related codes by the corresponding U.S. population for each year and expressed them per 100,000 population. We used age-specific CMRs for age-stratified analyses, as age adjustment is unnecessary within defined age strata. To quantify national annual trends in mortality involving IHD and medical/surgical procedure-related codes, we used the Joinpoint Regression Program (version 5.4.0.0, National Cancer Institute) to estimate the Annual Percentage Change (APC) and Average Annual Percentage Change (AAPC) with 95% CIs [19]. We fit log-linear regression models (ln(y) transformation of rates) to model temporal variation. We permitted a maximum of 4 joinpoints. Model selection was conducted using the Permutation Test with a statistical significance threshold of alpha = 0.05 and 4,499 permutations. We specified standard errors using the standard errors provided in the CDC WONDER rate estimates (heteroscedastic error specification). We assumed errors were uncorrelated over time. Confidence intervals for APCs and AAPCs were calculated using the Empirical Quantile method with 5,001 resamples.

We conducted subgroup analyses across prespecified demographic and geographic categories. We did not perform sensitivity analyses for sparse strata; therefore, we interpreted estimates based on small cell counts cautiously because of potential statistical instability. We considered APCs increasing or decreasing if the slope describing the change in mortality differed significantly from zero using a two-tailed t-test ($p < 0.05$).

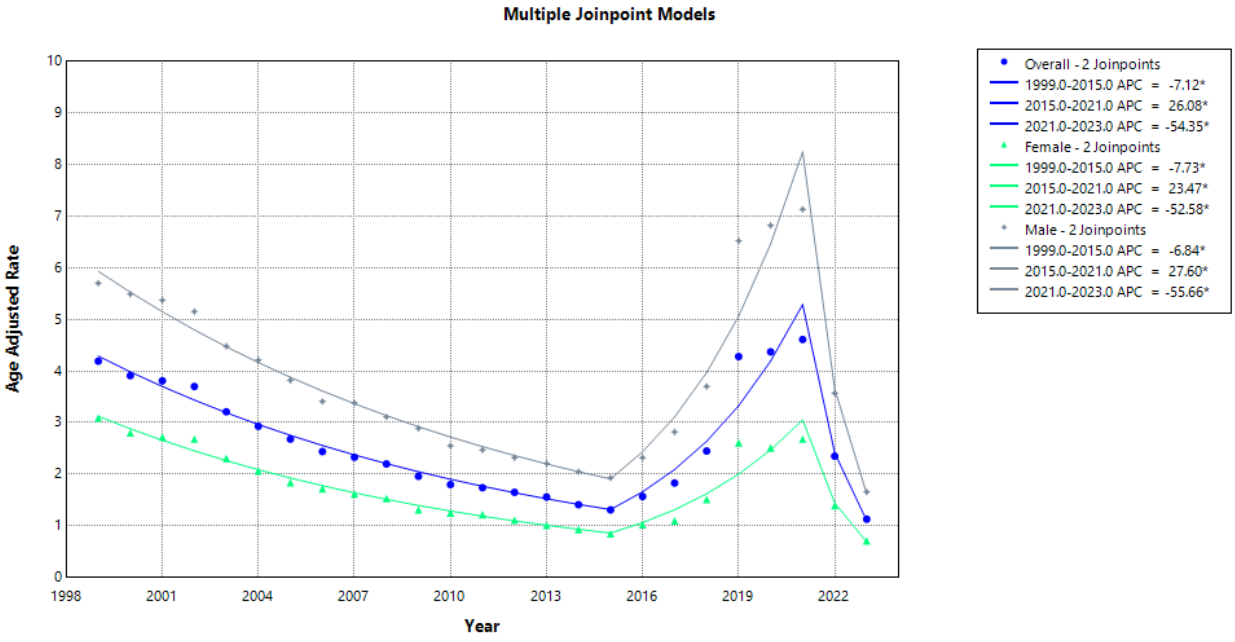

Figure 1: Overall and sex-stratified age-adjusted mortality rates per 100,000 for deaths involving ischemic heart disease and procedure-related conditions in U.S. adults, 1999–2023. In the figure legend, an asterisk denotes an APC significantly different from zero (two-sided *t*-test, $p < 0.05$).

3. Results

3.1. Overall trends

Between 1999 and 2023, a total of 144,644 deaths in the United States were identified in mortality records documenting both IHD and medical/surgical procedure-related conditions. Overall, AAMR declined from 4.19 (95% CI: 4.1 to 4.29) in 1999 to 1.13 (95% CI: 1.09 to 1.17) in 2023, with an AAPC of -5.51 (95% CI: -7.94 to -3.01) (p = 0.000021), thus reflecting a downward trend.

From 1999 to 2015, the AAMR declined from 4.19 (95% CI: 4.10–4.29) to 1.31 (95% CI: 1.26–1.36), with an APC of -7.12 (95% CI: -8.04 to -6.18; p < 0.000001). From 2015 to 2021, the AAMR increased again, increasing from 1.31 (95% CI: 1.26–1.36) to 4.61 (95% CI: 4.53–4.70) in 2021, with an APC of 26.08 (95% CI: 19.33 to 33.22; p < 0.000001). From 2021 to 2023, the AAMR declined from 4.61 (95% CI: 4.53–4.70) to 1.13 (95% CI: 1.09–1.17), with an APC of -54.35 (95% CI: -65.58 to -39.46; p = 0.000019) (Figure 1; Supplemental Tables 1, 2, 3).

3.2. Trends by sex

When stratified by sex, males accounted for more deaths than females among records documenting both IHD and medical/surgical procedure-related conditions. (90,561 deaths in males vs. 54,083 deaths in females). In males, the AAMR decreased from 5.7 (95% CI: 5.53 to 5.88) in 1999 to 1.66 (95% CI: 1.59 to 1.74) in 2023, yielding an AAPC of -5.26 (95% CI: -7.63 to -2.84; p = 0.000028). The AAMR also exhibited an overall downward trend in females, decreasing from 3.09 (95% CI: 2.98 to 3.19) in 1999 to 0.71 (95% CI: 0.67 to 0.76) in 2023. The AAPC for this period was -6.12 (95% CI: -8.81 to -3.35; p = 0.000021).

Among males, the AAMR declined from 5.7 (95% CI: 5.53 to 5.88) in 1999 to 1.93 (95% CI: 1.85–2.02) in 2015; this reduction yielded an APC of -6.84 (95% CI: -7.76 to -5.91; p < 0.000001). From 2015 to 2021, the AAMR increased from 1.93 (95% CI: 1.85–2.02) in 2015 to 7.13 (95% CI: 6.98–7.29) in 2021, with an APC of 27.60 (95% CI: 21.58 to 33.92; p < 0.000001). From 2021 to 2023, the AAMR trended downward, decreasing from 7.13 (95% CI: 6.98–7.29) in 2021 to 1.66 (95% CI: 1.59–1.74) in 2023, with an APC of -55.66 (95% CI: -66.55 to -41.23; p = 0.000012).

Among females, the AAMR also exhibited a similar downward trend during a similar time frame, decreasing from 3.09 (95% CI: 2.98–3.19) in 1999 to 0.85 (95% CI: 0.80–0.90) in 2015, with an APC of -7.73 (95% CI: -8.73 to -6.73; p < 0.000001). From 2015 to 2021, AAMR increased from 0.85 (95% CI: 0.80–0.90) in 2015 to 2.68 (95% CI: 2.60–2.77) in 2021, with an APC of 23.47 (95% CI: 16.04 to 31.36; p = 0.000002). From 2021 to 2023, the AAMR trended downward, decreasing from 2.68 (95% CI: 2.60–2.77) in 2021 to 0.71 (95% CI: 0.67–0.76) in 2023, with an APC of -52.58 (95% CI: -65.40 to -35.0; p = 0.000111) (Figure 1; Supplemental Tables 1, 2, 3).

3.3. Trends by race and ethnicity

Across the study period, NH White individuals accounted for the highest number of deaths (116,083 deaths), followed by NH Black/African American individuals (13,891 deaths), Hispanics (9,623 deaths), NH Asian or Pacific Islander (4,120 deaths), and NH American Indian or Alaska Native (927 deaths).

Among NH White individuals, the AAMR decreased from 4.35 (95% CI: 4.24 to 4.45) in 1999 to 1.18 (95% CI: 1.13 to 1.23) in 2023. Consequently, the AAPC was -5.50 (95% CI: -7.38 to -3.59; p < 0.000001). From 1999 to 2015, the AAMR decreased from 4.35

(95% CI: 4.24 to 4.45) in 1999 to 1.36 (95% CI: 1.30–1.41) in 2015, resulting in an APC of -7.08 (95% CI: -7.83 to -6.32; p < 0.000001). Then, the AAMR increased from 1.36 (95% CI: 1.30–1.41) in 2015 to 4.52 (95% CI: 4.42–4.61) in 2021, yielding an APC of 24.70 (95% CI: 19.17 to 30.49; p < 0.000001). This was followed by a downward trend, with the AAMR decreasing from 4.52 (95% CI: 4.42–4.61) in 2021 to 1.18 (95% CI: 1.13–1.23) in 2023, resulting in an APC of -52.93 (95% CI: -61.87 to -41.89; p = 0.000001).

Among NH Black/African American individuals, the AAMR decreased from 3.95 (95% CI: 3.63 to 4.27) in 1999 to 1.13 (95% CI: 1.00 to 1.26) in 2023, with an AAPC of -5.22 (95% CI: -7.42 to -2.96; p = 0.000008). From 1999 to 2015, the AAMR demonstrated a downward trend, decreasing from 3.95 (95% CI: 3.63 to 4.27) in 1999 to 1.35 (95% CI: 1.20–1.50) in 2015, and thus giving an APC of -6.84 (95% CI: -7.7 to -5.97; p < 0.000001). Then, from 2015 to 2021, the AAMR increased significantly, from 1.35 (95% CI: 1.20–1.50) in 2015 to 4.9 (95% CI: 4.63–5.18) in 2021. An APC of 27.51 (95% CI: 21.96 to 33.32; p < 0.000001) was recorded for that time frame. However, from 2021 to 2023, the AAMR decreased from 4.9 (95% CI: 4.63–5.18) in 2021 to 1.13 (95% CI: 1.00–1.26) in 2023, with an APC of -55.3 (95% CI: -65.61 to -41.90; p = 0.000006).

Among Hispanics, the AAMR also decreased, as noted in other demographics, decreasing from 2.61 (95% CI: 2.26 to 2.95) in 1999 to 0.95 (95% CI: 0.83 to 1.06) in 2023; the AAPC was -4.6 (95% CI: -8.53 to -0.5; p = 0.028). From 1999 to 2015, the AAMR decreased from 2.61 (95% CI: 2.26–2.95) in 1999 to 1.10 (95% CI: 0.96–1.25) in 2015, with an APC of -6.12 (95% CI: -8.18 to -4.01; p = 0.000014). Furthermore, from 2015 to 2021, the AAMR demonstrated a significant increase, trending from 1.10 (95% CI: 0.96–1.25) in 2015 to 4.98 (95% CI: 4.70–5.26) in 2021, with an APC of 32.94 (95% CI: 22.33 to 44.47; p = 0.000001). Then, from 2021 to 2023, the AAMR decreased significantly, from 4.98 (95% CI: 4.70–5.26) in 2021 to 0.95 (95% CI: 0.83–1.06) in 2023, recording an APC of -59.90 (95% CI: -74.40 to -37.18; p = 0.000491) for that time frame.

Among NH Asian/Pacific Islander individuals, the AAMR decreased from 2.98 (95% CI: 2.44 to 3.53) in 1999 to 0.78 (95% CI: 0.64 to 0.92) in 2023, with an AAPC of -5.11 (95% CI: -9.84 to -0.14; p = 0.000042). From 1999 to 2014, the AAMR demonstrated a downward trend, decreasing from 2.98 (95% CI: 2.44 to 3.53) in 1999 to 0.99 (95% CI: 0.80–1.19) in 2014, and thus giving an APC of -7.65 (95% CI: -10.44 to -4.76; p = 0.000042). Then, from 2014 to 2021, the AAMR increased significantly, reaching from 0.99 (95% CI: 0.80–1.19) in 2014 to 4 (95% CI: 3.66–4.34) in 2021, with an APC of 28.34 (95% CI: 17.86 to 39.75; p = 0.000010) recorded for that time frame. However, from 2021 to 2023, the AAMR decreased from 4 (95% CI: 3.66–4.34) in 2021 to 0.78 (95% CI: 0.64–0.92), with an APC of -59.61 (95% CI: -76.50 to -30.58; p = 0.0026), (Figure 2; Supplemental Tables 1, 2, 4).

3.4. Trends by age group

When stratified by age groups, individuals aged ≥65 years accounted for more deaths than individuals aged 45–64 years and 25–44 years (113,650 deaths, 28,870 deaths, and 2,124, respectively). Among adults aged ≥65 years, the CMR decreased from 17.06 (95% CI: 16.63 to 17.5) in 1999 to 4.22 (95% CI: 4.05 to 4.39) in 2023, with an AAPC of -5.65 (95% CI: -8.16 to -3.08; p = 0.000022). However, the CMR showed an overall downward trend among adults aged 45–64 years, decreasing from 2.3 (95% CI: 2.18 to 2.42) in 1999 to 0.77 (95% CI: 0.71 to 0.83) in 2023. The AAPC for this period was -5.07 (95% CI: -7.49 to -2.58; p = 0.00008). Furthermore, in adults aged 25–44 years, the CMR decreased from 0.11 (95% CI: 0.09 to 0.14) in 1999 to 0.06 (95% CI: 0.04 to 0.08) in 2023, with an AAPC of -2.24 (95% CI: -12.31 to 8.90; p = 0.68).

Among individuals aged ≥65 years, the CMR decreased from 17.06 (95% CI: 16.63 to 17.5) in 1999 to 5.1 (95% CI: 4.90–5.30) in 2015, at an APC of -7.21 (95% CI: -8.18 to -6.22; p < 0.000001). In addition, from 2015 to 2021, the CMR increased, trending from 5.1 (95% CI: 4.90–5.30) in 2015 to 17.55 (95% CI: 17.20–17.90) in 2021, with an APC of 26.37 (95% CI: 19.71 to 33.39; p < 0.000001). The CMR then decreased between 2021 and 2023, from 17.55 (95% CI: 17.20–17.90) in 2021 to 4.22 (95% CI: 4.05 to 4.39) in 2023. The APC between 2021 and 2023 was -55.16 (95% CI: -66.62 to -39.76; p = 0.000024).

On the other hand, among adults aged 45 to 64 years, the CMR initially decreased, from 2.3 (95% CI: 2.18–2.42) in 1999 to 0.84 (95% CI: 0.77–0.90) in 2015, at an APC of -6.90 (95% CI: -7.74 to -6.04; p < 0.000001). However, the CMR demonstrated a significant upward trend from 2015 to 2021, from 0.84 (95% CI: 0.77–0.90) in 2015 to 2.85 (95% CI: 2.74–2.97) in 2021. The APC for that time frame was 25.84 (95% CI: 20.30 to 31.63; p < 0.000001). In addition, from 2021 to 2023, the CMR decreased, trending from 2.85 (95% CI: 2.74–2.97) in 2021 to 0.77 (95% CI: 0.71–0.83) in 2023. The APC was -52.38 (95% CI: -64.60 to -35.95; p = 0.000061).

Among adults aged 25 to 44 years, the CMR decreased from 0.11 (95% CI: 0.09–0.14) in 1999 to 0.08 (95% CI: 0.06–0.10) in 2016, at an APC of -7.16 (95% CI: -9.61 to -4.63; p = 0.00002). In addition, from 2016 to 2019, the CMR increased, trending from 0.08 (95% CI: 0.06–0.10) in 2016 to 0.17 (95% CI: 0.14–0.19) in 2019, with an APC of 73.24 (95% CI: -26.78 to 309.94; p = 0.20). The CMR then decreased between 2019 and 2023, from 0.17 (95% CI: 0.14–0.19) in 2019 to 0.06 (95% CI: 0.04–0.08) in 2023; however, the APC between 2019 and 2023 was -20.73 (95% CI: -38.35 to 1.93; p = 0.068) (Figure 3; Supplemental Tables 2, 5).

3.5. Trends by census region

Between 1999 and 2023, the Midwest accounted for the most deaths involving IHD and medical/surgical procedure-related conditions. The South, West, and Northeast followed in descending order.

The AAMR in the South showed an overall downward trend, decreasing from 4.52 (95% CI: 4.35–4.68) in 1999 to 1.18 (95% CI: 1.11 to 1.25) in 2023, for an AAPC of -5.86 (95% CI: -7.42 to -4.27; p < 0.000001). From 1999 to 2015, the AAMR decreased from 4.52 (95% CI: 4.35–4.68) in 1999 to 1.42 (95% CI: 1.34–1.50) in 2015; the APC for that period was -7.33 (95% CI: -7.97 to -6.69; p < 0.000001). An upward trend was then observed between 2015 and 2021, with the AAMR increasing from 1.42 (95% CI: 1.34–1.50) in 2015 to 4.48 (95% CI: 4.35–4.61) in 2021, with an APC for that time frame of 23.67 (95% CI: 19.30 to 28.20; p < 0.000001). Then, the AAMR decreased from 4.48 (95% CI: 4.35–4.61) in 2021 to 1.18 (95% CI: 1.11 to 1.25) in 2023, with APC of -52.89 (95% CI: -60.60 to -43.66; p < 0.000001).

Similarly, AAMR in the West decreased overall, from 3.19 (95% CI: 3.01 to 3.38) in 1999 to 1.06 (95% CI: 0.97 to 1.14) in 2023; the AAPC was -4.57 (95% CI: -9.08 to 0.16; p = 0.058). Between 1999 and 2015, the AAMR decreased significantly from 3.19 (95% CI: 3.01 to 3.38) in 1999 to 1.16 (95% CI: 1.06–1.25) in 2015, with an APC of -5.87 (95% CI: -7.90 to -3.81; p = 0.000018). The AAMR then increased from 1.16 (95% CI: 1.06–1.25) in 2015 to 5.92 (95% CI: 5.72–6.12) in 2021, with an APC of 34.44 (95% CI: 22.12 to 48.01; p = 0.000005). The AAMR then decreased from 5.92 (95% CI: 5.72–6.12) in 2021 to 1.06 (95% CI: 0.97–1.14) in 2023, with an APC of -61.89 (95% CI: -77.5 to -35.46; p = 0.0013).

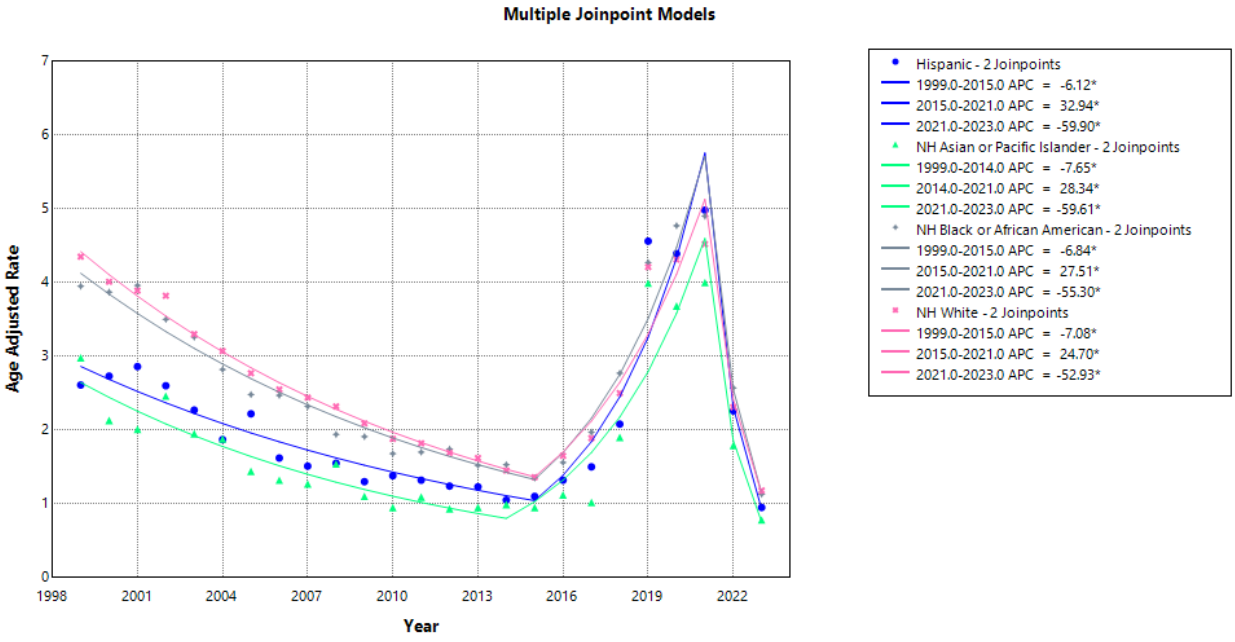

Figure 2: Race and ethnicity-stratified age-adjusted mortality rates per 100,000 for deaths involving ischemic heart disease and procedure-related conditions in U.S. adults, 1999–2023. In the figure legend, an asterisk denotes an APC significantly different from zero (two-sided *t*-test, $p < 0.05$).

The AAMR in the Midwest decreased from 4.65 (95% CI: 4.44 to 4.85) in 1999 to 1.13 (95% CI: 1.04 to 1.22) in 2023, at an AAPC of -6.08 (95% CI: -8.31 to -3.80; p < 0.000001). From 1999 to 2015, the AAMR trended downward, from 4.65 (95% CI: 4.44 to 4.85) in 1999 to 1.37 (95% CI: 1.27–1.47) in 2015, with an APC of -7.74 (95% CI: -8.49 to -6.99; p < 0.000001). The AAMR then increased from 1.37 (95% CI: 1.27–1.47) in 2015 to 4.08 (95% CI: 3.91–4.25) in 2021, with an APC of 23.27 (95% CI: 17.72 to 29.09; p < 0.000001). From 2021 to 2023, the AAMR decreased from 4.08 (95% CI: 3.91–4.25) in 2021 to 1.13 (95% CI: 1.04 to 1.22) in 2023, with an APC of -52.10 (95% CI: -63.43 to -37.27; p = 0.000023).

In the Northeast, the AAMR decreased from 4.05 (95% CI: 3.84 to 4.25) in 1999 to 1.13 (95% CI: 1.03 to 1.22) in 2023, and the AAPC was -5.04 (95% CI: -7.68 to -2.33; p = 0.00031). The AAMR declined overall between 1999 and 2015, from 4.05 (95% CI: 3.84 to 4.25) in 1999 to 1.23 (95% CI: 1.13–1.33), with an APC of -6.89 (95% CI: -7.85 to -5.93; p < 0.000001). The AAMR increased from 1.23 (95% CI: 1.13–1.33) in 2015 to 3.97 (95% CI: 3.79–4.15) in 2021, with an APC of 23.65 (95% CI: 17.01 to 30.68; p < 0.000001). The AAMR decreased from 3.97 (95% CI: 3.79–4.15) in 2021 to 1.13 (95% CI: 1.03–1.22) in 2023, with an APC of -49.67 (95% CI: -63.19 to -31.19; p = 0.00024) (Figure 4; Supplemental Tables 2, 6).

3.6. Trends by urbanization

Between 1999 and 2020, metro areas accounted for more deaths than nonmetropolitan areas (95,967 deaths vs. 26,963 deaths). Overall, AAMR in metro areas in 1999 was 3.99 (95% CI: 3.89 to 4.09) and increased to 4.17 (95% CI: 4.09 to 4.26) in 2020, with an AAPC of 0.39 (95% CI: -1.06 to 1.86; p = 0.6). In nonmetropolitan areas, the AAMR in 1999 was 5.07 (95% CI: 4.83–5.31), increasing to 5.42 (95% CI: 5.19–5.64) in 2020, with an AAPC of 0.46 (95% CI: -0.68 to 1.6; p = 0.43).

Among people living in metro areas, the AAMR declined from 3.99 (95% CI: 3.89 to 4.09) in 1999 to 1.24 (95% CI: 1.19–1.29) in 2015, with an APC of -7.58 (95% CI: -8.59 to -6.56; p < 0.000001). From 2015 to 2020, the AAMR increased from 1.24 (95% CI: 1.19–1.29) in 2015 to 4.17 (95% CI: 4.09–4.26) in 2020, with an APC of 30.8 (95% CI: 23.72 to 38.29; p < 0.000001).

Among people living in nonmetropolitan areas, the AAMR declined from 5.07 (95% CI: 4.83–5.31) in 1999 to 1.71 (95% CI: 1.58–1.84) in 2015, with an APC of -6.85 (95% CI: -7.63 to -6.06; p < 0.000001). From 2015 to 2020, the AAMR showed an increase from 1.71 (95% CI: 1.58–1.84) in 2015 reaching 5.42 (95% CI: 5.19–5.64) in 2020, with an APC of 27.93 (95% CI: 22.44 to 33.65; p < 0.000001) (Figure 5; Supplemental Tables 2, 7).

4. Discussion

Our nationwide analysis of mortality involving IHD and medical/surgical procedure-related codes among U.S. adults aged ≥25 years over 25 years identified three overarching patterns. First, mortality has declined substantially over the long term, with 2023 rates less than one-third of those in 1999. Second, this favorable trend was disrupted by a sharp rebound from the mid-2010s through 2021, followed by an equally steep decline thereafter – a U-shaped pattern mirrored across sex, race/ethnicity, age groups, and regions. Third, the burden remains concentrated in older adults, males, NH White and NH Black individuals, and residents of Midwest and nonmetropolitan areas, underscoring persistent demographic and geographic inequities despite overall progress.

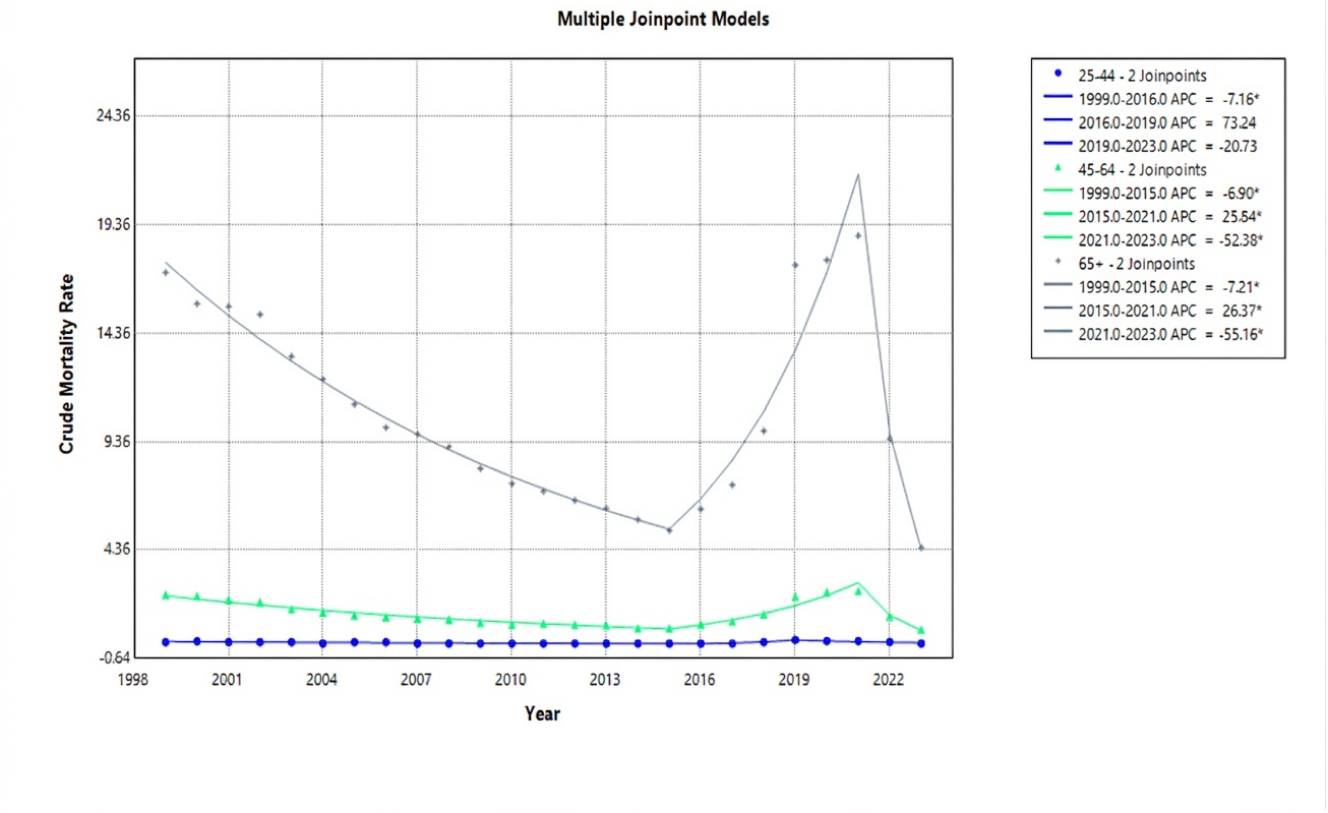

Figure 3: Age-stratified crude mortality rates per 100,000 for deaths involving ischemic heart disease and procedure-related conditions in U.S. adults, 1999–2023. In the figure legend, an asterisk denotes an APC significantly different from zero (two-sided t-test, $p < 0.05$).

Mortality rates were consistently higher among male individuals than female individuals, while both sexes experienced significant declines in mortality rates over time. The mortality patterns observed were similar to those reported for IHD and cardiovascular mortality more broadly, where males have historically had a greater overall burden of disease, supported by the earlier onset of atherosclerosis, a higher prevalence of multiple clustered risk factors, and differences in patterns of care for males versus females [20, 21]. In addition to our earlier observation, the study supports the hypothesis that this difference persists in mortality records documenting IHD and medical/surgical procedure-related conditions and underscores the need for sex-sensitive risk stratification and secondary prevention efforts to address the differences noted above. Our analysis supports the observations noted in the literature concerning race and ethnicity; in particular, the majority of deaths in our analysis occurred among NH White individuals, who had a higher mortality rate than NH Black individuals, with AAMRs of 2.65 and 2.61 per 100,000, respectively [22, 23]. The lower rates of IHD deaths documented among Hispanic and NH Asian/Pacific Islander groups were also noted in our analysis. Consistent with findings reported in the literature, previous studies have described differences in cardiovascular mortality and outcomes associated with medical and surgical care across racial and ethnic groups, including differences reported between Black and White adults, potentially reflecting variations in comorbidities, access to care, and broader social and health-system factors [24, 25]. In our study, we found that these inequities persisted even when we limited the analysis to deaths coded for both IHD and medical/surgical procedure-related conditions. The very rapid and symmetrical increase in mortality from 2015 through 2021 across all racial and ethnic groups may suggest the presence of a substantial system-wide stressor during this period, potentially reflecting the possible convergence of worsening cardiometabolic risk, rising obesity-related IHD mortality, and the COVID-19 pandemic, alongside longstanding structural disparities [26, 27].

Regionally, the Midwest consistently had the highest mortality rates, followed by the South, while the West and Northeast reported lower rates. These regional patterns are consistent with previously described geographic variation in the prevalence of obesity, diabetes, and hypertension, as well as differences in access to specialty and medical care across regions [28–30]. Our findings indicate that these regional patterns were also present in mortality records documenting both IHD and procedure-related conditions, consistent with regional differences reported for chronic IHD mortality [28–30].

As expected, patients aged ≥65 years accounted for the vast majority of deaths involving IHD and medical/surgical procedure-related conditions in our cohort. Younger patients, while contributing to a much smaller proportion of deaths involving IHD, still accounted for a significant share of the overall deaths documenting medical/surgical procedure-related conditions. This finding is consistent with the age gradient associated with CVD and IHD incidence [31, 32]. Older patients may have a higher prevalence of underlying atherosclerotic disease and a greater accumulated atherosclerotic burden, as well as multiple comorbidities and frailty, which may increase their susceptibility to hemodynamic (blood flow) stress and other physiological stressors associated with medical and surgical procedures

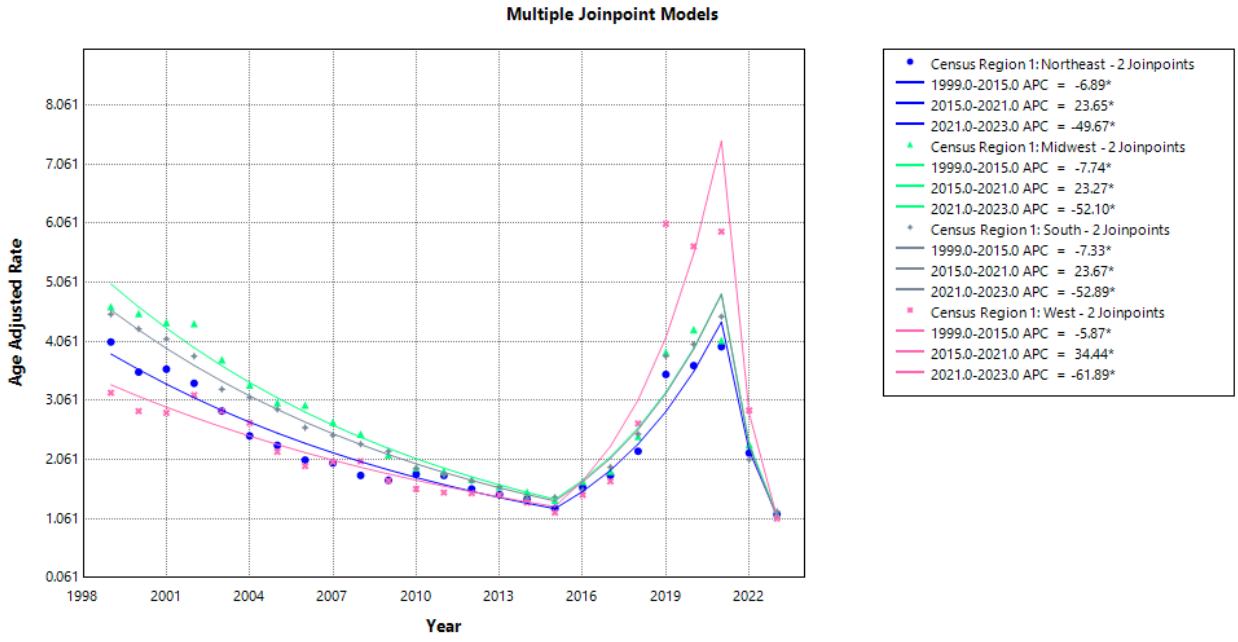

Figure 4: Census region-stratified age-adjusted mortality rates per 100,000 for deaths involving ischemic heart disease and procedure-related conditions in U.S. adults, 1999–2023. In the figure legend, an asterisk denotes an APC significantly different from zero (two-sided t-test, $p < 0.05$).

[33, 34]. In addition, recent studies have shown that postoperative acute heart failure and Myocardial Injury after Noncardiac Surgery (MINS) are particularly lethal among older patients, with one-year mortality rates for these events often exceeding those observed in comparable non-surgical patient cohorts [35–37]. These findings suggest prioritizing cardiovascular care optimization among older patients, with particular attention to comprehensive risk assessment, management of cardiovascular risk factors, and appropriate follow-up.

Although metropolitan areas had higher crude death counts, AAMRs declined in both metropolitan and nonmetropolitan areas through 2020, with mortality rates remaining relatively similar between the two groups toward the end of the study period [23]. Our findings suggest that the mid-2010s reversal and COVID-19-era changes in mortality involving IHD and procedure-related conditions may have affected metropolitan and nonmetropolitan settings in parallel, potentially reflecting shared factors such as changes in case mix, delayed elective surgical care, and health-system strain [38].

Temporal changes in mortality may partly reflect differences in death-certificate documentation and coding practices, which can influence observed IHD mortality trends [39]. Because MCOD data lack detailed patient-level clinical information, the observed patterns cannot establish underlying mechanisms or causal pathways.

4.1. Clinical implications

Cardiovascular risk assessment and optimization are important components of managing adults with IHD. Previous clinical research suggests that systematic risk assessment, including risk scoring and targeted troponin surveillance among patients considered at high risk, may help inform cardiovascular management in the context of medical and surgical procedures [40–42]. Further research is needed to determine whether these approaches improve population-level mortality outcomes.

Accordingly, the observed decline in mortality over the past several decades may reflect, in part, advances in IHD management and the broader evolution of medical and surgical care. Nevertheless, the observed patterns also suggest that these improvements may remain vulnerable to broader system-wide stressors.

Therefore, we hypothesize that future research should evaluate whether tailored cardiovascular care pathways for older adults, Black patients, rural populations, and populations residing in regions with a high burden of morbidity and mortality, particularly the Midwest, may improve cardiovascular outcomes compared with generalized approaches to cardiovascular care. At the health-system level, the observed mortality patterns were broadly consistent with existing disparities in cardiometabolic health across demographic and geographic groups, suggesting that cardiovascular care should be considered within the broader continuum of population-level cardiovascular prevention and care [43–45].

4.2. Strengths, limitations, and future directions

The study's main strengths are its national scope, 25-year duration, and large sample size, as well as its consistent use of CDC WONDER data and joinpoint regression across sex, race/ethnicity, age, region, and urbanization. By explicitly using both IHD (I20–I25) and medical/surgical procedure-related codes (Y83–Y84), we identify mortality records documenting IHD and procedure-related conditions, providing a focused analysis not performed in earlier national studies of IHD mortality or perioperative MI/MINS.

However, the following limitations should be noted. First, death certificate data are vulnerable to errors in identifying both the

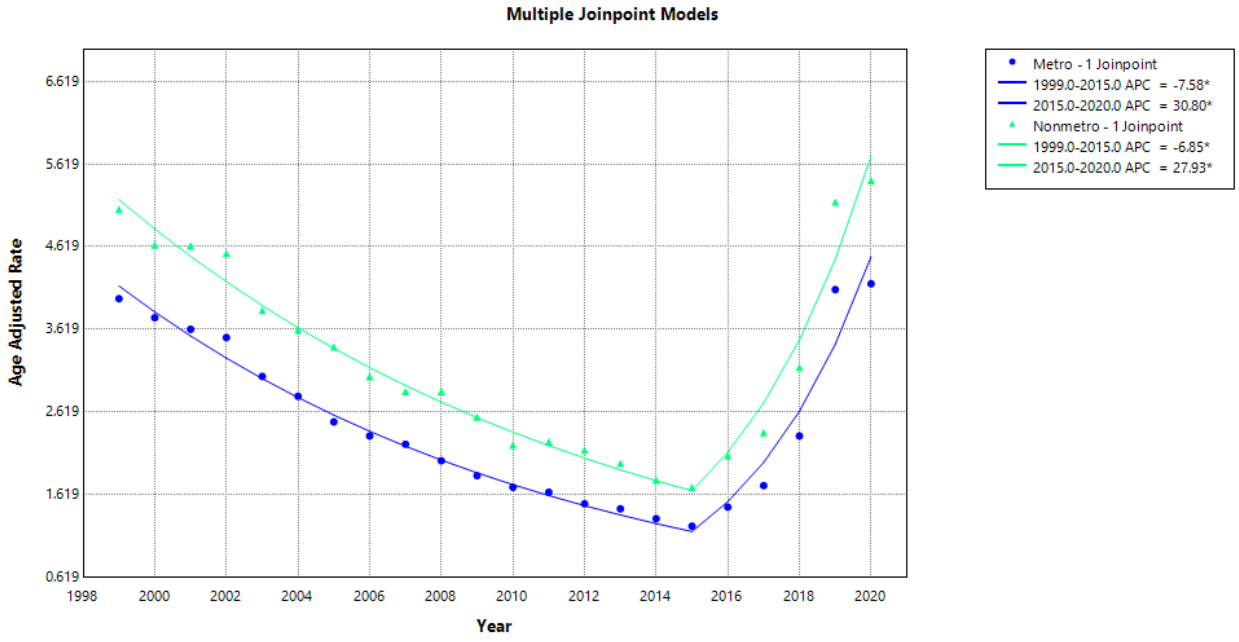

Figure 5: Urban–rural stratified age-adjusted mortality rates per 100,000 for deaths involving ischemic heart disease and procedure-related conditions in U.S. adults, 1999–2020. In the figure legend, an asterisk denotes an APC significantly different from zero (two-sided t-test, $p < 0.05$).

underlying cause of death and contributing conditions. Furthermore, Y83–Y84 coding may not capture all mortality records involving medical or surgical procedures and does not provide information on the timing, type of procedure performed, or clinical course surrounding the procedure. Second, CDC WONDER is not designed to include clinical variables such as coronary anatomy, revascularization strategy, prescribed medications, or hemodynamic parameters, which limits our ability to compare risk-adjusted outcomes or infer mechanisms underlying the observed mortality patterns. Third, urbanization data are available only through 2020, which prevents a complete understanding of urban–rural patterns during the height and immediate post-COVID-19 era. Lastly, as with all ecological studies, we cannot determine the causal impact of policies, clinical processes, or pandemic patterns on observed trends.

Researchers should integrate vital statistics with surgical registries and electronic health record databases to evaluate risks associated with specific types of procedures, identify variation in outcomes across hospitals, and better understand how guideline-based cardiovascular interventions may affect overall mortality rates. In addition, future studies should evaluate how the adoption of newer techniques for the management of IHD in vulnerable populations, including routine troponin monitoring, structured cardiovascular care pathways, telehealth-enabled prehabilitation, and other approaches, may impact mortality involving IHD and medical/surgical procedure-related conditions [46, 47].

5. Conclusion

In this nationwide analysis of U.S. adults aged ≥25 years, mortality involving IHD and medical/surgical procedure-related conditions declined substantially from 1999 to 2023, with 2023 rates less than one-third of those observed in 1999. However, this long-term improvement was interrupted by a marked increase from the mid-2010s through 2021, followed by a steep decline thereafter, producing a consistent U-shaped temporal pattern across demographic and geographic subgroups. Mortality was concentrated among older adults and males, with substantial mortality among NH White and NH Black individuals and across Midwestern and nonmetropolitan populations. These findings highlight substantial and persistent demographic and geographic disparities despite overall improvements in mortality. Continued efforts to strengthen perioperative cardiovascular risk assessment, prevention, and care, particularly among the highest-risk populations, are warranted.

Prior Presentation

This analysis was previously presented in abstract form at TCT 2025 and published as: Hemida M, Saghir M, Ibrahim A, et al. TCT-296 25-year trends in postoperative mortality in U.S. adults with ischemic heart disease. J Am Coll Cardiol. 2025;86(17 Suppl):B131–B132.

Conflicts of Interest

The authors declare no competing interests that could have influenced the objectivity or outcome of this research.

Funding Source

This research received no external funding.

Acknowledgments

None.

Informed Consent

Not applicable.

Institutional Review Board (IRB)

Institutional review board approval was not required because the study used publicly available, de-identified mortality data.

Large Language Model

None.

Authors Contributions

MA, YR, and MFH contributed to the conceptualization of the study and to the methodology, while MA, AHM, MS, AAI, AG, WQ, KP, MMAE, OKE, IE, SE, AE, and WB were responsible for investigation. YR, AHM, MS, AG, WQ, MMAE, and OKE were responsible for data curation, and YR performed the statistical analysis. MA, YR, AHM, MS, AAI, AG, WQ, KP, MMAE, OKE, IE, SE, AE, and WB assisted in drafting the manuscript, while YR and MFH supervised the study and were responsible for project administration. All authors reviewed and approved the final manuscript and agreed to be accountable for the work.

Data Availability

The data that support the findings of this study are openly available in CDC WONDER at https://wonder.cdc.gov/. Further inquiries can be directed to the corresponding author.

References

1. Martin SS, Aday AW, Allen NB, Almarzooq ZI, Anderson CAM, Arora P, et al. 2025 Heart Disease and Stroke Statistics: A Report of US and Global Data From the American Heart Association. Circulation. 2025;151(8):e41-e660. [PMID: 39866113, PMCID: PMC12256702, https://doi.org/10.1161/CIR.0000000000001303].
2. Khalid N, Haider S, Abdullah M, Asghar S, Laghari MA, Rajeswaran Y. Trends and disparities in coronary artery disease prevalence among U.S. adults from 2019 to 2022. Curr Probl Cardiol. 2024;49(8):102645. [PMID: 38796947, https://doi.org/10.1016/j.cpcardiol.2024.102645].
3. Centers for Disease Control and Prevention. Heart Disease Facts; 2024. National Center for Chronic Disease Prevention and Health Promotion. Updated 24 October 2024. Available from: https://www.cdc.gov/heart-disease/data-research/facts-stats/.
4. Mohebi R, Chen C, Ibrahim NE, McCarthy CP, Gaggin HK, Singer DE, et al. Cardiovascular disease projections in the United States based on the 2020 census estimates. J Am Coll Cardiol. 2022;80(6):565-78. [PMID: 35926929, PMCID: PMC9396356, https://doi.org/10.1016/j.jacc.2022.05.033].
5. Sweitzer B. Perioperative evaluation and optimization of patients at risk of cardiac complications for non-cardiac surgery. Mo Med. 2016;113(4):320-4. [PMID: 30228486, PMCID: PMC6139923].
6. Song MG, Kim CW, Song SY, Kim HG, Kim DH. Management of patients with ischemic heart disease in spine surgery. Asian Spine J. 2023;17(6):1168-75. [PMID: 38105637, PMCID: PMC10764142, https://doi.org/10.31616/asj.2023.0161].
7. Ruetzler K, Smilowitz NR, Berger JS, Devereaux PJ, Maron BA, Newby LK, et al. Diagnosis and management of patients with myocardial injury after noncardiac surgery: a scientific statement from the American Heart Association. Circulation. 2021;144(19):e287-305. [PMID: 34601955, https://doi.org/10.1161/CIR.0000000000001024].
8. Kashlan B, Kinno M, Syed M. Perioperative myocardial injury and infarction after noncardiac surgery: a review of pathophysiology, diagnosis, and management. Front Cardiovasc Med. 2024;11:1323425. [PMID: 38343871, PMCID: PMC10853429, https://doi.org/10.3389/fcvm.2024.1323425].
9. Hedge J, Balajibabu PR, Sivaraman T. The patient with ischaemic heart disease undergoing non cardiac surgery. Indian J Anaesth. 2017;61(9):705-11. [PMID: 28970628, PMCID: PMC5613595, https://doi.org/10.4103/ija.IJA_384_17].
10. Thompson A, Fleischmann KE, Smilowitz NR, de las Fuentes L, Mukherjee D, Aggarwal NR, et al. 2024 AHA/ACC/ACS/ASNC/HRS/SCA/SCCT/SCMR/SVM guideline for perioperative cardiovascular management for noncardiac surgery: a report of the American College of Cardiology/American Heart Association Joint Committee on Clinical Practice Guidelines. Circulation. 2024;150(19):e351-442. [PMID: 39316661, https://doi.org/10.1161/CIR.0000000000001285].
11. Cohn SL. 2024 ACC/AHA guideline on perioperative cardiovascular management before noncardiac surgery: what's new? Cleve Clin J Med. 2025;92(4):213-9. [PMID: 40169218, https://doi.org/10.3949/ccjm.92a.24125].
12. Ali MF, Ahmad H, Qadri M, et al. The weight of risk: epidemiological trends in mortality involving cardiac arrest and obesity in the United States (1999–2023). J Diabetes Metab Disord. 2026;25:236. [https://doi.org/10.1007/s40200-026-02037-9].
13. Faheem MSB, Fatima Y, Munir SU, Khabir M, Khatri N. Trends in ischemic heart disease and thromboembolism-related mortality in the United States, 1999–2024: a population-based analysis using CDC WONDER data. Thromb Res. 2025;255:109482. [PMID: 40987074, https://doi.org/10.1016/j.thromres.2025.109482].
14. Hemida M, Saghir M, Ibrahim A, et al. TCT-296 25-year trends in postoperative mortality in U.S. adults with ischemic heart disease. J Am Coll Cardiol. 2025;86(17 Suppl):B131-2. Conference abstract. [https://doi.org/10.1016/j.jacc.2025.09.395].
15. von Elm E, Altman DG, Egger M, Pocock SJ, Gøtzsche PC, Vandenbroucke JP. The Strengthening the Reporting of Observational Studies in Epidemiology (STROBE) statement: guidelines for reporting observational studies. J Clin Epidemiol. 2008;61(4):344-9. [PMID: 18313558, https://doi.org/10.1016/j.jclinepi.2007.11.008].
16. Aggarwal R, Chiu N, Loccoh EC, Kazi DS, Yeh RW, Wadhera RK. Rural-urban disparities: diabetes, hypertension, heart disease, and stroke mortality among Black and White adults, 1999–2018. J Am Coll Cardiol. 2021;77(11):1480-1. [PMID: 33736831, https://doi.org/10.1016/j.jacc.2021.01.032].
17. Ingram DD, Franco SJ. 2013 NCHS urban-rural classification scheme for counties. Vital Health Stat 2. 2014;(166):1-73. [PMID: 24776070].
18. Anderson RN, Rosenberg HM. Age standardization of death rates: implementation of the year 2000 standard. Natl Vital Stat Rep. 1998;47(3):1-16. [PMID: 9796247].
19. National Cancer Institute. Joinpoint Regression Program, Surveillance Research Program; 2025. Available from: https://surveillance.cancer.gov/joinpoint/.
20. Wang Y, Sun X, Zhang X, Wang X, Li J, Wang K. Global, regional, and national burden of early-onset ischemic heart disease: trends and projections among adults aged 15–44 years from 1990 to 2046. Front Cardiovasc Med. 2025;12:1653335. [PMID: 40951829, PMCID: PMC12426116, https://doi.org/10.3389/fcvm.2025.1653335].
21. Wolf S, Schievano E, Amidei CB, et al. Mortality trend of ischemic heart disease (2008–2022): a retrospective analysis of epidemiological data. Int J Cardiol. 2024;406:132042. [PMID: 38614362, https://doi.org/10.1016/j.ijcard.2024.132042].
22. Sosa D IV, Blankenship JC. Racial disparities in ischemic heart disease. J Clin Cardiol Cardiovasc Interv. 2022;5(7). [https://doi.org/10.31579/2641-0419/269].
23. Hemida MF, Ibrahim AA, Goel A, et al. Twenty-five years of angina-related mortality in elderly adults aged ≥65 years: a retrospective cohort study using real-world data from the USA. ASIDE Int Med. 2025;2(3):33-42. [https://doi.org/10.71079/ASIDE.IM.110925248].
24. Kibrik P, Rao A, Zhu J, Bai H, Storch J, Han D, et al. Impact of race on perioperative outcomes following carotid endarterectomy, transfemoral carotid artery stenting, and transcarotid artery revascularization. J Vasc Surg. 2023;78(2):e93-4. Conference abstract.

25. Kyalwazi AN, Loccoh EC, Brewer LC, et al. Disparities in cardiovascular mortality between Black and White adults in the United States, 1999 to 2019. Circulation. 2022;146(3):211-28. [PMID: 35861764, PMCID: PMC9310198, https://doi.org/10.1161/CIRCULATIONAHA.122.060199].
26. Wang Y, Li Q, Bi L, Wang B, Lv T, Zhang P. Global trends in the burden of ischemic heart disease based on the global burden of disease study 2021: the role of metabolic risk factors. BMC Public Health. 2025;25(1):310. [PMID: 39856644, PMCID: PMC11763131, https://doi.org/10.1186/s12889-025-21588-9].
27. Janus SE, Makhlouf M, Chahine N, Motairek I, Al-Kindi SG. Examining disparities and excess cardiovascular mortality before and during the COVID-19 pandemic. Mayo Clin Proc. 2022;97(12):2206-14. [PMID: 36336516, PMCID: PMC9300586, https://doi.org/10.1016/j.mayocp.2022.07.008].
28. Ferdinand AO, Akinlotan MA, Callaghan T, Towne SD Jr, Bolin J. Diabetes-related hospital mortality in the U.S.: a pooled cross-sectional study of the National Inpatient Sample. J Diabetes Complications. 2019;33(5):350-5. [PMID: 30910276, https://doi.org/10.1016/j.jdiacomp.2019.01.007].
29. Ashfaq F, Zain A, Ahmad K, et al. Trends in mortality from acute myocardial infarction among the obese population in the United States from 1999 to 2020: insights from CDC WONDER. Arch Med Sci Atheroscler Dis. 2025;10:e211-9. [PMID: 41142685, PMCID: PMC12550666, https://doi.org/10.5114/amsad/210584].
30. Brereton BJ, Desai RV, Yarrarapu SNS, Matos Urena JG, Jain AP. Regional disparities of cardiovascular risk factors and major cardiovascular events in non-electively hospitalized young adults. J Community Hosp Intern Med Perspect. 2023;13(2):1-6. [PMID: 37168061, PMCID: PMC10166212, https://doi.org/10.55729/2000-9666.1164].
31. Lagoo-Deenadayalan SA, Newell MA, Pofahl WE. Common perioperative complications in older patients. In: Principles and Practice of Geriatric Surgery. New York: Springer; 2011. p. 361-76. [https://doi.org/10.1007/978-1-4419-6999-6_29].
32. Chawan AP, Rathore YS, Chumber S, Kataria K. Surgical diseases and surgical outcomes in geriatric patients. Int Surg J. 2020;7(10):3315-20. [https://doi.org/10.18203/2349-2902.isj20204129].
33. Islam MS, Maruf AA, Mazumder MM, Rahman MA, Siraj SB. Cardiovascular challenges in geriatric anesthesia after induction of GA. Ann Int Med Dent Res. 2023;9:191-6. [https://doi.org/10.53339/aimdr.2023.9.28].
34. Au Yong PSA, Sim EYL, Ho CYX, et al. Association of multimorbidity with frailty in older adults for elective non-cardiac surgery. Cureus. 2021;13(5):e15033. [PMID: 34150384, PMCID: PMC8200322, https://doi.org/10.7759/cureus.15033].
35. Gewarges M, Frankfurter C, McDonald M. Perioperative assessment and management of patients with heart failure. Can J Gen Intern Med. 2022;17(SP1):28-37. [https://doi.org/10.22374/cjgim.v17iSP1.604].
36. Beattie WS, Wijeysundera DN. The growing burden of perioperative heart failure. Anesth Analg. 2014;119(3):506-8. [PMID: 25136995, https://doi.org/10.1213/ANE.0000000000000370].
37. Smilowitz NR, Redel-Traub G, Hausvater A, et al. Myocardial injury after noncardiac surgery: a systematic review and meta-analysis. Cardiol Rev. 2019;27(6):267-73. [PMID: 30985328, PMCID: PMC6776733, https://doi.org/10.1097/CRD.0000000000000254].
38. Mehta A, Awuah WA, Ng JC, et al. Elective surgeries during and after the COVID-19 pandemic: case burden and physician shortage concerns. Ann Med Surg (Lond). 2022;81:104395. [PMID: 35999832, PMCID: PMC9388274, https://doi.org/10.1016/j.amsu.2022.104395].
39. Chen L, Walker S, Tong S. The impact of the variation in death certification and coding practices on trends in mortality from ischaemic heart disease. Aust Health Rev. 2002;25(4):189-97. [PMID: 12404982, https://doi.org/10.1071/ah020189a].
40. Segerson KE. Ischemic heart disease. In: The Perioperative Medicine Consult Handbook. Cham: Springer International Publishing; 2020. p. 59-64. [https://doi.org/10.1007/978-3-030-19704-9_9].
41. Mahendran S, Thiagalingam A, Hillis G, Halliwell R, Pleass HC, Chow CK. Cardiovascular risk management in the peri-operative setting. Med J Aust. 2023;219(1):30-9. [PMID: 37302136, https://doi.org/10.5694/mja2.51988].
42. Fisher B. Peri-operative cardiovascular risk and the general internist. Can J Gen Intern Med. 2014;9(2):53-9. [https://doi.org/10.22374/cjgim.v9i2.40].
43. Gottumukkala V, Vetter TR, Gan TJ. Perioperative medicine: what the future can hold for anesthesiology. Anesth Analg. 2023;136(4):628-35. [PMID: 36928147, https://doi.org/10.1213/ANE.0000000000006412].
44. McLeod M, Signal V, Gurney J, Sarfati D. Postoperative mortality of indigenous populations compared with nonindigenous populations: a systematic review. JAMA Surg. 2020;155(7):636-56. [PMID: 32374369, https://doi.org/10.1001/jamasurg.2020.0316].
45. Bhave NM, Eagle KA. Trends in perioperative cardiovascular events: mostly sunny, with showers. JAMA Cardiol. 2017;2(2):188-9. [PMID: 28030654, https://doi.org/10.1001/jamacardio.2016.4786].
46. Azizi PM, Wijeysundera DN, Wijeysundera HC, et al. Troponin testing after noncardiac surgery: a population-based historical cohort study on variation and factors associated with testing in Ontario. Can J Anaesth. 2022;69(5):572-81. [PMID: 35386054, https://doi.org/10.1007/s12630-022-02219-y].
47. Jones C, Sritharan K, Abu-Habsa M. Identification and management of perioperative cardiovascular risk. Br J Hosp Med (Lond). 2010;71(1):M12-5. [PMID: 20081650, https://doi.org/10.12968/hmed.2010.71.Sup1.45984].